

Thesis for Doctor of Philosophy

δ -TRIP Steel

Yi, Hongliang (易 红 亮)

Department of Ferrous Technology

Graduate Institute of Ferrous Technology

Pohang University of Science and Technology

2010

δ -TRIP Steel

δ -TRIP Steel

by
Yi, Hongliang
Department of Ferrous Technology
Graduate Institute of Ferrous Technology
Pohang University of Science and Technology

A thesis submitted to the faculty of Pohang University of Science and Technology in partial fulfillments of the requirements for the degree of **Doctor of Philosophy** in the Graduate Institute of Ferrous Technology (Computational Metallurgy)

Pohang, Korea

June 30, 2010

Approved by

Prof. Bhadeshia, H. K. D. H.

Prof. Kim, Nack-Joon

Major Advisor

Co-advisor

δ -TRIP Steel

Yi, Hongliang

This dissertation is submitted for the degree of Doctor of Philosophy at the Graduate Institute of Ferrous Technology of Pohang University of Science and Technology. The research reported herein was approved by the committee of Thesis Appraisal

June 30, 2010

Thesis Review Committee

Chairman: Prof. Bhadeshia, H. K. D. H.

(Signature)

Member: Prof. Kim, Nack-Joon

(Signature)

Member: Prof. Suh, Dong-Woo

(Signature)

Member: Prof. Kim, Seon-Hyo

(Signature)

Member: Dr. Lee, Jae-Kon

(Signature)

Preface

This dissertation is submitted for the degree of Doctor of Philosophy at Pohang University of Science and Technology. The research reported herein was carried out under the supervision of Professor H. K. D. H. Bhadeshia in the Computational Metallurgy Laboratory of the Graduate Institute of Ferrous Technology, Pohang University of Science and Technology, and Professor of Physical Metallurgy, University of Cambridge, between March 2007 and February 2010.

This work is to the best of my knowledge original, except where suitable references are made to previous work. Neither this, nor any substantially similar dissertation has been or is being submitted for any degree, diploma or other qualification at any other university or institution. This dissertation does not exceed 60,000 words in length.

The research has been published as follows:

H. L. Yi, S. K. Ghosh, W. J. Liu, K. Y. Lee and H. K. D. H. Bhadeshia, Non-equilibrium Solidification and Ferrite in δ -TRIP Steel. *Materials Science & Technology*, 2010, in press.

H. L. Yi, K. Y. Lee and H. K. D. H. Bhadeshia, Stabilisation of Ferrite in Hot Rolled δ -TRIP Steel. *Materials Science & Technology*, 2010, in press.

H. L. Yi, S. Ghosh and H. K. D. H. Bhadeshia, Dual-Phase Hot-Press Forming Alloy. *Materials Science & Engineering A*, 527 (2010) 4870-4874.

H. L. Yi, K. Y. Lee and H. K. D. H. Bhadeshia, Extraordinary Ductility in

Al-bearing Delta-TRIP Steel. *Proceedings of the Royal Society A*, in press.

H. L. Yi, K. Y. Lee and H. K. D. H. Bhadeshia, Spot Weldability of δ -TRIP Steel Containing 0.4 wt% C. *Science and Technology of Welding & Joining*, submitted.

H. L. Yi, K. Y. Lee and H. K. D. H. Bhadeshia, Mechanical Stabilisation Phenomenon of Retained Austenite in δ -TRIP Steel. to be submitted.

Hongliang Yi, S. Ghosh, H. K. D. H. Bhadeshia and Kyooyoung Lee, Stabilization of δ -ferrite in δ -TRIP Steel. *Taiwan 2008 International Steel Technologies Symposium*, #A17, 2008.

MFT Yi, Hongliang

20073851 δ -TRIP Steel

Department of Ferrous Technology (Computational Metallurgy)

2010

Advisor: Bhadeshia, H. K. D. H., Prof. Kim, Nack-Joon

ABSTRACT

A new concept in steels which are considered by transformation plasticity was recently developed entirely by calculation. The steel relies on the presence of δ -ferrite in solidification, bainitic ferrite and retained austenite in the microstructure. δ -TRIP steel contains a small amount of silicon to avoid surface quality problems during hot rolling and galvanizing. The original concept steel was found to possess excellent properties for automotive applications. The limited experimental validation of this concept has been extended in the present work, almost to the point of advanced commercialisation.

An attempt to reproduce the work highlighted a number of δ -ferrite, the solidification process has been investigated in order to understand the stability of δ -ferrite as a function of solute content and non equilibrium cooling conditions. The solid-state transformation of δ -ferrite into austenite occurs without the required partitioning of solutes and this is responsible for the development of non-equilibrium microstructures, a conclusion supported by microanalytical data and through calculations of limiting phase diagrams based on para equilibrium rather than equilibrium. Kinetic simulations confirm that this interpretation is consistent with the majority of austenite growing in the solid state without the partitioning of the substitutional solutes.

Further, the stability of this δ -ferrite has been investigated during reheating into a temperature range typical of hot rolling conditions since the alloys are always used in the rolled condition. It is found that contrary to expectations from calculated phase diagrams, the steel becomes fully austenitic under these conditions and that a better balance of ferrite promoting solutes is necessary in order to stabilise the dendritic structure. New alloys are

designed for this purpose and are found suitable for hot rolling in the two-phase field over the temperature range 900–1200 °C.

Furthermore, the heat treatment profiles have been studied to achieve good properties for automotive application, which is consistent with practical production processes. The alloys exhibit impressive combinations of tensile strength and elongation. The alloys rely on significant concentrations of ferrite-stabilising solutes so that δ -ferrite which forms during solidification is retained in the microstructure. Except the role of retained austenite playing as TRIP effect, its plastic deformation is found to contribute to the overall mechanical behavior as well. The mechanical stabilisation phenomenon of retained austenite has been firstly observed experimentally in TRIP-assisted steels here. A physical model has been proposed for the estimation of mechanical stabilisation. The result of modeling is consistent with the experimental observations. This explains the reason why retained austenite cannot transform fully into martensite in TRIP-assisted steels.

The δ -TRIP steel is expected to be weldable even though its carbon equivalent is much higher than the conventionally permitted value 0.4 wt% because a dual phase (ferrite + martensite) is supposed to be achieved in both heat affected zone and fusion zone by introducing δ -ferrite into the microstructure. The δ -ferrite can persist in the entire temperature range during spot welding by addition of strong ferrite stabilising element, aluminium. The spot weldability of δ -TRIP alloys has therefore been investigated in this research with changing the aluminium contents.

Hot-press forming steels are formed in a fully austenitic state followed by die-quenching in order to generate martensite to achieve high strength. The ductility therefore, tends to be limited. A novel steel design, based on chemical compositions of a δ -TRIP alloy but different heat treatment, in which the forming operation is in the two-phase austenite and ferrite field, so that the quenching results in a dual-phase ferrite and martensite microstructure at ambient temperature. It is demonstrated that slightly better properties are achieved compared with current hot-press forming steels. The interpretation of the mechanisms of deformation during tensile testing indicates that the ductility can be further enhanced without compromising strength. The new steel also can be heated to temperature which is lower than that used for conventional hot-press forming steels, before transfer into the forming press.

Contents

Chapter 1	TRIP-assisted Steels and δ-TRIP Steel.....	1
1.1	Introduction.....	1
1.2	TRIP and TRIP-assisted steels	4
1.3	Alloying elements in TRIP-assisted steels.....	6
1.4	Microstructural evolution.....	12
1.5	Mechanical performance.....	19
1.6	Strain or stress induced martensite formation.....	22
1.7	Factors affecting performance.....	31
1.7.1	Phases	32
1.7.2	Stability of retained austenite	34
1.7.3	Test parameters	38
1.8	Special properties.....	42
1.8.1	Formability	43
1.8.2	Deep drawability.....	43
1.8.3	Stretch formability	44
1.8.4	Stretch flangeability.....	44
1.8.5	Crash-worthiness	45
1.8.6	Fatigue resistance	47
1.9	δ -TRIP.....	48
1.10	Summary	50
1.11	Scope of the research	52
Chapter 2	Stabilization of δ-ferrite during Solidification.....	53
2.1	Introduction.....	53
2.2	Alloy design and manufacture	54
2.3	Metallography.....	57
2.4	Microanalysis.....	60

2.5	Kinetic Simulations.....	64
2.6	Conclusions.....	67
Chapter 3	Stabilisation of Ferrite in Hot-rolled Process	69
3.1	Introduction.....	69
3.2	Experimental.....	70
3.3	Reheating experiments.....	71
3.4	New alloys	74
3.5	Conclusions.....	77
Chapter 4	Extraordinary Ductility in Al-bearing δ-TRIP Steel	79
4.1	Introduction.....	79
4.2	Experimental.....	81
4.3	Microstructure.....	83
4.4	Deformation	85
4.5	Conclusions.....	89
Chapter 5	Mechanical Stabilisation of Retained Austenite	91
5.1	Introduction.....	91
5.2	Experimental.....	92
5.3	Mechanical behavior and microstructure.....	92
5.4	Mechanical stabilisation of austenite in TRIP-assisted steels.....	94
5.5	Conclusions.....	99
Chapter 6	Spot Weldability	100
6.1	Introduction.....	100
6.2	Method and Alloys	101
6.3	Results and discussion	103
6.4	Conclusions.....	109
Chapter 7	Dual-Phase Hot-Press Forming Alloy.....	110
7.1	Introduction.....	110

7.2	Experimental Method.....	111
7.3	Results and Discussion.....	113
7.4	Conclusions.....	117
Chapter 8	Conclusions	119
Appendix 1	Design of High Aluminium Containing δ-TRIP Steel by Calculation.....	122
A1.1	Introduction.....	122
A1.2	Experimental	122
A1.3	Microstructure evolution.....	123
A1.4	Microstructure and mechanical properties.....	127
A1.5	Conclusions.....	131
Appendix 2	Medium carbon fully pearlitic steel obtained by slow cooling	132
A2.1	Introduction.....	132
A2.2	Experiment	133
A2.3	Metallography and properties	133
A2.4	Transformation driving force	138
A2.5	Conclusions.....	140
References	141
Acknowledgments	158
CURRICULUM VITAE	160

Chapter 1 TRIP-assisted Steels and δ -TRIP Steel

1.1 Introduction

The worldwide demand for a reduction in greenhouse gas emissions, better fuel economy and safety in automobiles has required the development of a variety of alloy steels. Steel is a material with a unique, inherent capacity to absorb an impact, and thus to diffuse the consequence of a crash. It can be engineered to collapse like an accordion. Therefore, in addition to the strength, automotive safety requires the alloys to have considerable ductility. Formability is required due to the complex shapes of automotive parts.

When selecting a material for a particular application, engineers must be confident that it will be suitable for the loading conditions and environment it will experience in service. The mechanical properties of steel can be controlled through its chemical composition, processing and heat treatment, all of which lead to its final microstructure. The relevant properties of steels have been illustrated through a series of projects completed by the global steel industry: UltraLight Steel Auto Body (ULSAB), UltraLight Steel Auto Closures (ULSAC), UltraLight Steel Auto Suspensions (ULSAS) and ULSAB-AVC (Advanced Technologies). The most recent project, ULSAB-AVC, contains a list of typical mechanical properties used to design for light vehicle weight, and it is often referred to by industry (Table 1.1).

Table 1.1: Typical mechanical properties of steels for automotive applications [ULSAB-AVC, 2002]. YS and UTS mean yield strength and ultimate tensile strength respectively; TEL represents total elongation; n and \bar{r} are strain hardening exponent and normal *Lankford* coefficient, respectively.

Steel type	YS* / MPa	UTS* / MPa	TEL / %	n	\bar{r}	Application Code
Mild 140/270	140	270	38-44	0.05-0.15	1.8	A,C,F
BH 210/340	210	340	34-39	0.23	1.8	B
BH 260/370	260	370	29-34	0.18	1.6	B
IF 260/410	260	410	34-38	0.13	1.7	C
DP 280/600	280	600	30-34	0.2	1.0	B
IF 300/420	300	420	29-36	0.21	1.6	B
DP 300/500	300	500	30-34	0.2	1.0	B
HSLA 350/450	350	450	23-27	0.16	1.0	A,B,S
DP 350/600	350	600	24-30	0.22	1.1	A,B,C,W,S
DP 400/700	400	700	19-25	0.14	1.0	A,B
TRIP 450/800	450	800	26-32	0.14	0.9	A,B
HSLA 490/600	490	600	21-26	0.24	1.0	W
DP 500/800	500	800	14-20	0.13	1.0	A,B,C,W
SF 570/640	570	640	20-24	0.14	1.0	S
CP 700/800	700	800	10-15	0.08	1.0	B
DP 700/1000	700	1000	12-17	0.13	0.9	B
Mart 950/1200	950	1200	5-7	0.09	0.9	A,B
MnB	1200	1600	1-5	n/a	n/a	S
Mart1250/1520	1250	1520	1-6	0.07	0.9	A

Application Code: A=Ancillary Parts, B=Body Structure, C=Closures, F=Fuel Tank, S=Suspension Chassis, W=Wheels; Note: Flat sheet, as shipped properties; *Yield strength and ultimate tensile strength are minimum values, others are typical values

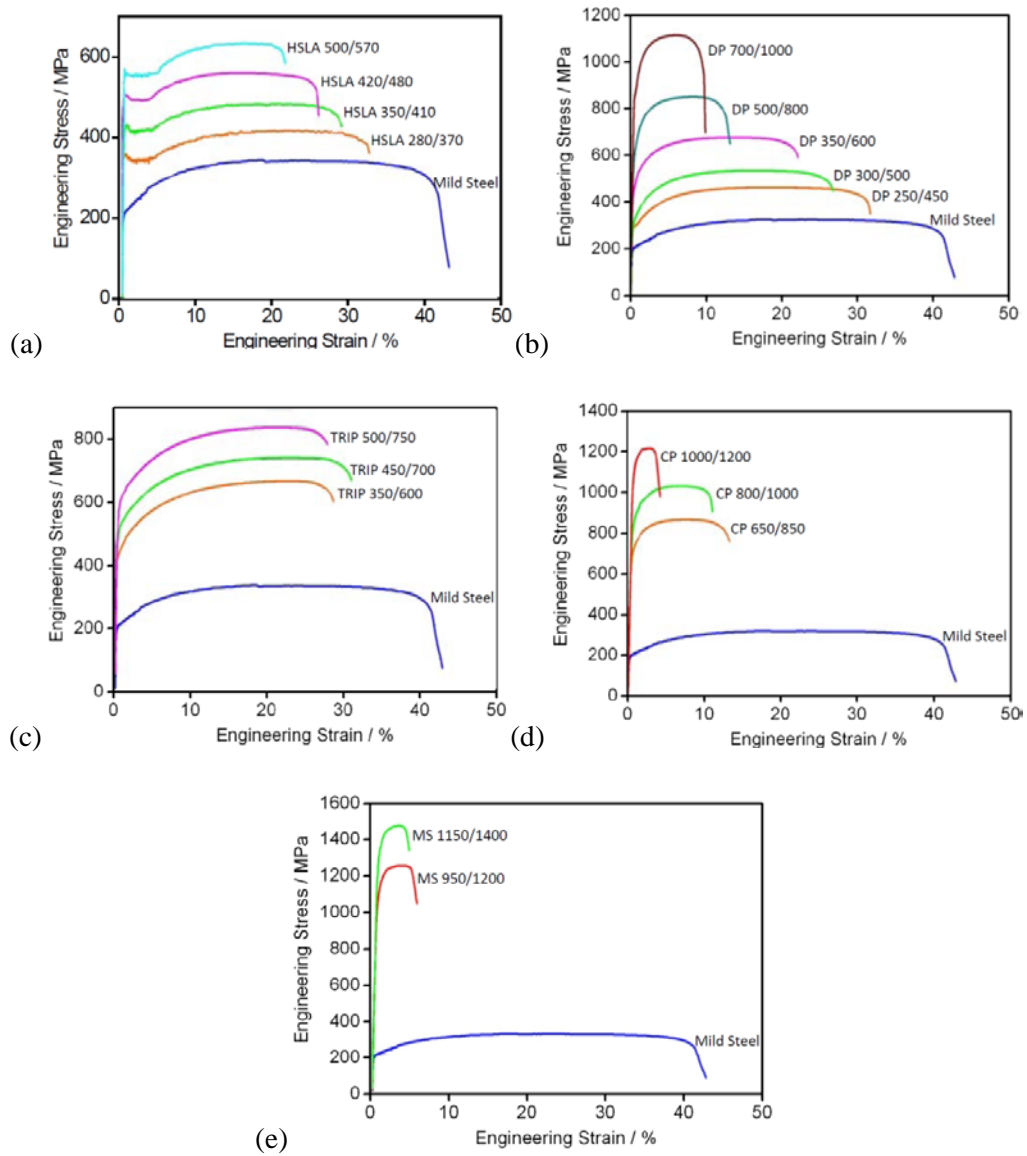


Figure 1.1: Engineering stress-strain curves for a series of steels. (a) cold-rolled high strength low alloy (HSLA) steels; (b) Dual phase (DP) steels; (c) Transformation-induced plasticity (TRIP) steels; (d) Complex phase (CP) steels; (e) Martensite (MS) steels. [Auto/Steel Partnership (A/SP), 2009].

The stress-strain curves are valuable for comparing different alloys (Figure 1.1). Any increase in strength is in general associated with a loss of ductility. The exceptions

are the transformation-induced plasticity (TRIP) steels, where considerable ductility is obtained in spite of the strength. These promising properties are thought to be due partially to the TRIP effect, where the plasticity is enhanced by martensitic transformation from retained austenite during deformation.

1.2 TRIP and TRIP-assisted steels

The first practical exploitation of TRIP came from Zackay and coworkers [1967] who developed steels with dramatically improved elongation, as a consequence of deformation-induced martensitic transformation. These alloys were fully austenitic at ambient temperature, achieved by large concentrations of expensive solutes which resulted in a high cost (Table 1.2).

In the 1980's, the TRIP effect was demonstrated in low-alloy steels made with 0.2 C, 1-2 Mn and 1-2 Si (wt%) [Matsumura *et al.*, 1987a, b; Takechi *et al.*, 1987]. The microstructures consisted of 50-60 vol.% allotriomorphic ferrite, 20-30 vol.% carbide-free bainite, the remainder being high-carbon retained austenite with or without martensite as shown in Figure 1.2. Such steels typically contained only 10-30 vol.% austenite [Hanzaki 1994; Matsumura *et al.*, 1992; Sakuma *et al.*, 1991a; Sugimoto *et al.*, 1993, 1992a]. They are henceforth referred to as "TRIP-assisted" to distinguish them from fully austenitic TRIP steels. The TRIP-assisted alloys are lean and hence affordable in large scale applications (Table 1.3).

Table 1.2: Typical chemical compositions (wt%) of early TRIP steels.

C	Si	Mn	Cr	Ni	Mo
0.31	1.92	2.02	8.89	8.31	3.8
0.25	1.96	2.08	8.88	7.60	4.04
0.25	1.90	0.92	8.80	7.80	4.00
0.25	-	-	-	24.4	4.10
0.23	-	1.48	-	22.0	4.00
0.24	-	1.48	-	20.97	3.57

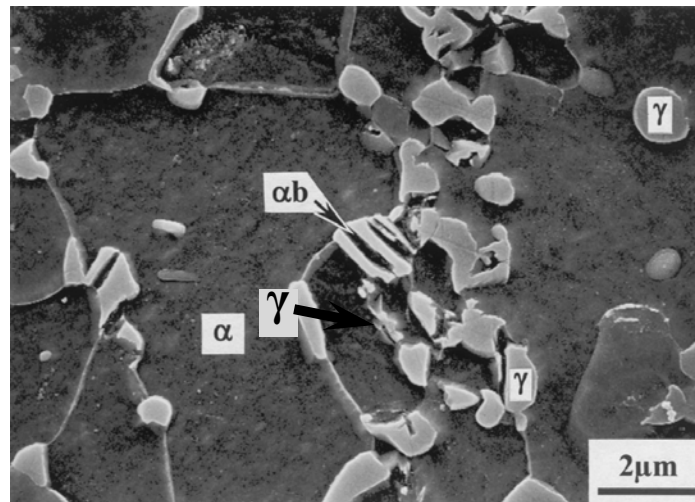


Figure 1.2: A typical multiphase microstructure of a modern TRIP-assisted steel. Austenite appears in white, ferrite in black. (α : ferrite, γ : retained austenite, α_b : bainitic ferrite) [Girault *et al.*, 2001].

Table 1.3: Typical chemical compositions (wt%) of TRIP-assisted steels [Hanzaki *et al.*, 1995; Hashimoto *et al.*, 2004; Jacques *et al.*, 2001a, b; Jiao *et al.*, 2002; Kim *et al.*, 2002, 2003; Matsumura *et al.*, 1987b; Sugimoto *et al.*, 1992a; Sugimoto *et al.*, 2006; Sugimoto 2007].

C	Si	Mn	Al	P	Nb	Mo	Cu	Cr	Ni
0.38	1.53	0.83		0.007					
0.18	2.0	1.5	0.037	0.015					
0.19	2.48	1.49	0.036	0.014					
0.11	0.59	1.55	1.5	0.012					
0.14	0.53	1.57		0.204					
0.22	1.55	1.55	0.028		0.035				
0.20	1.48	1.44	0.04	0.004	0.109				
0.20	1.47	1.51	0.028	0.004	0.047	0.2			
0.20	1.6	1.6	0.028		0.041	0.3			
0.21	1.49	1.49	0.028	0.005	0.017	0.1			
0.14	1.49	1.51	0.04	0.0012			0.51		
0.15	1.52	1.51					0.51	0.39	
0.15	1.55	1.50					0.51		0.41

1.3 Alloying elements in TRIP-assisted steels

Carbon plays a key role in the composition of TRIP-assisted steel. It strengthens austenite by interstitial solid solution hardening and enhances its stability. The carbon does diffuse and can enrich in austenite during bainitic transformation. TRIP steels use higher quantities of carbon than dual phase alloys to obtain sufficient carbon content for stabilizing the retained austenite to below ambient temperature. The stress or strain level at which retained austenite begins to transform to martensite can be controlled by adjusting the carbon content. At lower carbon levels, the retained austenite begins to

transform almost immediately upon deformation, increasing the work hardening rate and formability during the stamping process. At higher carbon contents, the retained austenite is more stable and begins to transform only at strain levels beyond those produced during forming. At these carbon levels the retained austenite persists into the final part. It transforms into martensite during subsequent deformation, such as during forming or in a crash event.

Solute other than carbon are added for the following reasons:

- to optimize the fraction of retained austenite,
- to control cementite precipitation,
- to increase the hardness of ferrite,
- to increase the hardenability so that pearlite formation can be avoided before bainite reaction.

The austenite can be stabilized by the enriched carbon only if the latter is not consumed by the formation of cementite. Silicon is actually well known to inhibit the formation of cementite during bainitic transformation. A high driving force is needed to force silicon into cementite due to its extremely low solubility in cementite, since silicon cannot diffuse away from cementite owing to the para equilibrium formation of cementite during bainitic transformation [Bhadeshia *et al.*, 2003]. The role of silicon in inhibiting cementite formation is therefore limited to its influence on the nucleation of cementite, the driving force for transformation. A buildup of silicon around a cementite nucleus could considerably increase the carbon activity locally and prevent carbon diffusion to the nucleus [Bhadeshia 2001]. In a Fe-0.2C-1.96Si-1.51Mn wt% alloy, cementite actually formed after isothermally holding for 60 min at 400 °C or for 20 min

at 450 °C [Jun *et al.*, 2004]. Addition of 0.6 wt% of silicon in a Fe-0.15C-1.5Mn wt% steel is not sufficient to retard the cementite precipitation during isothermal bainitic transformation [Pichler *et al.*, 1998]. The minimum level of silicon needed to effectively suppress cementite formation is probably ~0.8 wt. % [Girault *et al.*, 2001]. The typical silicon contents is ~1.5 wt% for modern TRIP-assisted steels and is sufficient to inhibit the formation of cementite [Jacques *et al.*, 1999]. Addition of 1.48 wt% silicon in Fe-0.1C-1.5Mn-0.5Cu wt% TRIP-assisted steels led to higher retained austenite fraction and improved mechanical properties than 0.94 wt% silicon addition [Lee *et al.*, 2002]. Increase of silicon content is beneficial for enhancing the combination of strength and ductility, and effectively retards the pearlite formation, but prolongs the bainitic transformation time required for the optimum mechanical properties [Sakuma *et al.*, 1991b].

The trend in research away from the conventional CMnSi composition is because galvanizing becomes difficult [Mintz 2001]. Silicon levels > 0.5wt% can cause problems during the galvanizing operation [Mahieu *et al.*, 2002; Mintz 2001; Pichler *et al.*, 2003, 2002]. The intercritical annealing is carried out in a furnace maintained with low oxygen partial pressure before hot-dip galvanizing. Under this condition, iron does not get oxidized but silicon can still be oxidized preferentially to form SiO₂ and mixed oxide Mn₂SiO₄ in manganese containing TRIP-assisted steels [Mahieu *et al.*, 2002]. This gives rise to a sheet surface with poor wettability in molten zinc. A decrease in silicon content diminishes the bare spot defects and hence improves the reactive wetting of TRIP steels [Bellhouse *et al.*, 2007]. Silicon also affects the nature of the surface scale formed in the hot rolled material. During hot rolling, the steel is exposed to air at high temperature. This leads to surface oxidation. Normally the oxide layer consists mainly of FeO attached to steel and minor Fe₃O₄ and Fe₂O₃ on the surface. They can be

easily descaled. But in silicon TRIP-assisted steels, the surface scale changes to the eutectic compound of FeO/Fe₂SiO₄ with relatively low solidus temperature of 1173 °C, which is generated in the furnace before hot rolling. This compound is located between steel and FeO and penetrates irregularly into both sides and also enters into the upper FeO grain boundaries [Fukagawha *et al.*, 1994]. This complex scale structure, therefore, is difficult to be descaled due to the anchor effect, by which the scale is firmly connected with steel [Okita *et al.*, 1989]. The remaining FeO scale is fractured easily by subsequent rolling and changed into Fe₃O₄ and finally into red Fe₂O₃. The red scale defect, therefore, is not directly due to the eutectic FeO/Fe₂SiO₄ compound [Fukagawa *et al.*, 1994].

Both aluminium and phosphorus retard cementite precipitation during bainitic transformation and hence can substitute for silicon because aluminium, like silicon, is not soluble in cementite and phosphorus reduces the kinetics of cementite precipitation [De Meyer *et al.*, 1999a, b, c; Mintz 2003]. Aluminium is less potent in retarding the formation of cementite than silicon at the same weight concentration [Girault *et al.*, 2001; Jacques *et al.*, 2001a, b]. The aluminium bearing steels actually exhibit a remarkable TRIP effect during tensile testing because of the large amount of austenite that can be retained. The aluminium, however, does not solid solution strengthen ferrite as strong as silicon [Jacques *et al.*, 2001b]. Consequently, full substitution of silicon by an equivalent amount of aluminium results in a deterioration of the strength/ductility balance [Jacques *et al.*, 2001b]. In the low silicon steels, replaced by aluminium, higher carbon is required to compensate the shortage of lower strength. High aluminium contents are required to inhibit pearlite formation during cooling from intercritical annealing in the silicon-free alloys [Mahieu *et al.*, 2002]. High aluminum concentration at low carbon level of conventional TRIP-assisted steels may result in problems due to

the formation of AlN during continuous casting. The addition of titanium can remove nitrogen and might prove beneficial here. Phosphorus, on the other hand, strengthens ferrite [Pichler *et al.*, 1998]. Addition of 0.1 wt% phosphorus leads to an increase of about 75 MPa in the strength of ferrite [Pickering 1978]. Aluminium and phosphorus, unlike silicon, don't cause problems during galvanizing steels with Al contents up to ~1.5wt% and P up to 0.1 wt%, although the phosphorus does slow down Zn-Fe reactions during galvannealing [Mintz 2001].

The typical Mn content in low alloy TRIP steel is ~1.5 wt% Mn, which is required to achieve hardenability. This content of manganese does not have any adverse effects on reactive wetting during coating [Bellhouse *et al.*, 2007]. Manganese, being an austenite stabilizer, lowers the temperature at which the cementite starts to precipitate. Mn also lowers the activity coefficient of C in ferrite and austenite and increases the C solubility in ferrite [DeCooman 2004]. Manganese is soluble in cementite. High manganese contents (~2.5 wt.%) are not favored as they lead to banding in the microstructure and excessively stabilized retained austenite [Kim *et al.*, 2001]. An increase in manganese may compensate for any reduction in silicon [Sakuma *et al.*, 1991a], but this shifts the T_0 curve to lower carbon concentrations, thereby limiting the amount of bainite that can form. Higher manganese concentration requires longer holding time for bainitic transformation to achieve maximum strength ductility balance [Sakuma *et al.*, 1991a, b]. Additionally, pronounced banding may occur in steels containing a large manganese concentration [Kim *et al.*, 2001].

Niobium in solid solution lowers the martensite-start temperature and retards carbide precipitation during bainitic transformation, thereby enhancing the quantity of retained austenite [Hanzaki *et al.*, 1995; Pereloma *et al.*, 1999; Sugimoto *et al.*, 2006].

The reason is not clear, as niobium is known to be a ferrite stabilizer. Fine precipitates of niobium carbides, nitrides or carbonitrides can strengthen the ferrite and refine the grain size [Hashimoto *et al.*, 2004]. The addition of 0.05 wt% of niobium increases yield strength by 50 MPa but has no effect on the tensile strength [Sugimoto *et al.*, 2006]. 0.08 - 0.11 wt% addition of niobium significantly improves the stretch-flangeability [Sugimoto *et al.*, 2006]. It does suppress the undesired pearlite formation during the production of TRIP-assisted steels [Sugimoto 2007].

Molybdenum is a solid solution strengthener of ferrite and strongly retards pearlite formation by decreasing both the nucleation rate and growth rate. It is the most effective elements to suppress pearlite formation and therefore is particularly good at decreasing the critical cooling rate for bainite formation [Coldren and Eldis, 1980]. In low-silicon steels, its addition (Fe-0.23C-1.1Si-1.6Mn-0.33Mo-0.036Nb wt%) can lead to mechanical properties comparable to high-silicon steels viz. ultimate tensile strength of 1270 MPa with a total elongation of about 36% [Bouet *et al.*, 1998]. Molybdenum in steels does not form oxide and therefore is beneficial for galvanising.

Copper, being an austenite stabiliser, helps to retain austenite [Im *et al.*, 2000a, b; Kim and Lee, 1999; Kim *et al.*, 2002]. Besides solid solution strengthening, fine ϵ -copper precipitates in ferrite can boost the overall strength [Kim *et al.*, 2002]. Thus copper can be thought to replace silicon in both the roles of retaining austenite and increasing the strength of ferrite.

The addition of nickel, like copper as austenite stabiliser, increases retained austenite fraction slightly and enhances both yield and tensile strength. Chromium, being a ferrite stabiliser, unlike copper and nickel, decreases the amount of retained austenite remarkably and increases strength with loss of ductility [Kim *et al.*, 2002,

2003].

Small concentrations of boron are known to significantly improve hardenability. Boron-containing low-silicon steels have been found to contain sufficient retained austenite and display a sensitive TRIP effect [Sadhukhan *et al.*, 2001].

All these alloying elements can increase the hardenability and be beneficial to produce desired bainite and hence retain austenite. The critical cooling rate (CR) to produce 5% martensite in dual phase steels can be expressed as following [Tobiyama *et al.*, 1999]:

$$\log (\text{CR} / \text{K s}^{-1}) = 3.95 - 1.73\text{Mn}_{\text{eq}} \quad (1.1)$$

$$\text{where, } \text{Mn}_{\text{eq}} = \text{Mn} + 0.26\text{Si} + 3.5\text{P} + 1.3\text{Cr} + 2.67\text{Mo} \text{ (wt\%)} \quad (1.2)$$

The molybdenum and phosphorus are more efficient in increasing hardenability than manganese. For TRIP-assisted steels, the cooling rate was modified as follows [Mintz 2003]:

$$\log (\text{CR}) = 4.4 - 1.73\text{Mn}_{\text{eq}} \quad (1.3)$$

Eq. 1.1-1.3 were derived based on data [Tobiyama *et al.*, 1999; Mintz 2001; Sakuma *et al.*, 1991a] in the following range: solutes C: 0.1-0.2, Si: 0.3-1.5, Mn: 1.5-2.2, P: ~0.7, Cr: ~0.5, Mo: 0.1-0.2, in wt%, and the cooling rate: 0.15-20 K s⁻¹ for Eq. 1.1 and 3.5-180 K s⁻¹ for Eq. 1.3.

1.4 Microstructural evolution

During bainitic transformation, silicon, or aluminium, phosphorus, retards cementite precipitation from untransformed austenite during bainite formation. The carbon partitioning into the untransformed austenite, enhances the stability of austenite and

allows it to be retained at ambient temperature.

Commercially supplied rolled TRIP-assisted steels are popular for the automotive industry. TRIP-assisted steel can be generated in both hot rolling and cold rolling processes. In hot rolling, the steels are heated above their recrystallization temperature and then deformed between rollers to form thinner cross sections. This process does reduce the average grain size of steels. The cooling rate is adjustable so that austenite can be controlled to transform to allotriomorphic ferrite firstly and then to bainite. However, a two-stage annealing treatment is required to produce the desired microstructure in cold rolled TRIP-assisted steels (Figure 1.3). The material is initially heated to a temperature in the $(\alpha+\gamma)$ phase region generating a mixture of ferrite and austenite (Intercritical annealing), which subsequently decomposes to bainite at a lower temperature (Isothermal transformation).

The retention of austenite in TRIP-assisted steels can be understood in the theory of the “incomplete reaction phenomenon” associated with bainitic transformation [Bhadeshia 2001]. Bainitic ferrite nucleates in para equilibrium condition and grows without diffusion of carbon but excess carbon subsequently partitions into the residual austenite (Figure 1.4). Diffusionless growth can only be sustained at temperatures below T_0 , at which ferrite and austenite of identical chemical composition have the same free energy. Some elements like silicon, aluminium and phosphorus retard cementite precipitation allowing the carbon to remain dissolved in austenite. It follows that in the absence of precipitation the bainite reaction stops when the carbon content in austenite equals the T'_0 limit (considering the stored energy of bainite), as illustrated in Figure 1.5. This was experimentally confirmed by isothermal bainitic transformation in a ~1.5 wt% silicon containing steel [Jacques *et al.*, 1999]. A certain amount of austenite can

remain untransformed during the isothermal process.

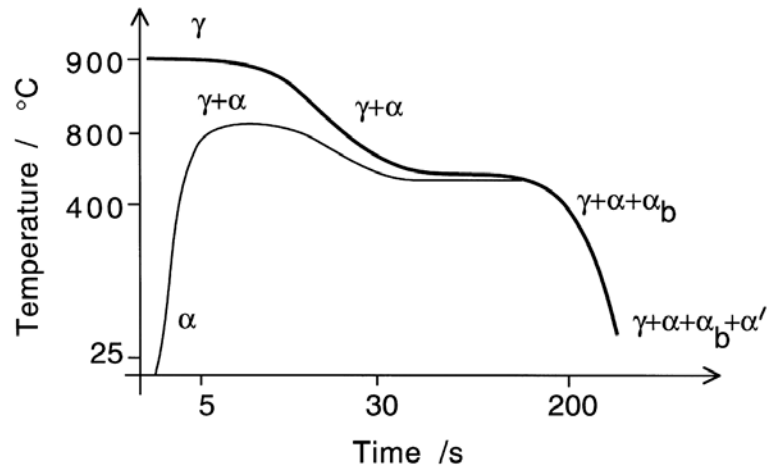


Figure 1.3: Schematic illustration of the two routes to generate the microstructure of TRIP-assisted steel, with typical temperature and time indicated. The upper curve and lower curve stand for the microstructure evolution in hot rolling process and intercritical annealing after cold rolling respectively. The terms γ , α , α_b and α' represent austenite, allotriomorphic ferrite, bainitic ferrite and martensite respectively [Bhadeshia 2001].

If the M_s temperature of the residual austenite can be depressed to below ambient temperature, it becomes stable against any further martensitic transformation during subsequent cooling [Andrews 1965], and hence is retained to ambient temperature. The pronounced effect of carbon in stabilizing austenite is therefore exploited in retaining austenite by isothermal bainitic transformation, thus permitting the concentration of other solutes to be kept to a minimum.

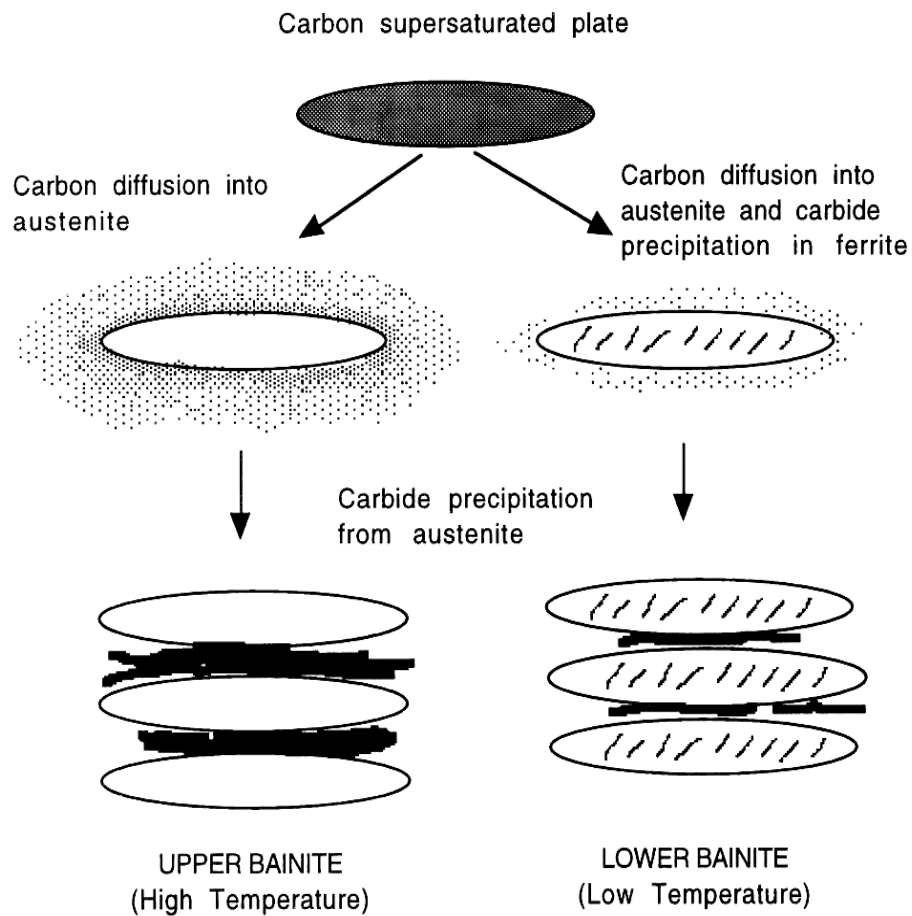


Figure 1.4: Schematic illustration of bainite reaction mechanism [Bhadeshia 2001].

Most alloying elements which enter into solid solution in austenite lower the M_s temperature, with the exception of cobalt and aluminium. However, the interstitial solutes carbon and nitrogen have a much larger effect than the metallic solute. The relative effect of alloying elements on the M_s temperature can be indicated by the following empirical relationship (concentrations in wt%) [Andrews 1965]:

$$M_s (^{\circ}\text{C}) = 539 - 423(\%C) - 30.4(\%Mn) - 17.7(\%Ni) - 12.1(\%Cr) - 7.5(\%Mo) + 10(\%Co) - 7.5(\%Si) \quad (1.4)$$

Later on, the other empirical equation to estimate the M_s temperature was proposed for the aluminum bearing TRIP-assisted steel as the follows [Mintz 2002]:

$$M_s \text{ (}^\circ\text{C)} = 539 - 423(\%C) - 30.4(\%Mn) - 17.1(\%Ni) - 12.1(\%Cr) - 7.5(\%Mo) - 7.5(\%Si) + 30(\%Al) \quad (1.5)$$

The M_s temperature can be conveniently estimated as well by software MUCG83, a powerful program for the modeling of transformations in steels [MAP].

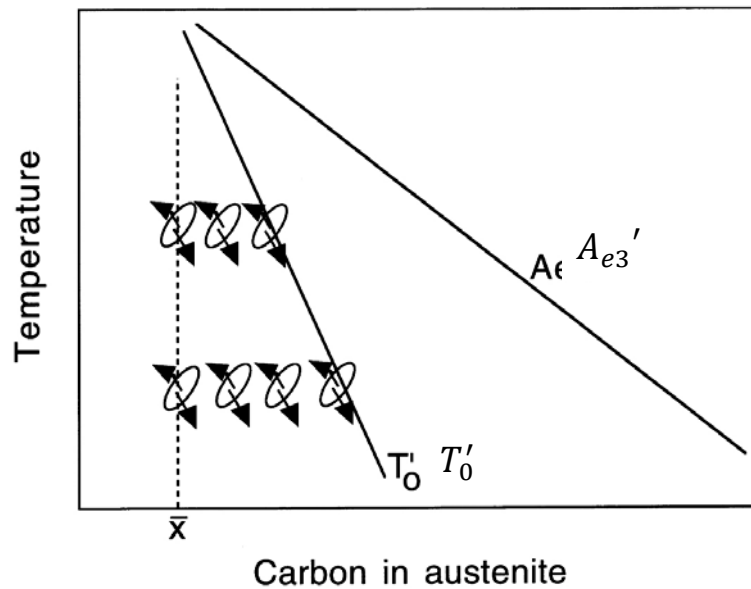


Figure 1.5: The incomplete reaction phenomenon: bainite reaction stops as carbon in austenite approaches T'_0 limit, \bar{x} is the bulk carbon content of the steel and A_{e3}' represents the para equilibrium $(\alpha+\gamma)$ - γ phase boundary [Bhadeshia 2001].

Microstructural evolution during the isothermal formation of bainite is identical for both hot and cold rolled TRIP-assisted steels. A typical transformation map is shown in Figure 1.6 [Jacques *et al.*, 2001c]. As the bainite reaction progresses, the residual austenite becomes enriched with carbon and gains stability against martensitic

transformation during cooling. When the enrichment is inadequate at low holding times, the austenite may decompose partly into martensite during further cooling. On the other hand, amount of untransformed austenite decreases, as more bainite forms with greater holding time. It follows that the quantity of retained austenite becomes maximum at an intermediate holding time during bainite reaction. The carbon content of retained austenite always increases with the holding time until it reach the T_0' in the case of suppressed cementite formation.

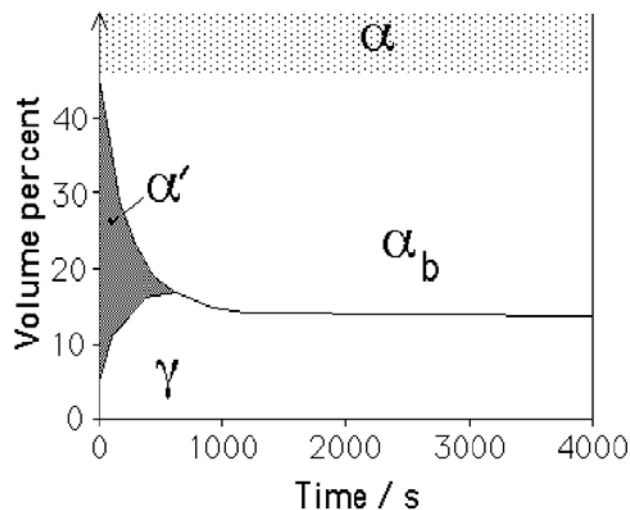


Figure 1.6: Typical microstructural evolution map during the bainite reaction. Retained austenite peaks at an intermediate holding time [Jacques *et al.*, 2001c].

In steels containing sufficient silicon or aluminium, bainite forms as an aggregate of ferrite plates separated by untransformed austenite. The individual plates are called sub-units while the aggregates of plates are known as sheaf (Figure 1.7). For the quite large grain size, sheaf of bainite therefore evolves by repeated nucleation of new sub-units predominantly at the tip of the pre-existing ones, rather on their sides. This process stops when the sheaf reaches the grain boundary [Jacques *et al.*, 2003].

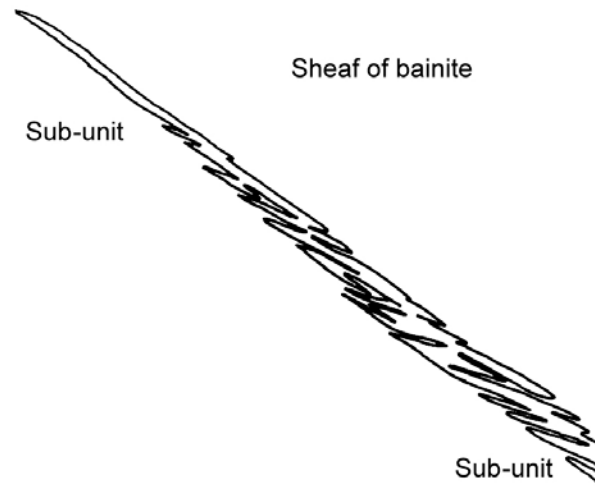


Figure 1.7: Schematic illustration of sub-units and sheaf of bainite [Bhadeshia 2001].

But such a mechanism may not occur in the intercritical austenite of TRIP-assisted steels because the size of the available austenite is only a few micrometers [Jacques 2003]. Bainite in these steels consists of adjacent platelets that span the whole of the austenite grain (Figure 1.8). The reduction of the austenite grains to the length of one platelet of bainitic ferrite changes the growth process from autocatalytic nucleation to grain boundary nucleation. The morphology also changes from a sheaf structure to adjacent platelets. These differences influence in a large way the transformation rate.

Epitaxial ferrite is also more likely to be present in the microstructures of cold rolled steels than the hot rolled products. After intercritical annealing some ferrite may form during cooling to the bainite transformation temperature. This occurs by the movement of an existing austenite-ferrite boundary i.e., epitaxial growth [Zaefferer *et al.*, 2004].

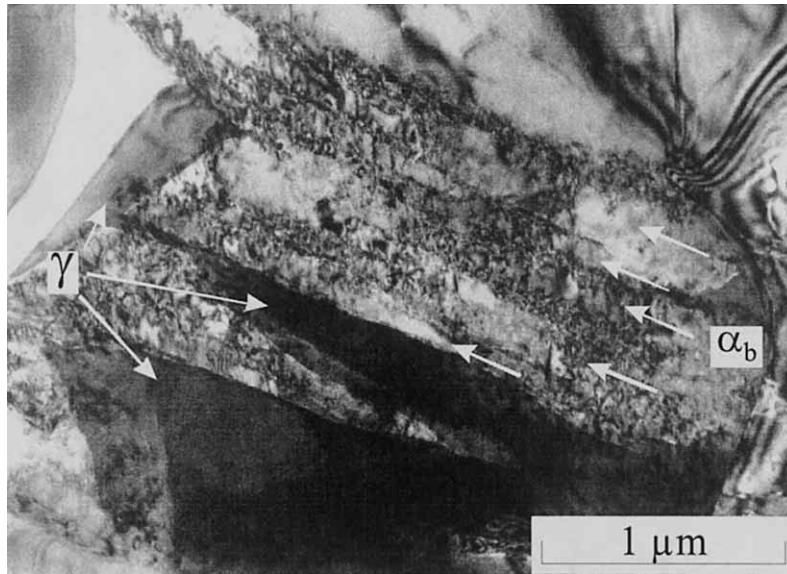


Figure 1.8: Bainite consisting of adjacent ferrite platelets in TRIP-assisted steels [Jacques *et al.*, 2001d].

1.5 Mechanical performance

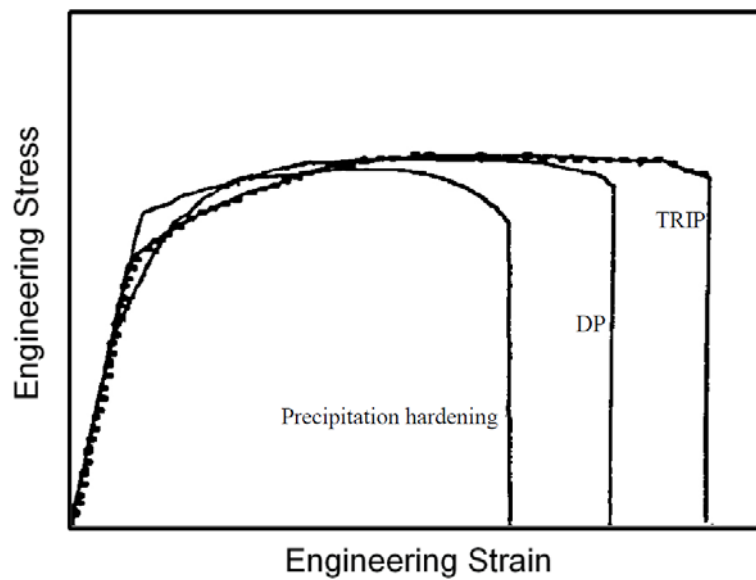


Figure 1.9: Stress-strain curves for precipitation hardening, dual phase and TRIP-assisted steels [Ojima *et al.*, 1998].

TRIP-assisted steels are reputed for the uniform elongation compared with other similarly strong steels like dual phase steels. The latter with microstructures of 10-15 vol.% low carbon ($C < 0.3$ wt%) martensite dispersed in ferrite have high strength. TRIP-assisted steel can be imagined to be a modification of the dual phase steel [Hassani and Yue, 1999].

In this TRIP-assisted steel as shown in Figure 1.2, the dispersion of hard second phases in soft ferrite creates a high work hardening rate during deformation, as observed in the dual phase steels. The work hardening rate persists at higher strains in TRIP-assisted steel where work hardening of the dual phase begins to diminish, shown in Figure 1.9. TRIP effects play important roles in TRIP-assisted steels since the retained austenite progressively transforms to martensite with increasing strain in the temperature range $M_s - M_d$.

TRIP-assisted steels yield greater elongation due to the substantial amount of retained austenite, as compared with dual phase steels. However, TRIP-assisted steels not containing martensite seem not to exhibit continuous yielding unlike dual phase steels [Sakaki *et al.*, 1983; Jacques *et al.*, 2001a]. Continuous yielding is advantageous in forming operations as this helps to avoid stretcher strain or Lüder bands. The gradual yielding of dual phase steels is mainly due to the free dislocations present in the ferrite grains generated by the formation of surrounding martensite. Formation of bainite, instead of martensite, in TRIP-assisted steels is not very effective to induce free dislocations in ferrite, resulting discontinuous yielding [Sakuma *et al.*, 1992a, b]. It's possible to avoid this by introducing martensite in TRIP-assisted steels [Choi *et al.*, 1988]. The discontinuous yielding of the intercritically annealed cold rolled TRIP-assisted steels could also be due to the strain ageing of ferrite at the temperature

where bainite forms [Choi *et al.*, 1988]. The ageing of ferrite can occur due to the difference in the solubility of the interstitial solutes at the intercritical annealing temperature and the bainite formation temperature.

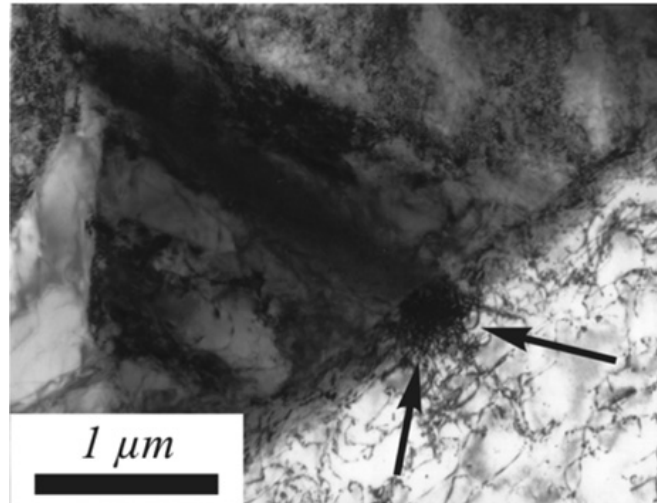


Figure 1.10: Dislocations generated in ferrite due to transformation of austenite during deformation [Jacques *et al.*, 2007].

The extra uniform elongation in TRIP-assisted steels, compared with in dual phase steels, is attributed mainly to the deformation-induced martensitic transformation of retained austenite. However, the transformation strains themselves can contribute at most 2% to the observed elongation by the small fraction of austenite present in these materials [Bhadeshia 2002]. The induced transformation generates some stresses and free dislocations in the adjacent grains of ferrite matrix due to the volume expansion and therefore enhances the dislocation density in the ferrite (Figure 1.10). The strain hardening rate arises because the freshly produced dislocations in the ferrite phase can then take part in the deformation process. The enhanced strain hardening does postpone the onset of necking to large strain hence achieve the large uniform elongation [Yu *et al.*,

2006]. Other phases in the microstructure must also influence the overall mechanical behaviour [Jacques *et al.*, 200c, d].

Martensite that forms in these steels inherits the high carbon content of the austenite. It is surprising that the freshly produced high-carbon martensite does not impair the ductility even carbon embrittles martensite. The tendency of the martensite to crack in a mixed microstructure of austenite and martensite depends on its absolute size. In these mixtures, hard martensite does not readily crack when it is sufficiently small in TRIP-assisted steels because it is difficult to transfer load onto the martensite when the composite mixture is strained. When the austenite grain size is coarse it's however prone to form long plates of martensite, which are easy to crack [Chatterjee and Bhadeshia, 2006].

1.6 Strain or stress induced martensite formation

Transformation-induced plasticity is a consequence of the formation of martensite from austenite. In steels, austenite can transform to ferrite either by breaking all the bonds and rearranging the atoms into an alternative pattern relying on the diffusion of atoms (reconstructive transformation), or by the homogeneous deformation of the original pattern into a new crystal structure (displacive or shear transformation) without diffusion. Martensitic transformation follows the latter mechanism and is diffusionless. It can occur at low temperatures where diffusion, even of interstitial atoms, is not conceivable over the time period of the experiment. It can grow at speeds which approach that of sound in the metal and such large speeds are inconsistent with diffusional transformation. The diffusionless character can be proven by chemical analysis.

The transformation starts only after cooling to a particular temperature called

martensite-start temperature or M_s . The fraction transformed increases with the undercooling below M_s . In the vast majority of cases, the extent of reaction is found to be virtually independent of time:

$$1 - V_{\alpha'} = \exp\{\phi(M_s - T)\} \quad \text{where } \phi \text{ is a constant and } \phi \cong -0.011 \quad (1.6)$$

where $V_{\alpha'}$ is the fraction of martensite and T is a temperature below M_s . This is the Koistinen and Marburger equation [1959]; notice that time does not feature in this relation, so that the fraction of martensite depends only on the undercooling below M_s . This athermal character is a consequence of rapid nucleation and growth, so rapid that the time taken can in normal circumstances be neglected. A *martensite-finish* temperature or M_f is usually defined as the temperature where 95% of the austenite has decomposed. Unlike M_s , M_f has no fundamental significance.

The face-centered cubic (FCC) austenite lattice cannot be transformed into a body-centered cubic (BCC) martensite lattice with the fully coherent interface by an Invariant-Plane Strain (IPS) [Bolling *et al.*, 1965]. The Bain strain, however, can ensure the lattice deformation **BR** to be an Invariant-Line Strain (ILS), which leaves one line unrotated and undistorted. This forms an interfacial dislocation line vector which joins the parent and product crystals without any rotation and distortion. These dislocations can glide as the interface moves, without any need for climb. It ensures that the semi-coherent interface connecting the martensite and the parent phase is glissile even at low temperatures.

The overall free energy change, ΔG , when nucleation takes place, is a result of the following three components:

-the change in chemical free energy: $\Delta G_{\text{Chem}} = G_{\text{Chem}}^{\alpha'} - G_{\text{Chem}}^{\gamma} \quad (1.7)$

-the strain energy stored due the shape deformation associated with martensitic transformation, shown in Table 1.4, the resulting strain energy has to be accounted for before the transformation can happen;

-the interfacial energy between matrix and martensite.

Table 1.4: Typical energies associated with martensitic transformation [Bhadeshia 2008b].

	J mol ⁻¹
Strain energy	600
Twin interface energy	100
γ/α interface energy	1
Stored energy due to dislocations	20

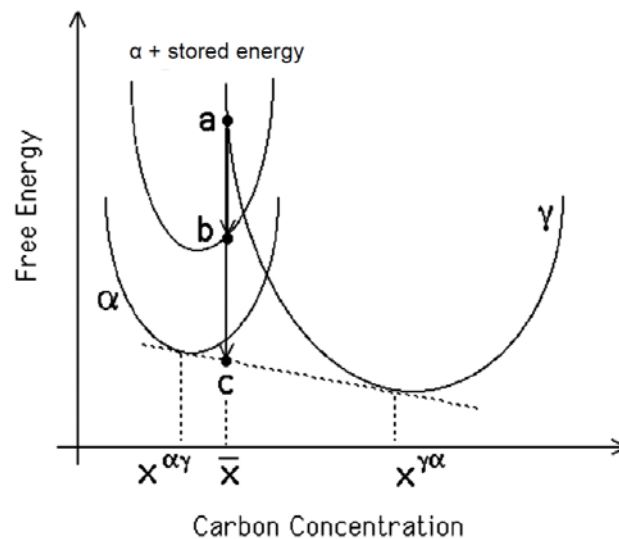


Figure 1.11: The distance **ac** represents the free energy decrease when austenite of composition \bar{x} decomposes into an equilibrium mixture of ferrite and austenite of compositions $x^{\alpha\gamma}$ and $x^{\gamma\alpha}$ respectively. The distance **ab** is the smaller decrease in free energy when martensite forms without any composition change, taking into account the stored energy associated with the transformation [Bhadeshia 2008b].

For a semicoherent nucleus of martensite with an oblate spheroid shape, radius r , semi-thickness c [Bhadeshia and Honeycombe, 2006]:

$$\Delta G = \frac{4}{3} \pi r^2 c \Delta G_{\text{Chem}} + \frac{4}{3} \pi r c^2 A + 2 \pi r^2 \sigma \quad (1.8)$$

where, ΔG_{Chem} = chemical free energy change per unit volume

A = strain energy factor

σ = free energy per unit area of γ/α' interface.

In an equilibrium transformation the chemical elements partition into the parent and product phase until they reach the same chemical potential in each phase, in a manner which leads to a minimization of free energy as shown in Figure 1.11. Martensite, however, grows without diffusion, so it inherits the composition of the austenite. The free energy change for martensite transformation can be represented as the **ac** on Figure 1.11.

The mechanical driving force due stress, can make the transformation possible above M_s temperature by supplying the shortfall of the necessary thermodynamic driving force. Martensitic transformation-induced by the deformation of austenite was first discovered in 1932 [Scheil *et al.*] and the thermodynamics of which was explained later [Patel *et al.*, 1953]. This is illustrated schematically in Figure 1.12. The free energy change, ΔG_1 , available at the M_s temperature is the critical driving force necessary for transformation. At a temperature T_1 above M_s , the magnitude of the free energy change for transformation, ΔG_2 , is less than the critical driving force, ΔG_1 . Martensite can form at this temperature only if the additional energy of a magnitude U , so that $U + \Delta G_2 = \Delta G_1$. This can be done by applying stress. The transformation becomes possible at the temperature higher than M_s through the work done by external stress, as a mechanical

driving force, adding to the available chemical free energy change. The higher the temperature above M_s , the greater is the magnitude of the stress required. However, the strength of the austenite diminishes at high temperatures. When the stress required for transformation exceeds that of austenite, plastic strain precedes transformation. This makes it difficult to provide further mechanical driving force so a temperature limit termed M_d is reached, above which austenite does not transform.

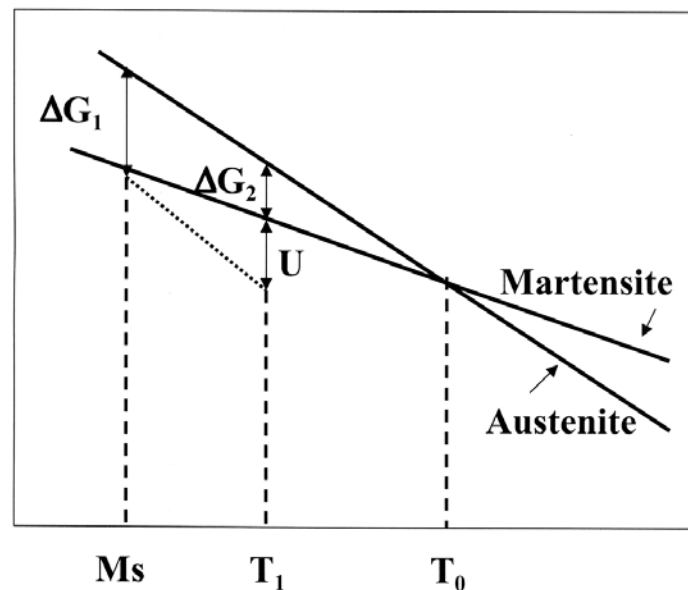


Figure 1.12: A shortfall in driving force for martensitic transformation above the M_s temperature can be compensated for by the application of stress [Chatterjee 2006].

TRIP-assisted steels contain a small quantity of carbon enriched retained austenite, which partially transforms into martensite during the course of plastic deformation. Most investigations into TRIP-assisted steels are based on tensile tests involving large plastic strains. It seems reasonable to assume that strain induced martensite is stimulated by introducing martensite nucleation sites. Each nucleus then transforms into a plate of martensite of a specified volume \bar{V} . Autocatalysis is also possible, in which the

formation of one plate stimulates others, but this is normally taken into account using a constant autocatalysis factor.

There are several empirical models based on strain for full austenite TRIP steels. One of these was proposed by Olson and Cohen [1975] to model the experimental data reported by Angel [1954],

$$f^{\alpha'} = 1 - \exp[-\beta\{1 - \alpha\epsilon\}^n] \quad (1.9)$$

where $f^{\alpha'}$ is the volume fraction of martensite obtained at a strain ϵ . The model contains two temperature dependant parameters, α and β . The former depends on the stacking fault energy of the steel, which in turn is affected by temperature. β defines the probability that a shear-band intersection creates a nucleation site, and therefore can be thought to depend on the chemical driving force, hence temperature. However, the exponent n in the model comes from fitting to experimental data. A value of 4.5 is appropriate for the steels studied by Angel.

Guimaraes [1972] studied a group of Fe-Ni-C alloys and proposed a similar exponential fit:

$$f^{\alpha'} = 1 - \exp(-k\epsilon^Z) \quad (1.10)$$

with empirical constants $k = 28$ and $Z = 3.7$.

A different parabolic type of dependence was proposed by Gerberich *et al.*, [1970]:

$$f^{\alpha'} = A_2\epsilon^{1/2} \quad (1.11)$$

where A_2 is an empirical constant.

Angel [1954], Ludwigson and Berger [1969] proposed the following model for metal stable austenite stainless steels:

$$f^{\alpha'} = A_1 \epsilon^B V_\gamma \quad (1.12)$$

Where A_1 and B are constants, with $B = 3$ fitted from stainless steels.

As can be seen, all of these models are formulated on the basis of the experimental data for fully austenitic TRIP steels and don't include original volume fraction of austenite and therefore exclude any possible interaction between the parent and the transformed phases. The first model for TRIP-assisted steels was expressed by Sugimoto *et al.*, [1992b] as:

$$\ln(V_\gamma^0) - \ln(V_\gamma) = k\epsilon \quad (1.13)$$

where V_γ^0 is the original retained austenite volume fraction and V_γ is the volume fraction of the untransformed austenite at a plastic strain ϵ , k is constant and a lower k value corresponds with higher retained austenite stability against strain-induced transformation.

A development of the model of Sugimoto *et al.*, [1992b] in TRIP-assisted steels has been proposed based on the assumption that k is proportional to the martensitic transformation driving force as $k = k_1 \Delta G^{\alpha'\gamma}$ since deformation temperature, chemical composition of retained austenite should be considered as well [Sherif *et al.*, 2004]. The fraction of untransformed austenite is expressed as a function of plastic strain, driving force and the original amount of austenite as follows:

$$\ln(V_\gamma^0) - \ln(V_\gamma) = k_1 \Delta G^{\alpha'\gamma} \epsilon \quad (1.14)$$

where k_1 is independent of the steel composition and is fitted from experimental data as a value of $0.00446 \text{ J mol}^{-1}$.

The hydrostatic pressure on the retained austenite enhances its stability against

martensitic transformation due to the accompanied volume expansion. A modified model was proposed including hydrostatic pressure parameters as following [Sugimoto and Kobayashi, 1994]:

$$\ln(V_{\gamma}^0) - \ln(V_{\gamma}) = (k - \beta P)\epsilon \quad (1.15)$$

where β is an empirical constant and P is the hydrostatic compression. This model was further developed as [Sherif *et al.*, 2004]

$$\ln(V_{\gamma}^0) - \ln(V_{\gamma}) = (k_3 + k_4 \Delta G^{\alpha\gamma}) \Delta G^{\alpha\gamma} \epsilon \quad (1.16)$$

where $k_3 = 0.008478 \text{ J mol}^{-1}$ and $k_4 = -0.242 \times 10^{-6} \text{ J mol}^{-1}$.

All these models were developed based on the kinetics of strain-induced formation of martensite. In this mechanism, the dislocations introduced in the austenite during plastic deformation assist in the nucleation of martensite [Olson and Cohen, 1975; Sherif *et al.*, 2004; Chatterjee and Bhadeshia, 2007]. In contrast, stress affected transformation occurs because the interaction of the applied stress with the shape deformation of martensite contributes a mechanical component ΔG_{mech} to the free energy change driving the transformation [Patel and Cohen, 1953; Chatterjee and Bhadeshia, 2007]. For uniaxial loading, the ΔG_{Mechl} per MPa is $\sim 0.86 \text{ J mol}^{-1}$ [Denis *et al.*, 1985]. Rapid transformation at first is due to the nucleation sites introduced by the deformation. However, an excessive plastic strain in austenite may cause the transformation to halt in that the motion glissile interface becomes impossible [Machlin *et al.*, 1951; Leslie *et al.*, 1964; Bhadeshia 1999]. This phenomenon is known as *mechanical stabilization* is a sure way of distinguishing the displacive and reconstructive mechanisms of solid state transformations [Bhadeshia 2004; Chatterjee *et al.*, 2006]. The critical plastic strain causing it can be predicted by balancing the force

which drives the transformation interface against the resistance from dislocation debris in the austenite [Chatterjee *et al.*, 2006]. The potential mechanical stabilization at large plastic strains however has never been taken into account in above equations. The strain-induced martensitic transformation model does not work well when the carbon content exceeds ~1.1 wt% [Chatterjee and Bhadeshia, 2007].

Based on stress-induced transformation, the total driving force ΔG_{total} for martensite transformation can be expressed as $\Delta G_{total} = \Delta G_{chem} + \Delta G_{Mech} - 600$, where ΔG_{chem} and ΔG_{Mech} are the chemical and mechanical driving force respectively and -600 J mol^{-1} is the strain energy stored energy. For uniaxial loading, the ΔG_{Mech} per MPa increases in M_s per unit of tensile stress is $\sim 0.1375\text{K}$. In the point view of driving force, a novel way to explain the stress-induced martensite transformation has been proposed taking the tensile stress as the increase of M_s in the athermal martensite formation equation *Eq. 1. 1*.

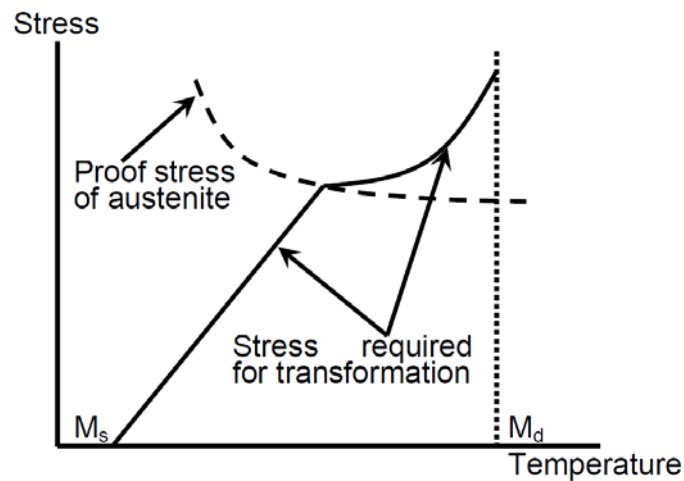


Figure 1.13: Stress requirement for martensitic transformation above M_s increases at higher temperatures; formation of martensite is not possible beyond M_d [Chatterjee 2006].

The yield strength of carbon enriched retained austenite is high to 1000MPa measured by neutron diffraction [Jacques 2007]. According to the continuum theory, strain on the strong austenite can initialize when the specimen accumulates a certain amount of overall strain in TRIP-assisted steels. The strain-induced decomposition of austenite model based on the overall strain is just the experimental fitted one but not physically meaningful, the constant k can indicate the stability of austenite qualitatively but not quantitatively. On the other hand, the stress-induced martensitic transformation is physically reasonable. As shown in Figure 1.13, without the necessary energy supply by stress to compensate the shortfall for the martensitic transformation, the induced martensitic transformation becomes impossible in any temperature between M_s and M_d , the strain in austenite cannot solely induce the transformation. It can be just assisted by the strain by supplying more nucleation sites and autocatalysis mechanism. In conclusion, the TRIP effect can be explained by that martensite transformation is induced by stress but assisted by strain as autocatalysis to stimulate the further transformation, hence the transformation strain on the adjacent ferrite grains, due to the formation of martensite by shear transformation, consequently attributes to the postponed onset of necking. The other explanation is that the stress-induced martensitic transformation does relax the stress concentration there and therefore results in the delayed onset of necking [Sugimoto *et al.*, 1999; Wei *et al.*, 2003]. This yields the extra uniform elongation in TRIP-assisted steels compared with dual phase steels.

1.7 Factors affecting performance

There are many factors that have been thought to control the mechanical properties of these steels, as summarized in this section.

1.7.1 Phases

TRIP-assisted steels consist of allotriomorphic ferrite, carbide-free bainitic ferrite, carbon enriched retained austenite with or without traces of martensite. Large retained austenite volume fraction enhanced ultimate tensile strength, total elongation, uniform strain and total absorbed energy compared with low austenite fraction in dual phase type steels, as shown in Figure 1.14 and Figure 1.15.

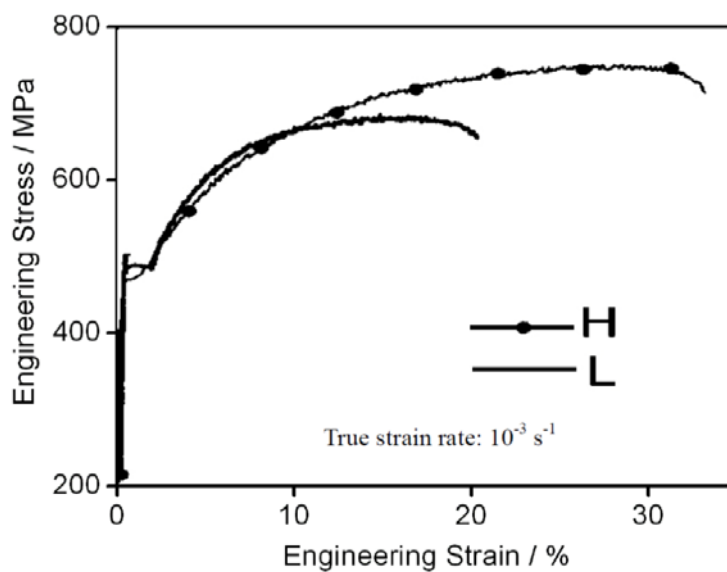


Figure 1.14: Quasi-static engineering stress-strain curves for TRIP steels (Fe-0.14C-1.51Mn-1.49Si-0.51Cu wt%) containing different volume fraction of retained austenite. H-type sample contains 16% of retained austenite and L-type contains less than 3% of that [Choi *et al.*, 2002].

However, a high retained austenite volume fraction implies less bainite which may adversely affect the strength. Similarly, high ferrite fraction during intercritical annealing finally results in less bainite, leading to a reduction in strength [Imai *et al.*, 1992]. Aluminium-containing steels contain more ferrite as compared with steels relying

on silicon. This is because in aluminium-containing steels, austenite starts transforming into allotriomorphic ferrite at a higher temperature and with a faster kinetics than in steels made with silicon.

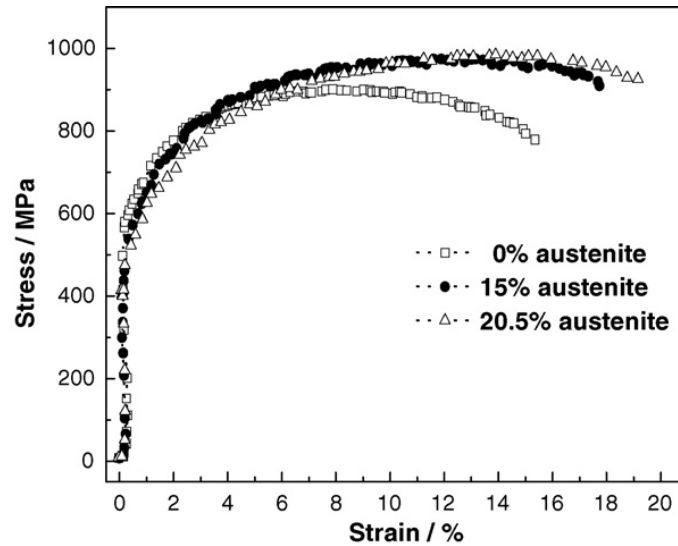


Figure 1.15: Stress-strain curves of TRIP-assisted steels with different volume percentage of the retained austenite [Zrník *et al.*, 2006]

Steels with reduced silicon content have been shown to possess properties similar to high-silicon steels although low-silicon steels contain only a small amount of retained austenite, the composite effect gives uniform elongation which is superior compared with high silicon bearing steels [Jacques *et al.*, 2001a, b]. This is due to the presence of some martensite in the low-silicon material. It seems that phases other than retained austenite can influence the mechanical behaviour of these steels. It is likely that the good uniform elongation properties of TRIP-assisted steels are due to the composite deformation behaviour of the major phases with the retained austenite playing a minor role [Bhadeshia 2002].

1.7.2 Stability of retained austenite

A moderate stability of retained austenite is required to achieve strength/ductility balance. It should transform to martensite progressively in order to retard the onset of necking during deformation. Its stability is determined by its morphology, M_S temperature and carbon concentration in TRIP-assisted steels. The maximum combination of strength and ductility happens always not at the maximum retained austenite fraction since greater austenite fraction leads to lower carbon concentration and less stability [Sakuma *et al.*, 1991a, b].

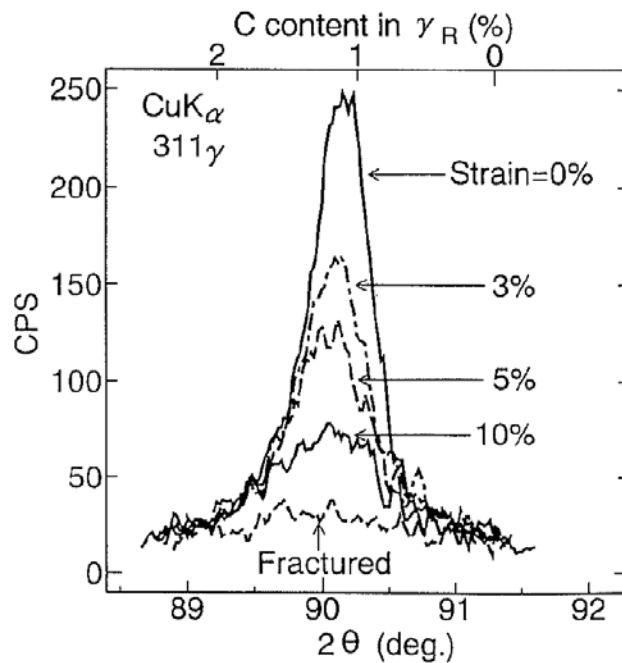


Figure 1.16: With increasing plastic strain, volume fraction of austenite decreases along with the increase in carbon content, which is apparent from the shift in the positions of the austenite, γ_R , peaks [Itami *et al.*, 1995].

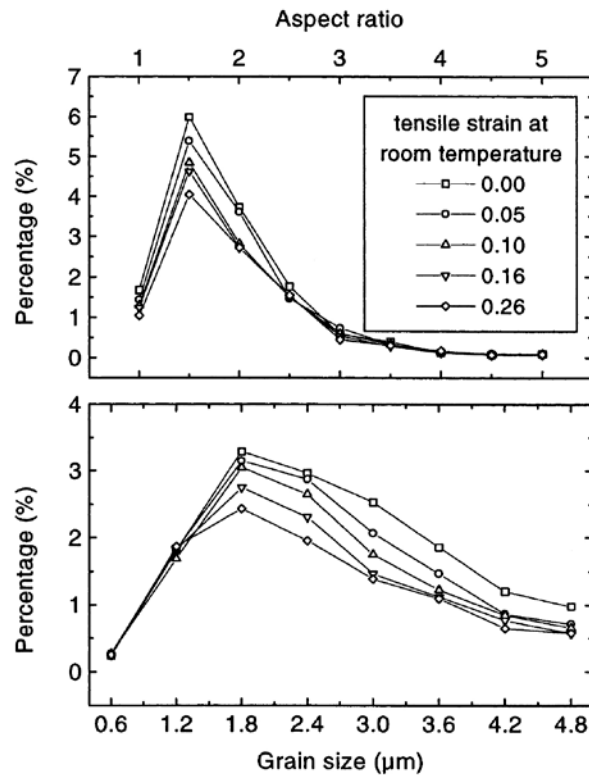


Figure 1.17: Effect of grain size and morphology of austenite on its stability, retained austenite with an aspect ratio larger than 2.5 and grain size finer than 1.2 μm remains unchanged with increasing tensile deformation [Basuki *et al.*, 1999a, b].

Carbon is more effective to strengthen austenite and hence to lower the martensite start temperature than the other substitutional elements. The austenite of TRIP steels can be enriched in carbon and become stable against the further martensitic transformation after isothermal bainitic formation. The carbon content is the most important parameters to enhance the stability of austenite. The retained austenite is however not homogeneously enriched with carbon by bainitic transformation [Schrader and Wever, 1952]. Regions in the vicinity of the bainite sheaves or the films of austenite trapped between bainite are richer in carbon. This may even lead to the observation of two different lattice parameters of austenite formed in the same sample [Matas and

Hehemann, 1961]. Austenite with low carbon content is easy to transform at the early stage of deformation. The carbon concentration of untransformed austenite increases with plastic strain, which can be proven by the increased lattice parameter observed from the X-ray diffraction results as shown in Figure 1.16 [Itami *et al.*, 1995].

The morphology of retained austenite generally is classified into two groups as follows: (1) isolated retained austenite islands lying in a soft ferrite matrix or on the grain boundary; (2) retained austenite thin films along martensite or bainite lath boundary or blocky one in these hard second phases [Sugimoto *et al.*, 1993]. The yield strength of allotriomorphic ferrite and bainite are measured by neutron diffraction as 500 MPa and 800 MPa respectively [Jacques *et al.*, 2007]. The harder bainite can constrain the deformation of retained austenite films and therefore increase the hydrostatic pressure on austenite compared with the softer allotriomorphic ferrite during straining, which is expressed by the following equation [Sakaki *et al.*, 1983]:

$$\sigma_p = \frac{2}{3\{Y_0 + 2H_0\varepsilon^*\}} + \frac{2}{3Y_0 \ln\left\{\frac{E\varepsilon^*}{1-\nu Y_0}\right\}} \quad (1.17)$$

where σ_p means resultant hydrostatic pressure, ε^* is isotropic transformation strain on martensitic transformation and $\varepsilon^* = 0.0058 + 0.0045C_\gamma$, Y_0 and H_0 are yield stress and strain hardening rate of phases surrounding austenite respectively, E and ν are Young's modulus and Poisson's ratio respectively. The M_S temperature of retained austenite can be affected by the hydrostatic pressure from the surrounding phases. An increase of 100 MPa of the hydrostatic pressure results in a decrease of 20-25 °C and 6.7 °C of M_S in TRIP-assisted steels and plain carbon steels respectively [Radcliffe and Schatz, 1962; Pyshmintsev *et al.*, 2002]. The morphology of retained austenite in group (2) may result in greater hydrostatic pressure and hence lower its M_S temperature and enhance its stability. According to Sugimoto *et al.*, [1993], the steels with morphology

of retained austenite of group (1) performed much better elongation at similar tensile strength than with morphology in group (2). However, the author did not notice that the steel of group (1) contained much more retained austenite compared with that of group (2). In fact, the effects of morphology of retained austenite on mechanical performance depend on the case by case in TRIP-assisted steels.

Except the enriched carbon, the refinement of austenite grain size (Figure 1.17) and increase of dislocation density in retained austenite can improve the austenite stability as well, which increases the rate of diffusion of interstitial elements to dislocations and creates solute atmospheres, hence strengthens austenite. It is confirmed again that the austenite thin film is more stable than that of isolated islands lying in a soft ferrite matrix or on the grain boundary [Basuki and Aernoudt, 1999].

The M_s temperature of austenite decreases with its grain size quantitatively as the following equation [Yang and Bhadeshia, 2009]:

$$M_s^0 - T = \frac{1}{b} \ln \left[\frac{1}{aV_\gamma} \left\{ \exp \left(-\frac{\ln(1-f)}{m} \right) - 1 \right\} + 1 \right] \quad (1.18)$$

where M_s^0 is defined as a fundamental martensite start temperature for an infinitely large austenite grain size; a and b are empirical fitting constants; m is the aspect ratio of the martensite plate; V_γ is the average austenite grain volume and f is the fraction of martensite. In other words, the refinement of austenite grain size improves the stability of retained austenite.

1.7.3 Test parameters

Temperature

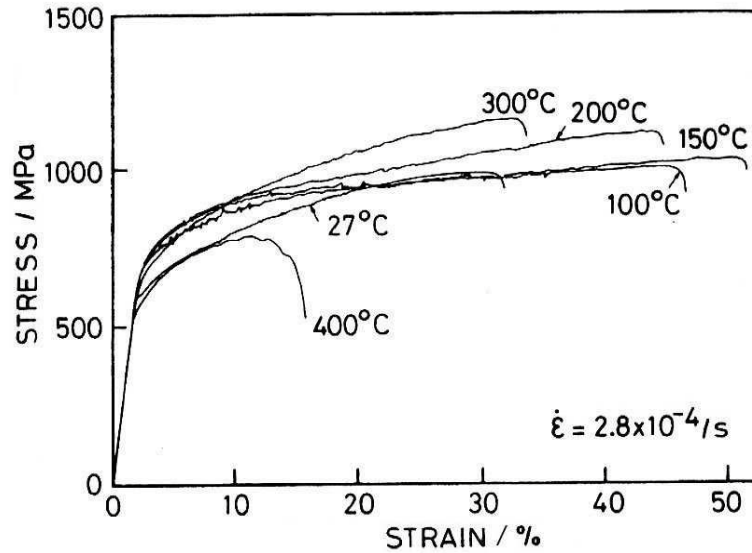


Figure 1.18: Effect of test temperature on the stress flow curve of TRIP-assisted steels [Sugimoto *et al.*, 1992b].

Enhanced temperature increases the stability of austenite against martensitic transformation due to reduced chemical driving force for transformation. Temperature can therefore exert a significant influence the mechanical properties (Figure 1.18 and Figure 1.19). The ultimate tensile strength and total elongation, unlike the yield strength, appear to vary much more strongly with temperature. However, the properties seem to improve only up to a certain maximum temperature, the peak temperature T_P ($^{\circ}\text{C}$) increases with increase in silicon and manganese contents (namely with decrease in carbon concentration in retained austenite) and is related to M_S temperature ($^{\circ}\text{C}$) of retained austenite as the following equation [Sugimoto *et al.*, 1993, 1992a]:

$$T_P = 3.04M_S + 187 \text{ (}^{\circ}\text{C)} \quad (1.19)$$

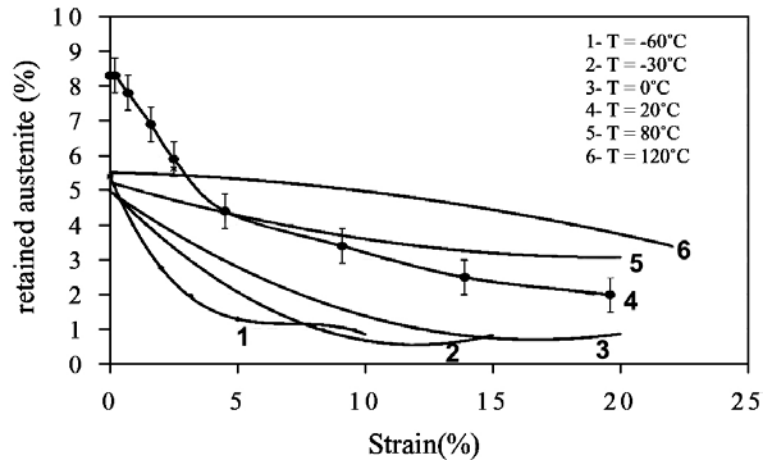


Figure 1.19: Influence of test temperature on the volume percent of retained austenite as function of strain [Berrahmoune *et al.*, 2004].

In a special case, the total elongation of an Al-Nb-Mo bearing TRIP-assisted steel (0.4C-0.5Si-1.5Mn-1.0Al-0.05Nb-0.2Mo wt%) can be improved to 78% combined with 1000 MPa tensile strength tested at an enhanced temperature of 150°C and strain rate of $3.3 \times 10^{-3} \text{ s}^{-1}$ compared with the 20% total elongation performed at 20°C [Mukherjee *et al.*, 2006]. A TRIP600 steel (Fe-0.08C-1.70Mn-1.55Si-0.015P-0.029Al wt%) showed the maximum TRIP effect and the best mechanical performance at 70°C and deteriorated with increase of temperature higher than 70°C [Berrahmoune *et al.*, 2004].

The characteristics of TRIP-assisted steels are beneficial for warm forming. Consequently, the martensitic transformation of retained austenite is suppressed by the enhanced stability of austenite during warming forming and much of them therefore can be retained in the formed parts and supply sufficient ability of energy absorption by TRIP effect in the case of crash.

Strain rate

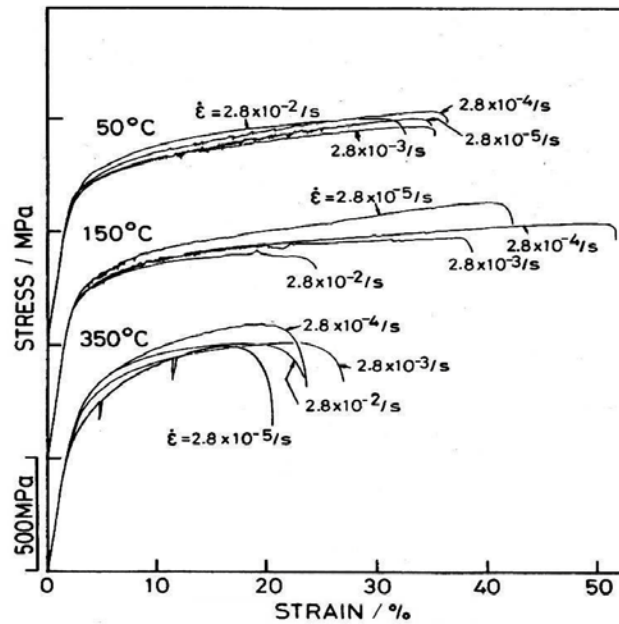


Figure 1.20: Effect of strain rate on the nature of the flow curve at different test temperatures [Sugimoto *et al.*, 1992b].

The strain rate strongly influences the tensile behavior of TRIP-assisted steels at different temperatures shown in Figure 1.20. An intermediate strain rate seems to maximize elongation, consistently at all the testing temperatures. Increasing strain rate from 10^{-3} to $2.5 \times 10^{-2} \text{ s}^{-1}$ raises both yield strength and ultimate tensile strength while the strain-hardening behaviour remains almost the same [Choi *et al.*, 2002]. Similar results were found in high chromium and nickel containing full austenite TRIP steels [Goldberg and Hoge, 1974]. However, a dynamic test of aluminium containing TRIP steel showed a positive effect of strain rate on the mechanical property at very high strain rate $> 1000 \text{ s}^{-1}$ due to the enhanced stability of retained austenite probably by the adiabatic heating during dynamic deformation [Van Slyckn *et al.*, 2007].

State of stress or strain

Both uniaxial tension and compression can aid the martensite transformation due to the positive shear component. The applied uniaxial tension however increase the M_S temperature more than compression since the normal component of tension is positive but is negative for the compression [Patel and Cohen, 1953]. Unlike uniaxial tension or compression, deformation-induced martensitic transformation is always known to be suppressed by hydrostatic pressure. Hydrostatic pressures increase the shear-to-normal stress ratio. The latter stress state considerably “softens” the hard phase present in the material during plastic deformation. The stability of the austenite can therefore be enhanced by applying hydrostatic pressure during tensile test, resulting higher uniform elongation.

Strain-induced martensitic transformation is retarded under plane-strain conditions relative to uniaxial loading [Im *et al.*, 2002]. This is due to lower applied stress and strain under plane-strain condition. By contrast, under biaxial stretching, the transformation is promoted relative to uniaxial testing, although the results vary with the sample orientation relative to the rolling direction [Streicher *et al.*, 2002]. This may be related to the texture of austenite grains [Reisner *et al.*, 1998].

The mechanical properties of TRIP steels are strongly dependent on the tensile direction with respect to the rolling direction and the specimens tested on the rolling direction perform the highest elongation [Hall *et al.*, 1969]. This is likely due to a texture effect of the retained austenite that can be highly textured [De Meyer *et al.*, 1999a, b, c; Mintz 2001]. The pre-strain improves the flow stress of TRIP-assisted steels slightly due to the increase of nucleation sites [Li *et al.*, 2007].

Gauge length

The product of tensile strength and total elongation is often used for evaluate the stretch

formability, which as high as 25-30 GPa% can be found with TRIP steels [Sugimoto *et al.*, 1992b]. However, the measure of total elongation is strongly affected by the gauge length. The shorter the gauge length, the greater the total elongation is measured. The gauge lengths are generally 50 mm (Japanese) or 80 mm (European), with occasionally 25 mm being used. Reducing the gauge length from 80 to 50 mm can lead to an approximate 3% increase in total elongation. Therefore, the gauge lengths have to be quoted when

1.8 Special properties

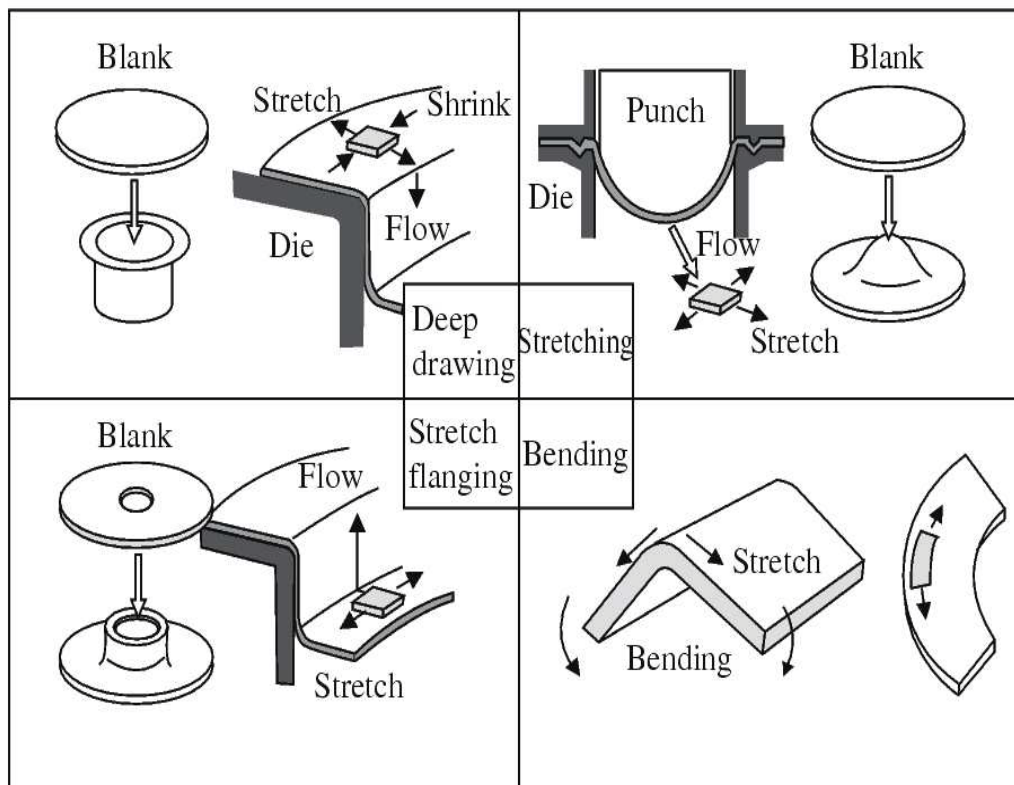


Figure 1.21: State of stress existing during different modes of forming operations [Takahashi 2003].

1.8.1 Formability

Formability is defined as the ease with which an object having a complex geometry can be manufactured using the material. This can approximately be related to plasticity or ductility which tends to deteriorate with increasing strength. TRIP-assisted steels are unique in this respect, they exhibit better formability than several other steels of comparable strength [Konieczny 2003]. Formability is not assessed by a single attribute but expressed as a combination of properties such as deep drawability, stretch formability, stretch flangeability and bendability. The state of stress is different in each of these forming operations, as illustrated schematically in Figure 1.21. The stability of retained austenite plays more significant role for the formability under the biaxial stress state than its volume fraction [Lee *et al.*, 2004].

1.8.2 Deep drawability

This is expressed by the r value, which means Lankford coefficient or plastic anisotropy coefficient, the ratio of true strain in the width direction to that in thickness direction for sheet metals. \bar{r} is the average of r values measured on specimens obtained at different directions respect to the rolling direction such as at 0° , 45° and 90° to the rolling direction. Generally, the higher the \bar{r} value, the better the deep drawability can be fulfilled in general. Although the \bar{r} values of TRIP-assisted steels are poor, they exhibit good deep drawability [Hiwatashi *et al.*, 1994; Nagasaka *et al.*, 1999a, b; Mintz 2001]. Both the volume fraction of the retained austenite and its stability enhanced by enriched carbon strongly improve the deep drawability based on the limiting drawing ratio ($LDR=D_0/d_p$), where the D_0 and the d_p are a maximum blank diameter and a punch diameter respectively. This excellent deep drawability is resulted from the large local necking resistance in TRIP steels at the cup wall just above the punch bottom due to

transformation hardening and stress relaxation owing to the deformation induced martensite transformation [Nagasaka *et al.*, 2001].

1.8.3 Stretch formability

In this test, rectangular blanks marked with circular grids on the surface by electrochemical etching method are deformed under a punch until local fracture occurs. This is also sometimes referred to as Limiting Dome Height test [Im *et al.*, 2000a, b; Lee *et al.*, 2004]. After the test, the circular grids turn into oval shape. The strain values on the major and the minor axes are measured and used to construct a Forming Limit Curve.

The volume fraction of retained austenite is beneficial to improve the value of product $UTS \times TEL$, its stability is more significant for better stretch formability. Microstructures with isolated retained austenite islands in ferrite away from bainite have better stretch formability than networks of austenite. The work hardening rates of TRIP steels are substantially higher than for conventional high strength steels, providing significant stretch formability. This is particularly useful when designers take advantage of the high work hardening rate (and increased bake hardening effect) to design a part utilizing the as-formed mechanical properties.

1.8.4 Stretch flangeability

Stretch flangeability is a more complex property assessed by a two step process viz. (a) hole punching and (b) hole expanding [Sugimoto *et al.*, 1999]. A hole is first punched on the steel blank and followed by the expansion of the hole until the first cracks are observed. The ratio of the increase in diameter of the hole to the original diameter is measured in this test [Mintz 2001].

Carbon-enrichment of the retained austenite enhance its stability and therefore suppress the strain-induced transformation at a punched surface layer and the void formation at the matrix/second phase interface and/or second phase/second phase interface. The stretch-flangeability is affected by carbon concentration of the retained austenite rather than by the volume fraction of retained austenite. In the successive hole-expanding, it enhances the localized ductility due to the effective TRIP of the untransformed retained austenite [Sugimoto *et al.*, 1999]. The morphology of retained austenite as well as the temperature of operation is significant for the stretch flangeability [Nagasaka *et al.*, 1996, 1998].

TRIP steels are expected to perform better stretch flangeability due to the gradual transformation of martensite from retained austenite compared with dual phase steels where martensite particles encourage the propagation of ductile cracks [Mintz 2001].

1.8.5 Crash-worthiness

The safety of automobile requires the automobile steels to be of crash-resistance. To simulate a real car crash, a dynamic testing is performed by a drop hammer falling on the column, where the strain rate of 2500 s^{-1} is chosen being based on a collision speed of $50\text{-}55 \text{ km h}^{-1}$ [Yoshitake *et al.*, 1996]. Static and quasi-static tensile tests performed with a slow strain rate of about 0.005 s^{-1} are therefore not sufficient. Such dynamic tests, however, are expensive and it is attempted to relate the energy absorbed in dynamic situation to it found in the simple slow strain rate tensile test. The area under the load-elongation tensile curve can be considered as a measure of the absorbed energy [Yoshitake *et al.*, 1996]. Both thickness and strength influence the energy absorption and the former is more significant.

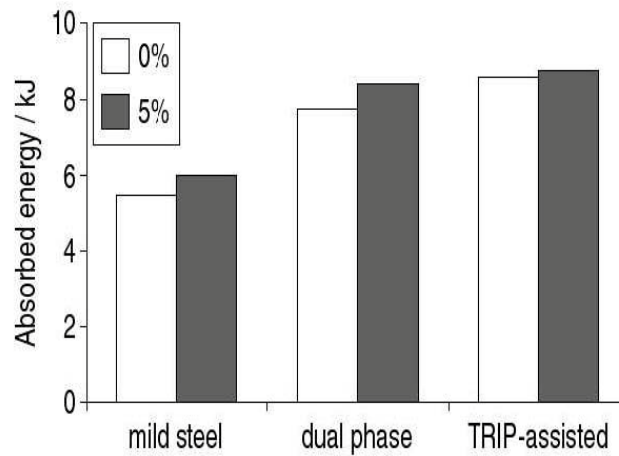


Figure 1.22: Superior crash-worthiness of TRIP-assisted steels compared with other types, the steels are tested with a prestrain of 0% and 5% in each case [Uenishi *et al.*, 2000].

TRIP-assisted steels, like all other steels, exhibit a positive strain-rate sensitivity index, which means that an increase in strain rate increases the flow stress but elongation is reduced. However, superior elongation has been reported for TRIP-assisted steels even at high strain rate [Uenishi *et al.*, 2000; Wei *et al.*, 2002a, b], presumably due to the TRIP effect. A comparison on crash-worthiness of different types of steels can be found in Figure 1.22 [Uenishi *et al.*, 2000]. TRIP steels perform better crashworthiness than dual phase steels. The crashworthiness is for the formed automotive parts but not for the steel sheets themselves. To ensure that, the transformation of martensite from retained austenite during press forming has to be limited and the majority of retained austenite should transform to martensite on impact and absorb much of the impact energy in the event of crash [Mintz 2001].

For some crash-worthiness models, stress-strain data up to 10% strain are the most important [ULSAB-AVC 2001]. The energy absorption up to 10% engineering strain

under the engineering stress-strain curves is considered to evaluate the crashworthiness as well.

1.8.6 Fatigue resistance

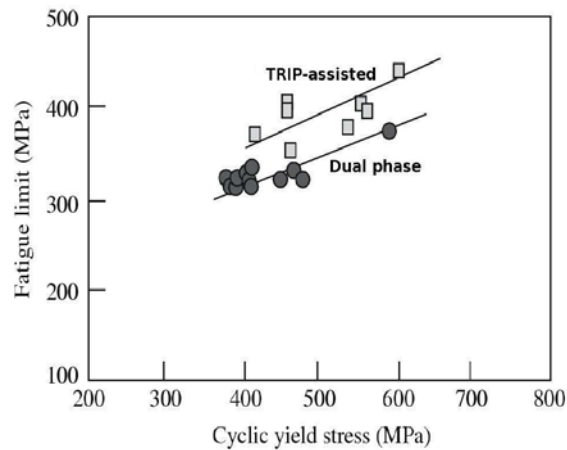


Figure 1.23: Effect of cyclic yield stress on fatigue limit of dual phase and TRIP-assisted steels [Takahashi 2003].

The importance of fatigue resistance is obvious for a steel to be used in automobile components that are routinely subjected to cyclic loading [Yan 2002]. Prestraining has been identified to be the most effective factor increasing fatigue strength. In TRIP-aided steels, prestraining to 10% in tension improves the fatigue limit. Steels with allotriomorphic ferrite matrix performs better fatigue property compared those with bainitic ferrite matrix. This is not only because of TRIP effect of retained austenite but also the high compressive internal stress in the allotriomorphic ferrite matrix resulting from a second hard phase on prestraining. The internal stress is the most effective parameter to increase the fatigue strength in TRIP-aided steels [Song *et al.*, 2001, 2003].

Dual phase steels are known to exhibit high fatigue strength. TRIP-assisted steels perform a little better fatigue property as shown in Figure 1.23 [Takahashi 2003]. The

fatigue behaviour, especially in high strength steels, is strongly affected by the zinc coating. The intermetallic layers have low fracture toughness and serve as crack nucleation sites in the galvanized high strength steels during fatigue [Mintz 2001].

1.9 δ -TRIP

A neural network model for the combination of alloying elements and processing has been established, which can lead to an optimum quantity of retained austenite in the microstructure and yet minimize the silicon concentration. Combining with genetic algorithm, the composition of steel was optimized and then manufactured at cast condition, illustrated in Table 1.5.

Table 1.5: Chemical composition of model perceived optimum alloy and experimental alloy, wt% [Chatterjee *et al.*, 2007]

Alloy	C	Si	Mn	Al	Cu	P
Optimum	0.4	0.5	2.0	2.0	0.5	0.02
experimental	0.36	0.73	1.96	2.22	0.52	0.022

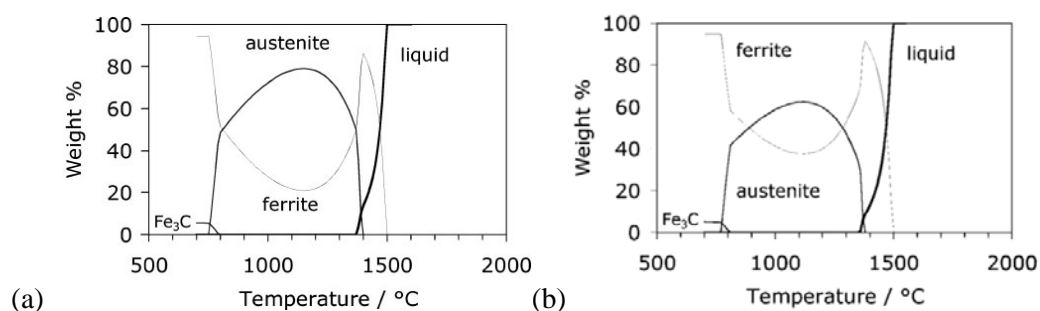


Figure 1.24: Calculated quantities of phases as function of temperature. (a) Optimised alloy; (b) Experimental alloy [Chatterjee, *et al.*, 2007]

Unexpectedly, the full austenite can't be achieved at any temperature based on the equilibrium phase diagram of both optimum and experimental alloy shown in Figure

1.24. This indicates the dendritic δ -ferrite should persist in the cast alloy. The novel microstructure consisting of δ -ferrite dendrites and a residual phase which at high temperatures is austenite is revealed as shown in Figure 1.25.

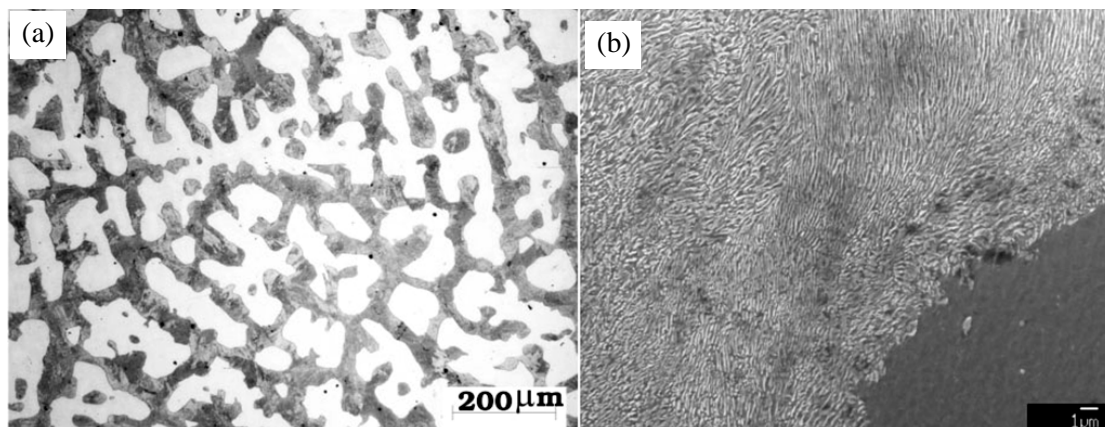


Figure 1.25: Microstructures of as-cast alloy. (a) optical micrograph; (b) Field emission gun scanning electron microscope (FEG-SEM) image [Chatterjee, *et al.*, 2007]

This austenite, with appropriate heat treatment, evolved into a mixture of bainitic ferrite and carbon enriched retained austenite (Figure 1.26). By such heat treatment of as-cast steel, it retained 13.5 ± 0.9 wt% austenite containing about 1.17 ± 0.03 wt% carbon revealed by X-ray diffraction analysis, where the stable dendritic δ -ferrite sustained which differentiates it from the conventional TRIP-assisted steel containing allotriomorphic ferrite and residual phases. It is therefore designated as δ -TRIP steel [Chatterjee, *et al.*, 2007]. The heat treated specimens of as-cast steel were tested to reveal a tensile strength of ~ 1 GPa and a uniform elongation of 23% (Figure 1.27).

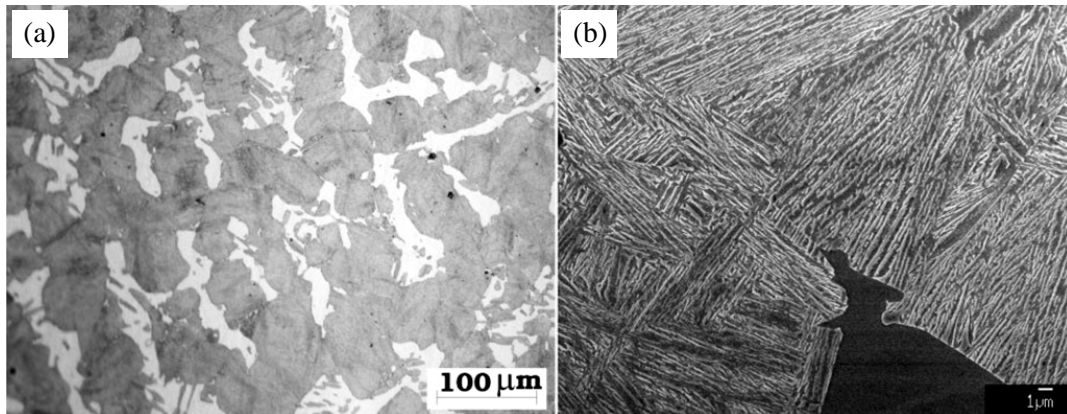


Figure 1.26: Microstructures of heat treated sample. (a) optical micrograph; (b) Field emission gun scanning electron microscope (FEG-SEM) image [Chatterjee, *et al.*, 2007]

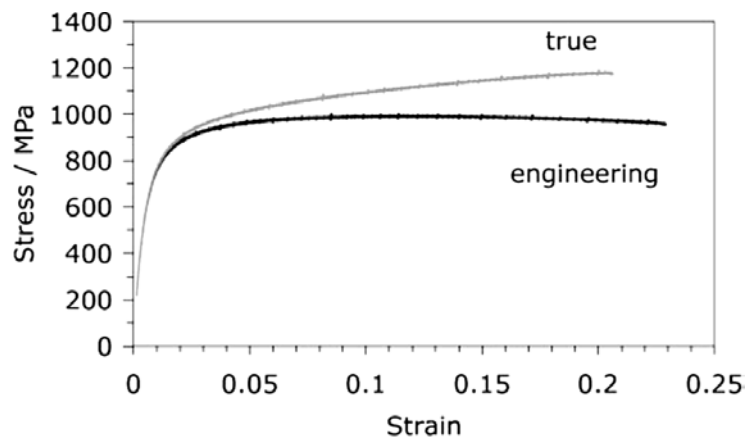


Figure 1.27: Stress-strain curve of heat treated material at room temperature: almost all elongation is uniform [Chatterjee, *et al.*, 2007]

1.10 Summary

TRIP-assisted steels play important roles in the safety of car bodies due to the strength combined ductility. This results from the characteristic of dual phase mechanism and transformation-induced plasticity (TRIP) effect because they contain soft allotriomorphic ferrite, hard carbide free bainite and retained austenite with or without a

few martensite. A moderate stability of retained austenite is required because the retained austenite has to transform to martensite progressively during straining in order to postpone the onset of necking. The martensitic transformation from retained austenite during deformation is induced by stress and assisted by strain. The morphology and constituent phases should be controlled carefully to achieve this. The carbon concentration in retained austenite is important in influencing its stability. The addition of silicon can effectively retard the formation of cementite and therefore enrich carbon into austenite during isothermal bainitic transformation in the para equilibrium condition. Aluminium and phosphorus are considered to partially or fully replace silicon in TRIP-assisted steels because silicon causes surface problems. Manganese is used to increase hardenability. The other elements, such as niobium, molybdenum, copper, nickel, chromium and boron, are added sometimes. The test temperature, strain rate and state of stress or strain also strongly influence their mechanical performance.

Generally, TRIP steels have better formability, crash-worthiness and fatigue resistance than dual phase steels. Compared with dual phase steels, they are however more complicated to be produced and of worse resistance spot-weldability due to their higher carbon contents in order to obtain sufficient TRIP effect. Novel δ -TRIP steel contains only a small amount of silicon to avoid the surface problems during hot rolling and galvanizing. It revealed excellent mechanical properties especially huge uniform ductility even in cast condition. It's potential to achieve much better performance after rolling to smaller more uniform and smaller grains. The stable δ -ferrite formed by solidification persists at all temperature. This is possible to avoid the full brittle martensite microstructure at the heat affected zone during resistance spot welding and therefore improve the bad weldability in conventional TRIP-assisted steels.

1.11 Scope of the research

δ -TRIP steel contains only a small amount of silicon to avoid the surface problems during hot rolling and galvanizing. It has revealed excellent mechanical properties especially huge uniform ductility even in the cast condition. It's potential to achieve much better performance after rolling.

In this research, the solidification process will be investigated firstly to understand the stability of δ -ferrite corresponding to the alloying elements and cooling condition in details. Further, the hot rolling and cold rolling of δ -TRIP steel will be performed followed by optimizing the two-stage heat treatment profiles to fulfill proper mechanical property for automotive application (ultimate tensile strength \times total elongation $>$ 30,000 MPa %). The mechanism for the super ductility should be understood as well.

The δ -TRIP steel is expected to be weldable even though its carbon equivalent is much higher than conventionally permitted value 0.4 wt% because a dual phase of ferrite and martensite is supposed to persist in the "Heat Affected Zone" of spot welds due to the stabilising δ -ferrite.

The final goal is to manufacture a δ -TRIP steel with sufficiently good surface quality in the rolled condition, good strength and ductility, formable into complicated shapes and spot weldable for automotive applications.

Chapter 2 Stabilization of δ -ferrite during Solidification

2.1 Introduction

Transformation-induced plasticity (TRIP) assisted steels contain allotriomorphic ferrite as the major phase, with the rest of the microstructure consisting of carbide free bainitic ferrite and carbon enriched retained austenite. An unconventional TRIP assisted steels has recently been invented, designated δ -TRIP [Chatterjee *et al.*, 2007], because the usual allotriomorphic ferrite grains are replaced by dendritic δ -ferrite, which grows from the liquid steel. Furthermore, the δ -ferrite persists at all temperatures and cannot be removed by heat treatment because it is a thermodynamically stable phase. Otherwise, the residual microstructure in the interdendritic regions is still the same, consisting of a mixture of bainitic ferrite with enriched austenite. The steel has interesting properties: an ultimate tensile strength in the as-cast condition of about 1000 MPa and a total elongation, almost all of which is uniform, of 23%. It has been demonstrated that the combination of strength and ductility is due partly to the deformation induced transformation of the retained austenite into martensite, resulting in an enhanced resistance to plastic instabilities [Chatterjee *et al.*, 2007].

The alloy contains only 0.5 wt% of silicon in order to avoid surface quality and galvanising problems [Chatterjee *et al.*, 2007; Jacques *et al.*, 2001a, b; Kizu *et al.*, 2001;]. However, one role of the silicon is to stop the precipitation of cementite during the bainite reaction [Deliry 1965; Pomey 1966; Kozeschnik and Bhadeshia, 2008], and 0.5 wt% can be insufficient to achieve this [Jacques *et al.*, 2001a]. To cope with this difficulty, δ -TRIP also contains aluminium, which is known to retard the precipitation of cementite [Allten 1954; Langer 1968; Bhat 1977]; the aluminium also helps to ensure

the presence of δ -ferrite during the solidification phase. The presence of δ -ferrite is crucial in this novel system, and the authors' experiments have indicated that its occurrence is temperamental and sometimes inconsistent with what is expected at thermodynamic equilibrium. Non-equilibrium solidification and any consequences of this on solid state transformation could play an important role in the management of the microstructure. Thus, the goal of the work presented in this chapter was to study the vagaries of the formation of ferrite during solidification in the context of δ -TRIP steel.

2.2 Alloy design and manufacture

The presence of δ -ferrite is crucial in this novel δ -TRIP steel which differentiates it from conventional TRIP-assisted steels. The fraction of phases as a function of temperature in both equilibrium and para equilibrium, therefore, were calculated to design stable δ -ferrite using MTDATA [2005] in combination with the TCFE (version 1.21) database. Liquid, ferrite, austenite and cementite were allowed coexist under equilibrium but cementite was omitted in the case of para equilibrium due to a lack of appropriate thermodynamic data. Miscibility gaps were not permitted in the liquid or austenite.

The role of each solute in TRIP steels has been discussed in Chapter 1. The significance of each solute in the content of preserving δ -ferrite is, however, not clear. The effects of Al, Mn, Si, Cu, on the fraction of δ -ferrite in the final microstructure were compared according to the phase diagrams based on a previously optimized composition of δ -TRIP steel [Chatterjee *et al.*, 2007], as shown in Figure 2.1. It is found that the most significant solute in stabilizing δ -ferrite is aluminium while the others have a minor influence. Accordingly, three alloys, with increasing aluminium concentration with the other alloying elements similar to previous work [Chatterjee *et al.*, 2007], were manufactured. The 34 kg ingots of 100×170×230 mm dimensions were cast in a vacuum

furnace in POSCO, the compositions are listed in Table 2.1.

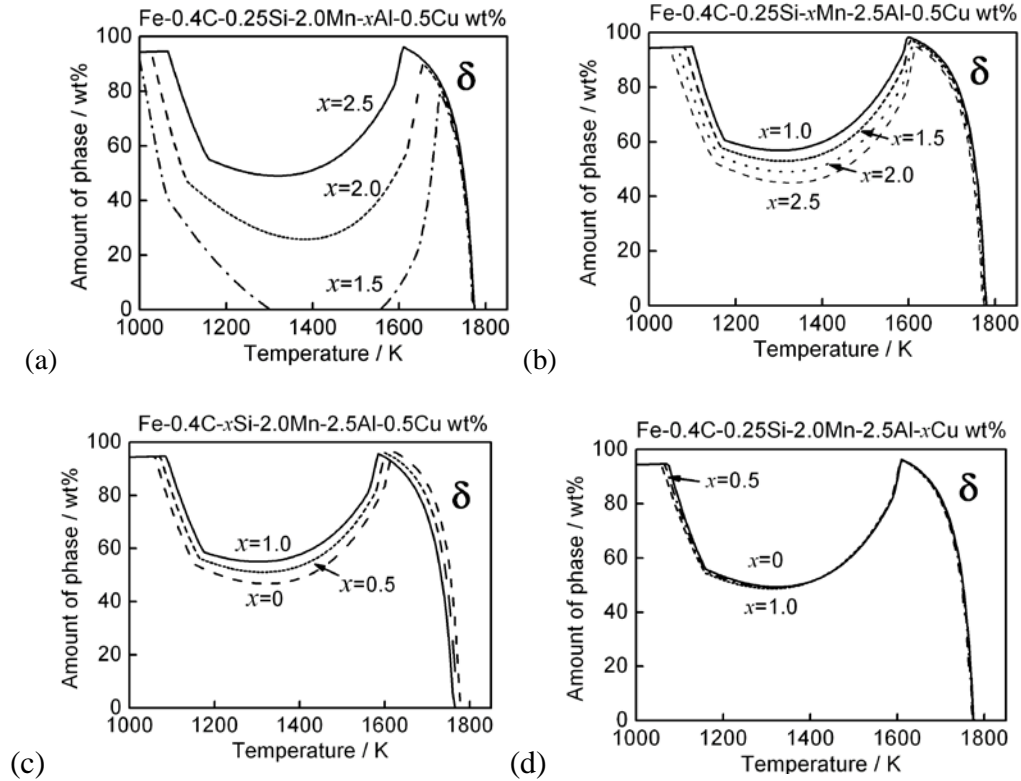


Figure 2.1: Change of ferrite fraction with alloying elements, (a) aluminium, (b) manganese, (c) silicon, (d) copper.

Table 2.1: Design compositions and those actually achieved during manufacture.

wt%	Alloy 0		Alloy 1		Alloy 2	
	Design	Actual	Design	Actual	Design	Actual
C	0.4	0.36	0.4	0.36	0.4	0.37
Si	0.25	0.26	0.25	0.26	0.25	0.23
Mn	2.0	1.99	2.0	2.02	2.0	1.99
Al	2.0	1.97	2.2	2.13	2.4	2.49
Cu	0.5	0.49	0.5	0.49	0.5	0.49
P	0.02	0.03	0.02	0.02	0.02	0.02
S		0.0036		0.0036		0.0036
N		0.0048		0.0048		0.0048

The calculated equilibrium phase diagrams for the manufactured alloys are presented in Figure 2.2a, b and c; they show that under equilibrium conditions, the minimum amount of ferrite to be expected in the microstructure is 27, 35 and 51 wt% for Alloy 0, Alloy 1 and Alloy 2. Furthermore, alloys start solidification with δ -ferrite which remains the only solid phase until most of the liquid has been consumed. The few percent of liquid that remains then converts into austenite, which on cooling continues to grow in proportion by consuming the δ -ferrite. After the amount of ferrite reaches the minimum, the austenite starts to transform in allotriomorphic ferrite or pearlite again, which, however, was a different morphology when compared with dendritic δ -ferrite.

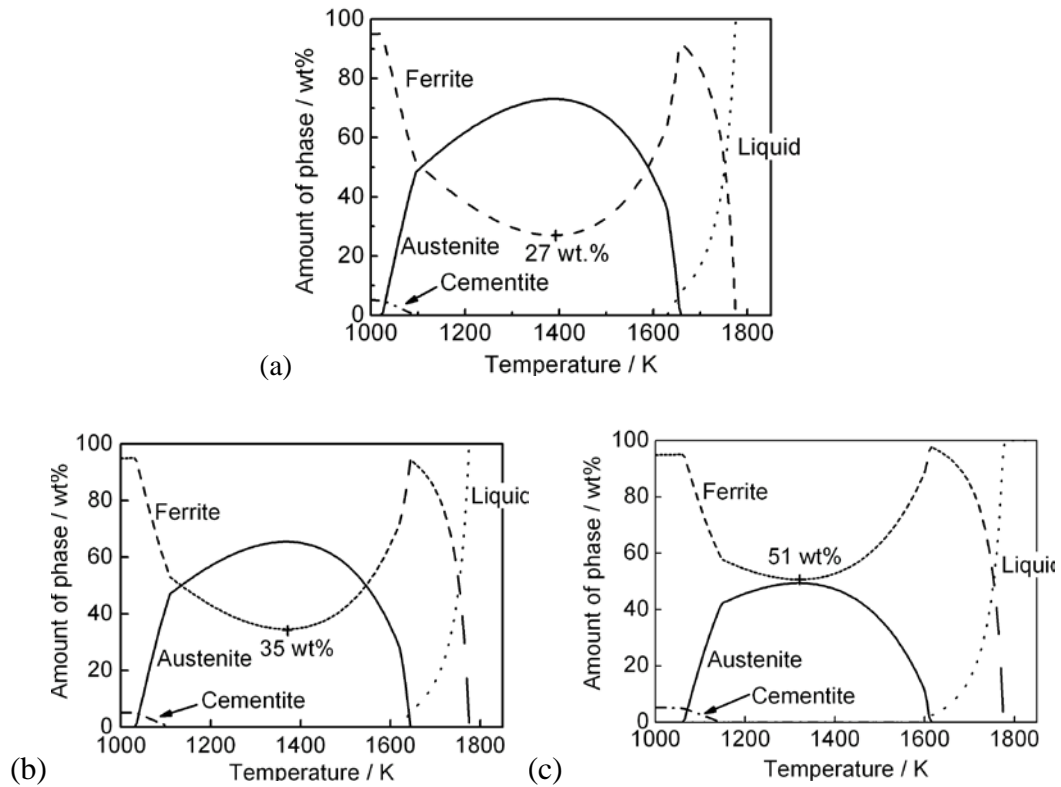


Figure 2.2: Calculated phase percentages as a function of temperature in equilibrium. (a) Alloy 0. (b) Alloy 1. (c) Alloy 2.

2.3 Metallography

Optical microscopy samples were prepared using standard methods and etched in 2% nital for study using optical microscopy (Olympus: BX60). Higher resolution observations were done using the secondary electron imaging in a field-emission scanning electron microscope (ZEISS ULTRA55) operating at 10 kV accelerating voltage. The machine had an energy dispersive X-ray microanalysis facility operating at 15 kV accelerating voltage.

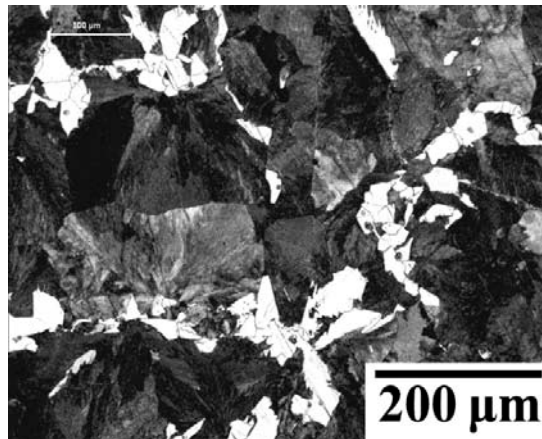


Figure 2.3: Microstructure of Alloy 0 in cast condition. The white regions are allotriomorphic ferrite and the dark are pearlite.

No trace of dendritic solidification could be found in Alloy 0 in its cast condition shown in Figure 2.3, whose microstructure consisted predominantly of pearlite with some allotriomorphic ferrite. The optical microstructures of Alloy 1 in the cast condition, on the other hand, shows remnants of the dendritic solidification process through coring effects, but the δ -ferrite dendrites themselves are almost absent, Figure 2.4. Instead, the microstructure has evolved through the complete transformation of δ -ferrite into austenite, which then transforms into a small amount of allotriomorphic and

Widmanstätten ferrite but predominantly into pearlite on cooling. This is quite inconsistent with the phase calculations in Figure 2.2 b which indicate that under equilibrium conditions, as a minimum, some 35 wt% of the microstructure should consist of δ -ferrite. The microstructure for Alloy 2 is more as-expected, with prominent dendrites of δ -ferrite and pearlite resulting from the solid-state transformation of austenite (Figure 2.4 c and d). However, even in this case, the total amount of δ -ferrite, 32.9 ± 1.4 wt%, which is estimated in volume percentage, being consistent with weight percentage in the condition that the difference in density between ferrite and austenite is ignored, by optical microscopy image analysis using *ImageJ* software, is much less than the minimum of 51 wt% indicated by the equilibrium phase diagram calculations in Figure 2.2 c. Indeed, the total ferrite content (δ and α) is expected to be much higher on reaching ambient temperature.

It is likely that solidification occurs under conditions which deviate from equilibrium. The solutes, particularly those which are substitutional, may not in such circumstances partition to the fullest extent required by thermodynamic equilibrium. To assess this, para equilibrium phase diagrams were calculated. Para equilibrium is a state of constrained equilibrium in which the substitutional to iron atom ratio is maintained constant everywhere, but subject to this constraint, the carbon partitions to achieve a uniform chemical potential [Hultgren 1951; Hillert 1952, 1953; Aaronson *et al.*, 1966a, b, c; Bhadeshia 1985]. The results are shown in Figure 2.5, where it is evident that under para equilibrium conditions, Alloy 0 and Alloy 1 can become fully austenitic and that the minimum quantity of δ -ferrite possible in Alloy 2 could be dramatically reduced.

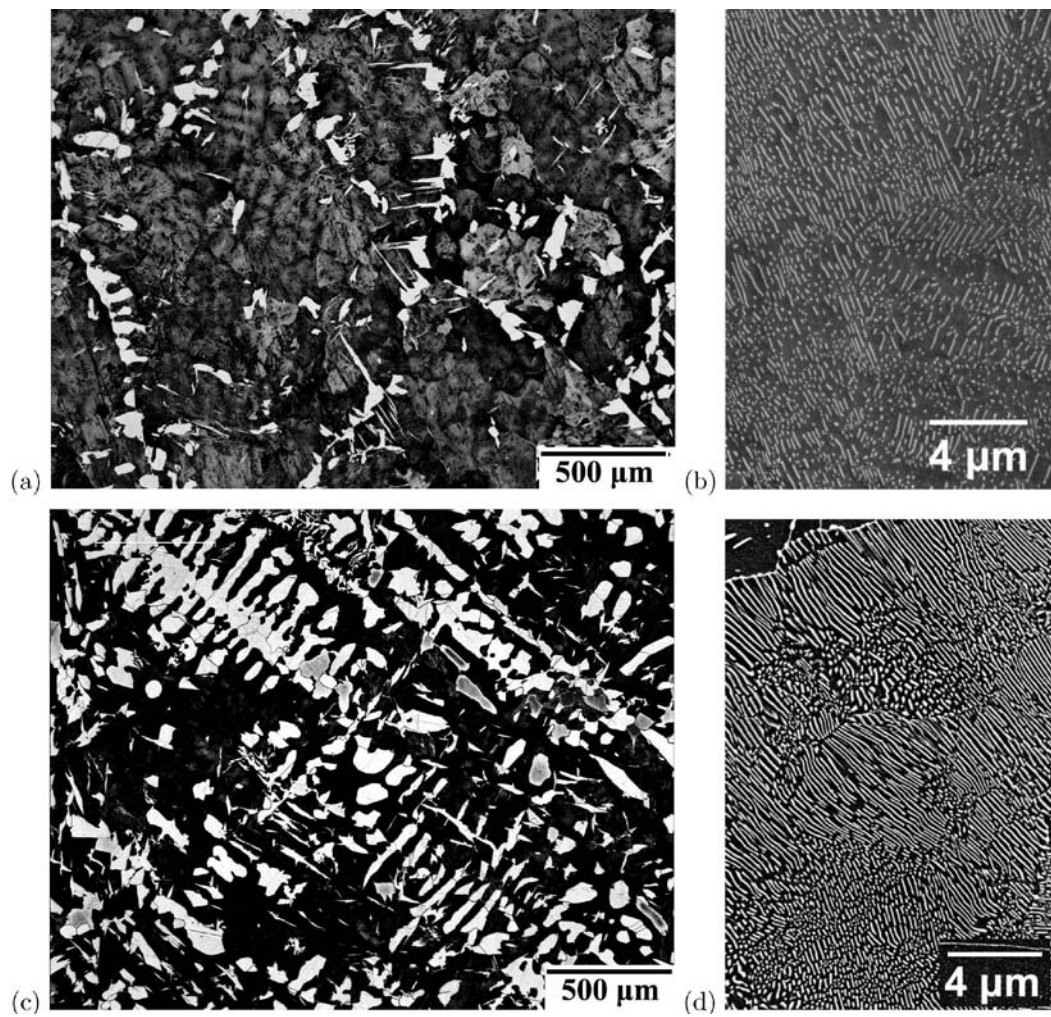


Figure 2.4: Microstructure of the cast alloys; the dark regions are fine pearlite and the white, ferrite. (a) General microstructure of Alloy 1; (b) higher magnification image of the dark areas of Alloy 1 showing pearlite. (c) General microstructure of Alloy 2; (d) higher magnification image of the dark areas of Alloy 2 showing pearlite.

2.4 Microanalysis

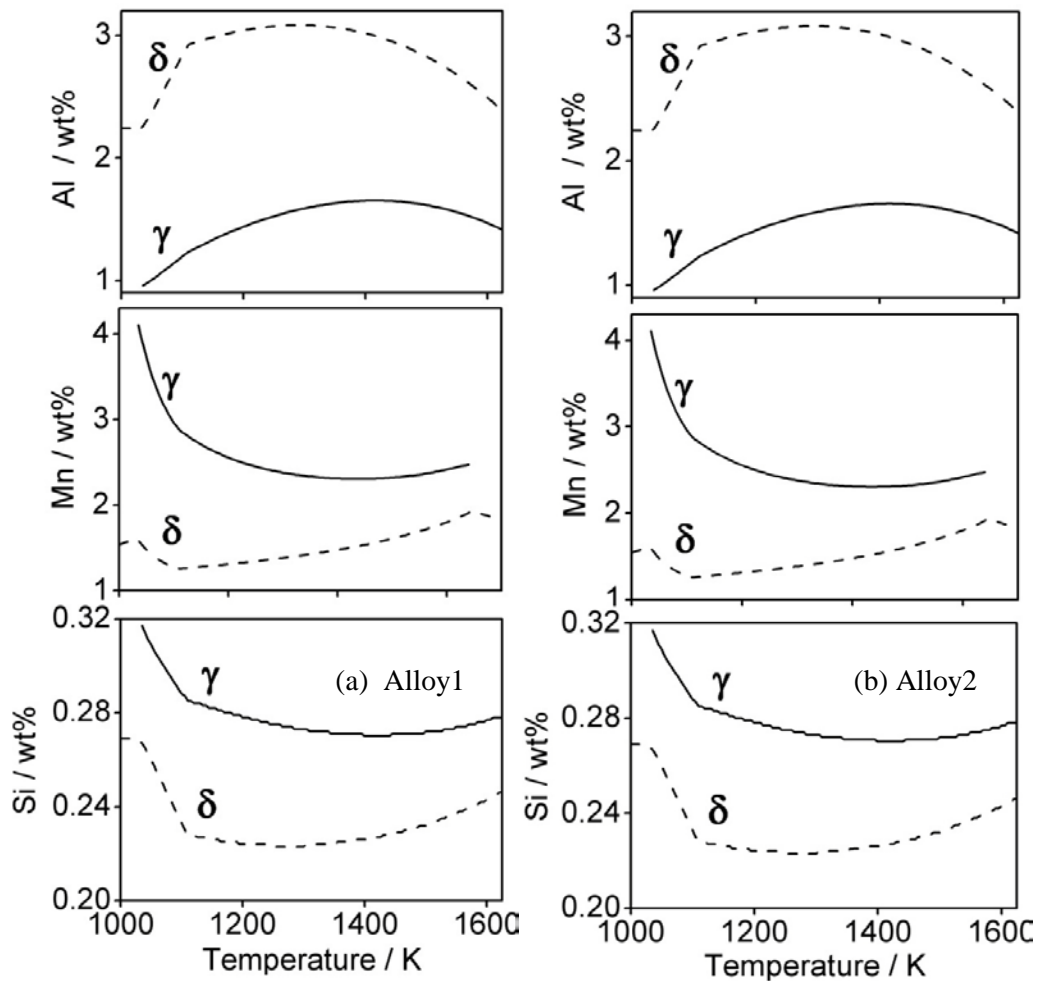


Figure 2.6: Calculated equilibrium compositions of the phases as a function of temperature. (a) Alloy 1; (b) Alloy 2.

Full equilibrium data for the key solutes of Alloy 1 and Alloy 2 are presented in Figure 2.6, both to illustrate the partitioning behaviour and to form the basis for comparisons with measurements. The real state of solidification with respect to the substitutional solutes is likely to be between equilibrium and para equilibrium (an infinite number of intervening states is possible). Microanalysis experiments were conducted to assess the

fine-scale distribution of solutes between the dendrites and interdendritic spaces where austenite initiates. These experiments were not conducted on Alloy 1 where the δ -ferrite dendrites were absent in their original state in the final microstructure. The discussion focuses on the major substitutional solutes Mn and Al but the interpretations are consistent with the behaviour of the minor solutes, with the exception of carbon which cannot be determined quantitatively with the microanalysis technique used.

The locations where microanalysis experiments were carried out are illustrated in Figure 2.7, the intention was to measure the composition of the δ -ferrite dendrites in general, and that of austenite at two locations. The latter is necessary because there are effectively two kinds of austenite, that which forms from the liquid residue left after δ -ferrite, and the second type which grows by solid-state transformation as it consumes the δ -ferrite. Thus, locations 2 and 3 in Figure 2.7b correspond to austenite from solid whereas location 4 is at the core of the austenite, i.e., which originated from interdendritic liquid.

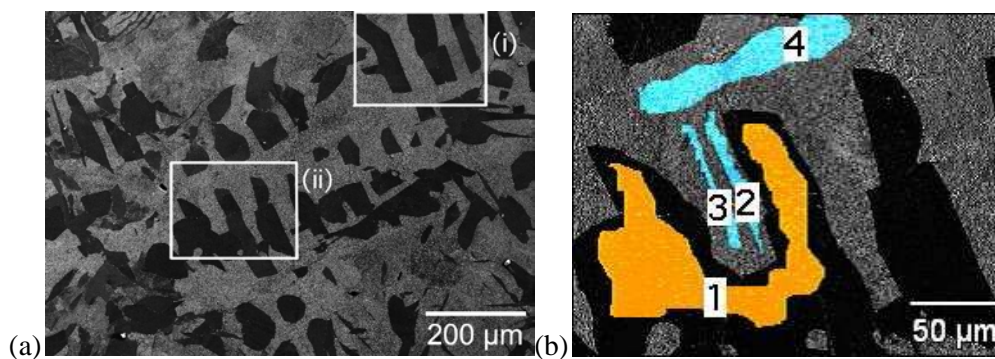


Figure 2.7: (a) Location of regions examined in detail. (b) Higher magnification of region (ii). The orange colour marks the region of δ -ferrite subjected to microanalysis, and the blue the austenite similarly analyzed.

The results, quantitatively listed in Table 2.2 and plotted in Figure 2.8, show that

the composition of the δ -ferrite corresponds essentially to that expected from equilibrium at the temperature (1612 K) where solidification is almost complete and austenite formation from liquid commences. Not surprisingly, the austenite which forms from the residual liquid is rich in Mn and depleted in Al, consistent with the equilibrium calculations. This is not the case for the austenite that grows in the solid-state, which inherits the concentrations in the δ -ferrite. In summary, the composition of the δ -ferrite ceases to change significantly during cooling following solidification, and much of the austenite evolves by growing into the δ -ferrite without the partitioning of substitutional solutes, i.e., by a process which may not be far from para equilibrium. Figure 2.9 shows the same effect more vividly, as a scan across the core of an austenite region. These results explain why the expected quantities of δ -ferrite are not obtained in contradiction to the equilibrium phase diagram but more consistent with the para equilibrium estimates (Figure 2.10).

Table 2.2: Microanalytical results for manganese and aluminium; in wt%.

	δ -ferrite		'Austenite'	
	Mn	Al	Mn	Al
Equilibrium for 1612K	1.95	2.52	3.77	1.15
Measured, Figure 2.7a, region (i)	2.13 \pm 0.20	2.46 \pm 0.03	2.47 \pm 0.40	2.23 \pm 0.03
Measured, Figure 2.7b, locations 1	1.19 \pm 0.19	2.52 \pm 0.03		
Measured, Figure 2.7b, locations 2,3			2.29 \pm 0.39	2.12 \pm 0.06
Measured, Figure 2.7b, location 4			3.33 \pm 0.40	2.01 \pm 0.03

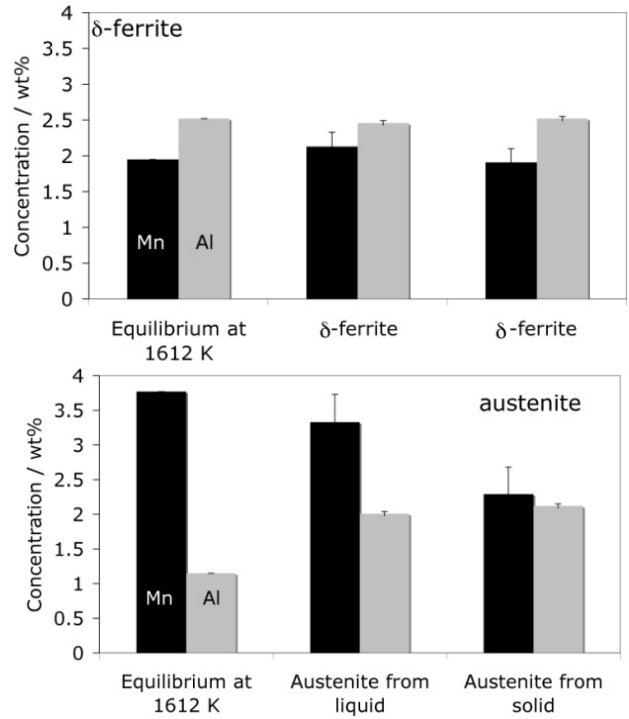


Figure 2.8: Illustration of data from Table 2.2.

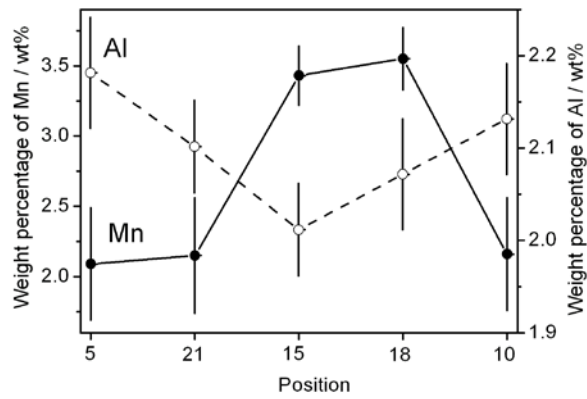


Figure 2.9: Microanalysis scan across the core of an austenite region in Alloy 2. The distance between successive microanalytical results is approximately 20 μm .

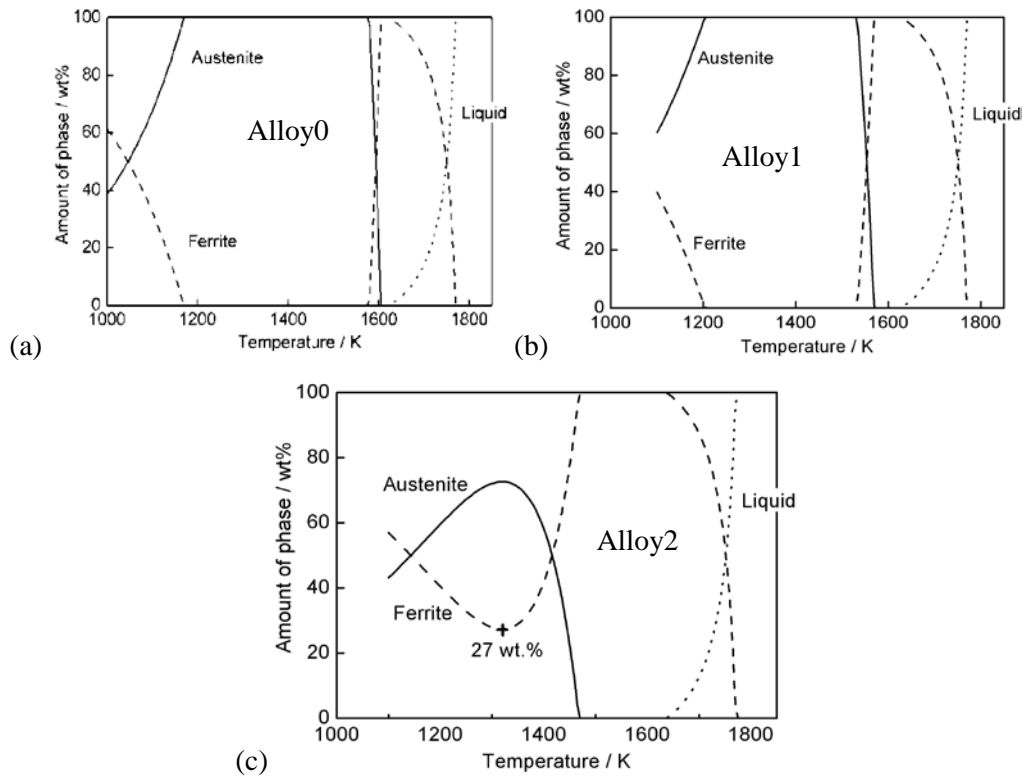


Figure 2.10: Calculated phase percentages as a function of temperature in para equilibrium. (a) Alloy 0. (b) Alloy 1. (c) Alloy 2.

2.5 Kinetic Simulations

The experimental observations indicate that the microstructure obtained is inconsistent with equilibrium, and that para equilibrium solid-state transformation may explain the excessive amount of austenite obtained. To confirm this, simulations have been conducted using DICTRA combined with thermodynamics database TCFE (version 1.21) and mobility database MOB2, capable of dealing with diffusional growth in multicomponent systems given the availability of thermodynamic and atomic-mobility data [Ågren 1991,1992; Egnström. *et al.*, 1994; Borgenstam, *et al.*, 2000]. The scale of the microstructure selected for simulation is the approximate distance between δ -ferrite

dendrites, i.e., 100 μm . Since the cooling rate of the 34 kg ingots used is not known, we have assumed a slow rate of 20 K s^{-1} , which also is representative of many continuous casting operations. Figure 2.11 shows simulations on the one-dimensional solidification of a 100 μm bar with the average composition of Alloy 2. As expected, the austenite that forms during the course of solidification is rich in manganese and depleted in aluminium; this is consistent with the microanalytical data presented in Table 2.2 for location 4. Furthermore, the simulated concentrations averaged over the extent of this austenite are in reasonable quantitative agreement with the tabulated data for location 4. The major discrepancy is that the amount of austenite that formed did not increase significantly beyond about 12% at 1500 K (Figure 2.11 a). The experiments described earlier suggest much larger austenite content. Allowing partitioning of all solutes does not therefore explain the observations even at the slow cooling rate used. To assess the alternative scenario that more austenite may form via a mechanism which does not result in the redistribution of substitutional solutes, a simulation was conducted on the limiting assumption that the δ -ferrite that remains at 1500 K, is permitted to undergo para equilibrium transformation into austenite. However, para equilibrium transformation does not occur before approximately 1400 K is reached because of a lack of sufficient driving force.

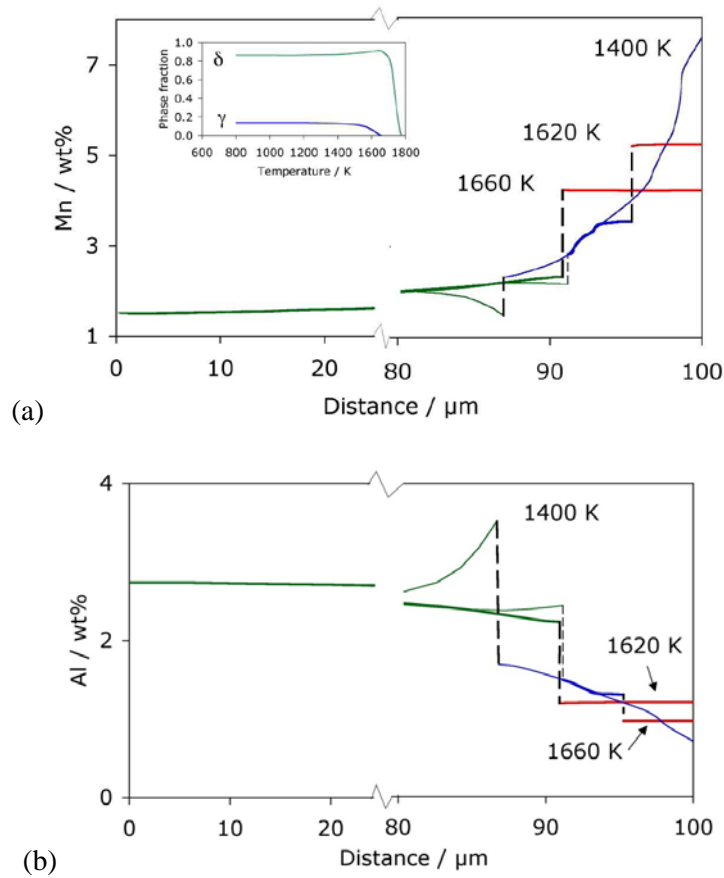


Figure 2.11: Simulation of the solidification of a 100 μm bar at 20 K s^{-1} with cooling beginning from 1800 K. Red represents liquid, green the δ -ferrite and blue, austenite. The vertical dashed lines represent interface positions. (a) Distribution of manganese. The inset shows how the phase fractions evolve with time. (b) Distribution of aluminium.

To do this, the composition of the δ -ferrite was taken to be the average of that remaining at 1500 K to do a DICTRA para equilibrium simulation. The simulation size set to 40 μm to account for the reduced region available for further austenite to form, and allowing for the fact that growth is expected from both the adjacent δ -ferrite regions. The composition used was therefore, Fe-0.325C-0.21Si-1.8Mn-2.62Al wt% and the

computation was initiated with a thin ($0.001 \mu\text{m}$) layer of austenite of the same composition as the ferrite. The results shown in Figure 2.12 are fascinating in that they prove that it is quite feasible for excess austenite to form at the slow cooling rate of 20 K s^{-1} .

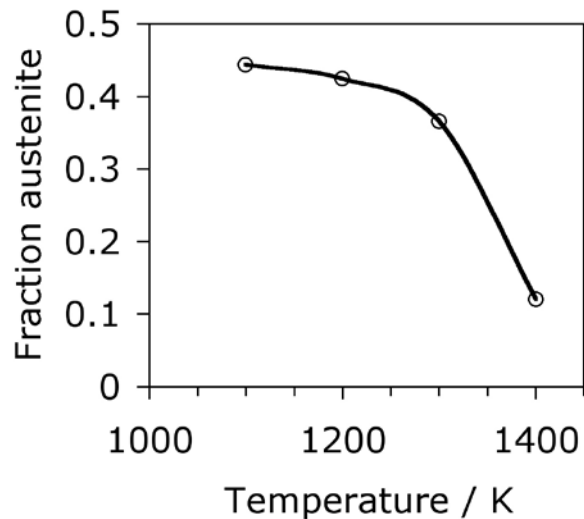


Figure 2.12: A kinetic calculation of the austenite fraction as a function of temperature

It is emphasized again, that the para equilibrium calculation is a limiting estimate since the real process can be anywhere between local equilibrium and local para equilibrium. The interpretation presented here explains not only the heterogeneous nature of the austenite by differentiating that which forms during solidification and the subsequent solid-state transformation under conditions where partitioning does not follow expectations from local equilibrium at the advancing interfaces.

2.6 Conclusions

Based on the equilibrium phase diagram, the most significant alloying element to stabilize δ -ferrite is aluminium, which for kinetic reasons has to be as high as 2.49 wt% to retain substantial amounts of δ -ferrite. Even then, the amount retained is less than

expected from equilibrium. For the cooling rate considered, a lower aluminium content results in a final microstructure without δ -ferrite, consisting mainly of pearlite, and small quantities of allotriomorphic and Widmanstätten ferrite. It is concluded that this is because the austenite that forms during cooling by solid-state transformation, does so without the required partitioning of substitutional solutes. This is responsible for the diminished quantities of δ -ferrite found in the cast microstructures. This conclusion is supported by microanalytical data and through calculations of limiting phase diagrams based on para equilibrium rather than equilibrium. Kinetic simulations support the conclusion that there are two stages involved in the formation of austenite, first when the latter forms as a part of the solidification process, and then through solid-state transformation of ferrite under circumstances where the substitutional solutes do not partition as expected from a local equilibrium condition at the transformation front. This explains the excessive amount of austenite obtained when compared with the equilibrium phase diagram.

Chapter 3 Stabilisation of Ferrite in Hot-rolled Process

3.1 Introduction

A transformation-induced plasticity steel is based on an unconventional microstructure in which the major constituent is δ -ferrite, which forms during solidification and is permanently retained after solidification [Chatterjee *et al.*, 2007]. The rest of the structure can be transformed into a mixture of bainitic ferrite and austenite, which is stabilised by the partitioning of carbon between these two allotropic forms of iron. It is this austenite, which behaves as in conventional TRIP assisted steels, and undergoes deformation induced transformation to martensite and, as a result, enhances the ductility of the alloy. Hence, the acronym TRIP, which stands for transformation-induced plasticity [Gerberich *et al.*, 1970]. The steel has interesting properties in its as-cast state: an ultimate tensile strength of ~ 1000 MPa and a total elongation, almost all of which is uniform, of 23%.

There is a difficulty with the alloy design. In spite of cooling rates as slow as $\sim 20 \text{ K s}^{-1}$, solid state transformation after solidification is completed exhibits large deviations from equilibrium conditions. Compositions which should, according to phase diagram calculations, show large quantities of δ -ferrite dendrites, often display zero or much reduced fractions on casting. This is because the austenite that forms during cooling by the solid state transformation of cored δ -dendrites does so without the required partitioning of substitutional solutes, particularly aluminium.

It is important in the δ -TRIP concept to maintain, as far as is possible, the ferrite produced during solidification because its presence at all temperatures should improve

its resistance spot weldability. If the material fails to become fully austenitic in the heat affected zone (HAZ), then it also becomes impossible to obtain a fully martensitic structure there. This should result in better welds because large gradients in properties in the affected region are known to dramatically reduce the shear resistance of spot welds [Santella, *et al.*, 1999]. Indeed, current TRIP assisted steels are known to be difficult to spot weld because of the production of fully martensitic regions in the HAZ.

The problem of retaining the δ -ferrite can, of course, be solved by adding aluminium in concentrations greater than required by equilibrium. This increases the fraction of δ -ferrite in the cast structure, even in the absence of equilibrium partitioning. However, it is necessary to examine the stability of the δ -ferrite also in the reheated condition since the casting must ultimately be hot rolled in order to produce the form required for potential applications, such as in the car industry.

The purpose of the work presented in this chapter is to assess the capability of the alloy system to sustain the ferrite during the reheating required for the hot rolling process, which is usually in the range 1200-900 °C. It is hoped that the work will form the basis of a future development programme, where the steel can be produced by hot rolling with the required quantity of ferrite, followed by the formation of the mixture of bainitic ferrite and retained austenite in a continuous process.

3.2 Experimental

The ingot manufacture and microscopy observations are referred in Chapter 2.2 and 2.3. The ingot was reheated to 1200 °C for rough rolling to make 25-30 mm slabs followed by air cooling. These slabs were then reheated to 1200 °C (heating rate to 1200 °C not monitored) and hot rolled to 3 mm in thickness with the temperature always maintained above 900 °C followed by cooling. Heat treatments were conducted on cylindrical

dilatometric samples of as-cast alloys of diameter 3 mm and length 10 mm using a push rod ‘BAHR DIL805’ high speed dilatometer with radio frequency induction heating; the equipment has been described elsewhere [Yang and Bhadeshia, 2007].

Table 3.1: Compositions achieved during manufacture, wt%.

	Alloy 3		Alloy 4		Alloy 5		Alloy 6		Alloy 7	
	D	A	D	A	D	A	D	A	D	A
C	0.4	0.40	0.4	0.40	0.4	0.41	0.4	0.37	0.4	0.39
Si	0.25	0.26	0.75	0.74	0.25	0.26	0.75	0.76	0.75	0.77
Mn	2.0	2.02	2.0	1.99	1.5	1.53	1.5	1.53	1.5	1.50
Al	2.5	2.50	2.5	2.39	2.5	2.30	3.0	2.91	3.5	3.35
Cu	0	0	0.5	0.49	0.5	0.49	-	-	-	-
P	0.02	0.02	0.02	0.02	0.02	0.02	-	-	-	-
S	-	0.0013	-	0.0015	-	0.0014	-	0.0042	-	0.0045
N	-	0.0032	-	0.0024	-	0.0030	-	0.0020	-	0.0022

The sample temperature is measured by a thermocouple welded to its surface using a precision welder and jig supplied by the dilatometer manufacturer. The cast structure of the alloy identified as ‘Alloy 2’ in Table 3.1 has been investigated in the Chapter 2. The alloy is new melt of the original δ -TRIP design, needed to provide more material for experiments.

3.3 Reheating experiments

The microstructure of the as-cast state of Alloy 2 (Table 2.1) is illustrated in Figure 2.2 and Figure 2.4 of Chapter 2, along with the calculated equilibrium phase diagram, which indicated that a large fraction of the δ -dendrites generated during solidification should, under equilibrium conditions, persist during reheating at all temperatures. Samples of the steel were heated at 20°C s^{-1} to peak temperatures of 800, 850, 900, 1000, 1100 and 1290°C for 5 min; further samples were similarly heated to 1360, 1380 and 1400°C for 1 min. After the small holding period, the samples were all quenched at -80°C s^{-1} . The

heat treatments were conducted on the dilatometer. The heating rate and transformation times used here will be different from those practised in an industrial environment, but the difference is unlikely to be significant given the rapid rate of austenite formation at high temperatures.

Metallographic studies were conducted on all the samples, but only selected examples are presented here. Figure 3.1a shows the effect of heating to 800 °C; there is clear evidence for the partial transformation of pearlite into austenite, so that quenching leads to martensite in the centres of the interdendritic regions, where austenite stabilising elements are partitioned. The austenite that forms from pearlite then begins to penetrate the δ -dendrites. The amount of austenite obtained is inconsistent with the equilibrium phase diagram (Figure 2.2), although these observations are not surprising given that the austenite grows without the required level of solute partitioning between the parent and product phases. By 950 °C, the δ -dendrite arms are no longer visible as uniform features, but on a microscopic scale, consist of martensite and remnants of ferrite, which are in the form of a network, presumably reflecting segregation patterns (Figure 3.1b).

The sample heat treated to a peak temperature of 1100 °C became almost fully austenitic, although the overall structure remained fine because of the pinning of austenite grain boundaries by remnants of ferrite (Figure 3.2a). The ferrite content only recovered slightly when the peak temperature reached 1400 °C, in a form reminiscent of the δ -ferrite, presumably following the solidification induced chemical segregation patterns existing in the sample.

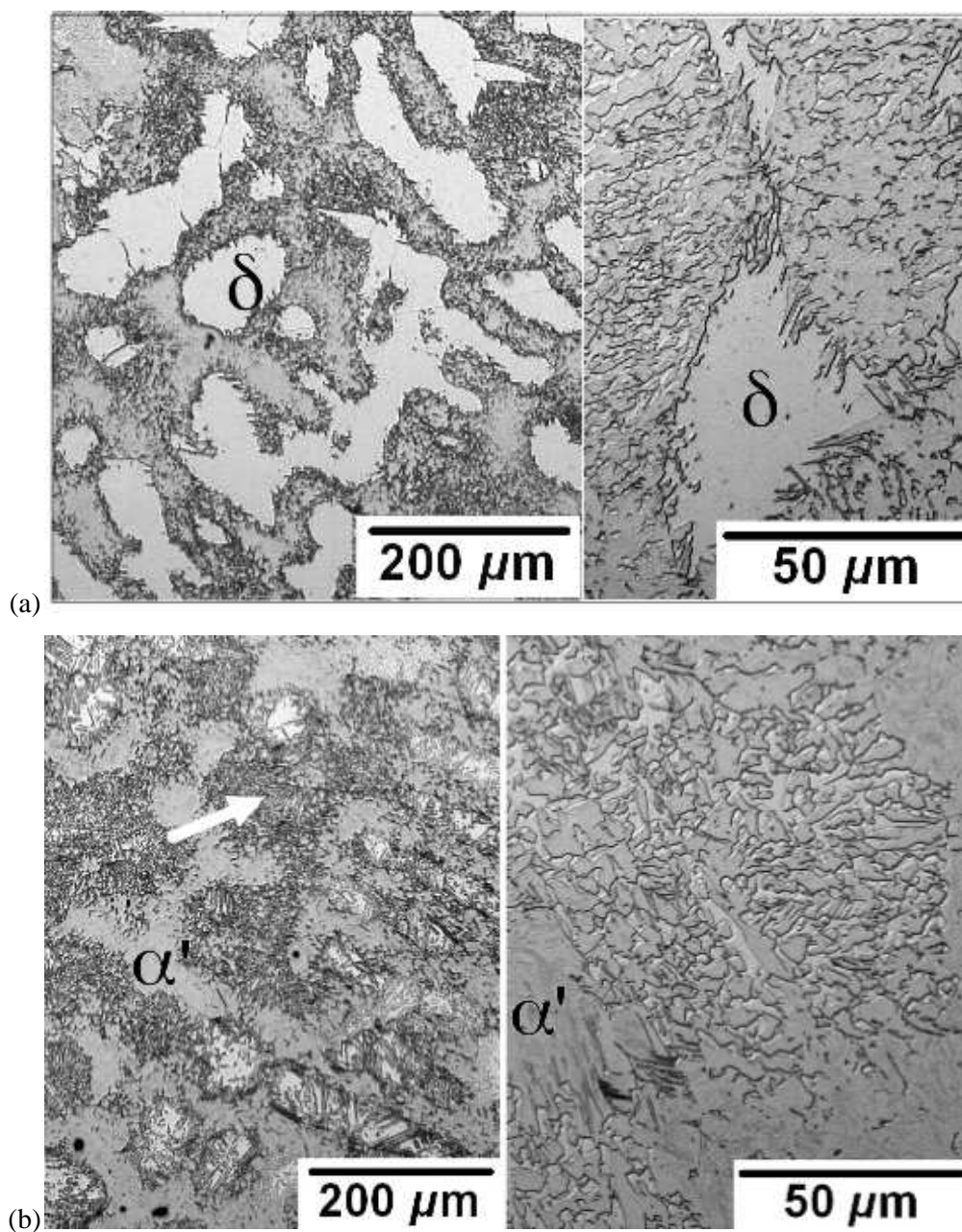


Figure 3.1: Alloy 2. (a) Heated to 800 °C and quenched. The light-etching regions represent dendrites and the darker regions are mixtures of martensite (austenite at 800°C) and ferrite. (b) Heated to 900 °C and quenched. The arrow shows that the region which used to be the δ -ferrite, and which is now a mixture of martensite and residual ferrite.

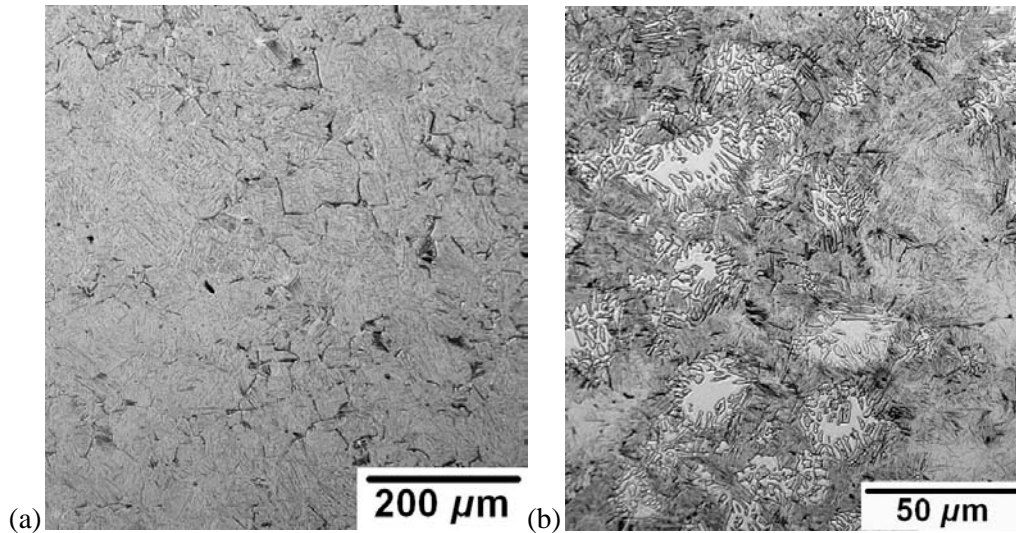


Figure 3.2: Alloy 2. (a) Heated to 1100 °C and quenched. (b) Heated to 1400 °C and quenched. The arrow indicates a ferrite forming in segregated regions of the sample, in shapes reminiscent of the solidification structure.

It is evident the alloy would not be suitable for a process in which substantial δ -ferrite must be retained in the microstructure during the hot rolling process, even though the equilibrium phase diagram suggests otherwise. These large deviations from expectation make it difficult to design suitable alloys; in Chapter 2, DICTRA was used, which allows growth to be modeled, to establish that the magnitudes of the kinetic effects are reasonable, but the method requires assumptions about shape and scale, which make its use for alloy design in the present context difficult. Therefore, a pragmatic approach was adopted in which new alloys were designed based essentially on experience, with the broad aim of stabilising the ferrite.

3.4 New alloys

Referring to Table 3.1 and using Alloy 2 as a reference, Alloy 3 is based on the removal of copper, which is an austenite stabilising element. The silicon concentration is

increased in Alloy 4 since both aluminium and silicon [Bentle and Fishel, 1956] have the same c-loop forming tendency and hence favour the formation of δ -ferrite. Alloy 5 is based on a reduction in the manganese concentration and Alloy 6 is based on a simultaneous reduction in Mn and increase in the silicon and aluminium concentrations. Alloy 7 has a lower Mn, high Si and particularly high Al concentrations. Phase diagram calculations for the new alloys are illustrated in Figure 3.3, which shows that the greatest potential for increasing the stability of δ -ferrite should be in Alloy 6 and Alloy 7. The microstructures in as-cast conditions are shown in Figure 3.4.

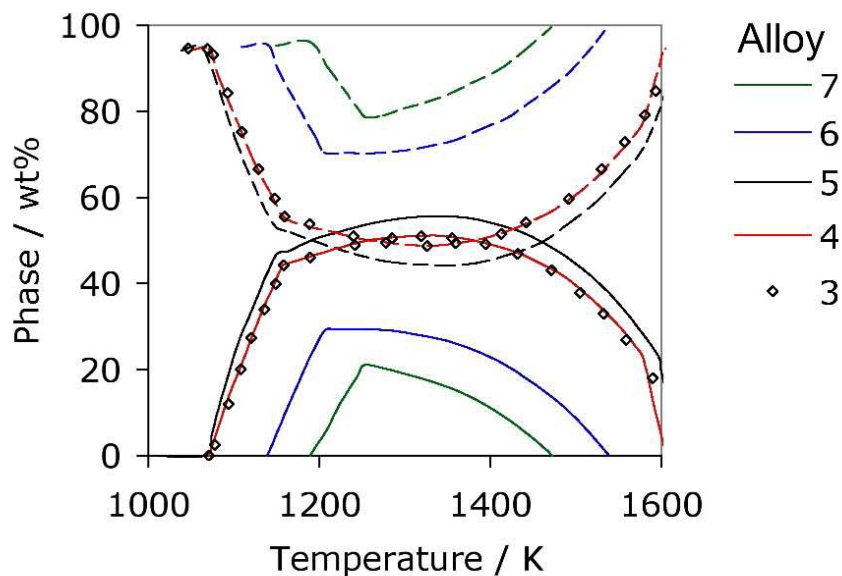


Figure 3.3: Calculated quantities of austenite (continuous lines) and ferrite (dashed lines). Alloy 3 is plotted as points in order to avoid confusion with Alloy 4. Although only austenite and ferrite are illustrated for clarity, the liquid and cementite phases were allowed to exist.

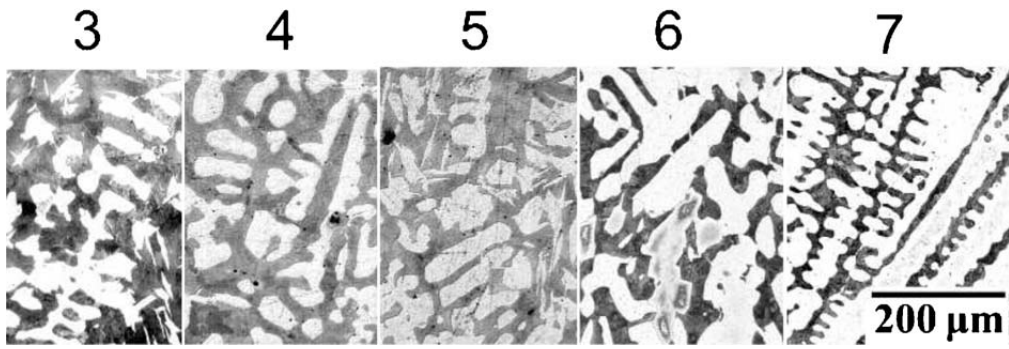


Figure 3.4: As-cast microstructures of Alloy 3-Alloy 7

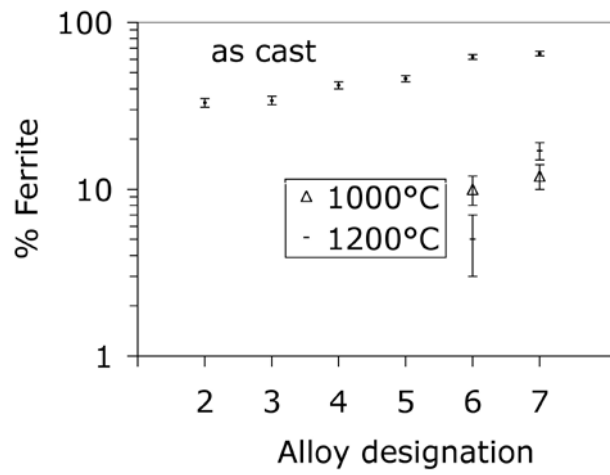


Figure 3.5: Volume percent of optically resolvable ferrite for cast and reheated samples.

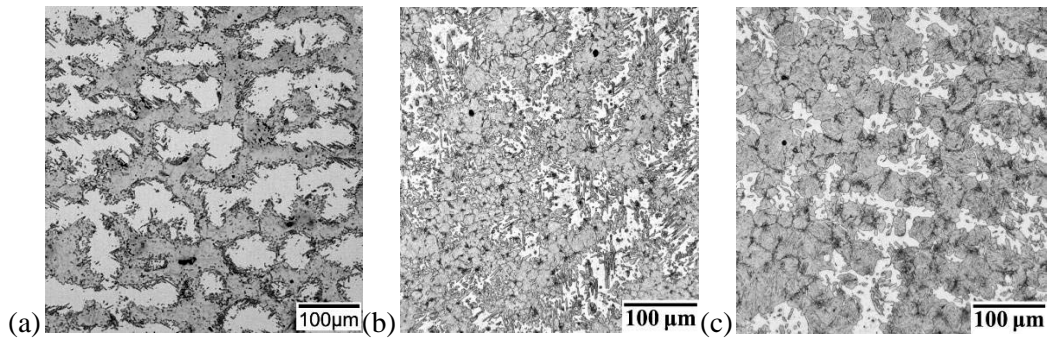


Figure 3.6: Alloy 7 following reheating to (a) 900 °C, (b) 1000 °C, (c) 1200 °C.

Reheating experiments were conducted as described for Alloy 2, and quantitative

data are presented in Figure 3.5. δ -ferrite did not persist in Alloy 2-5 on reheating, but dendrites of this phase survived in Alloy 6 and Alloy 7, although the fraction of δ -ferrite is much less than expected from equilibrium (Figure 3.6). The microstructure after hot rolling is illustrated in Figure 3.7, where it is evident that there are two kinds of ferrite present: the first, the δ -ferrite, which has been elongated by deformation and then the allotriomorphic ferrite, which precipitates as the temperature during rolling reduces towards 900 °C. It is seen that the presence of ferrite at all temperatures maintains a fine austenite and ferrite grain structure.

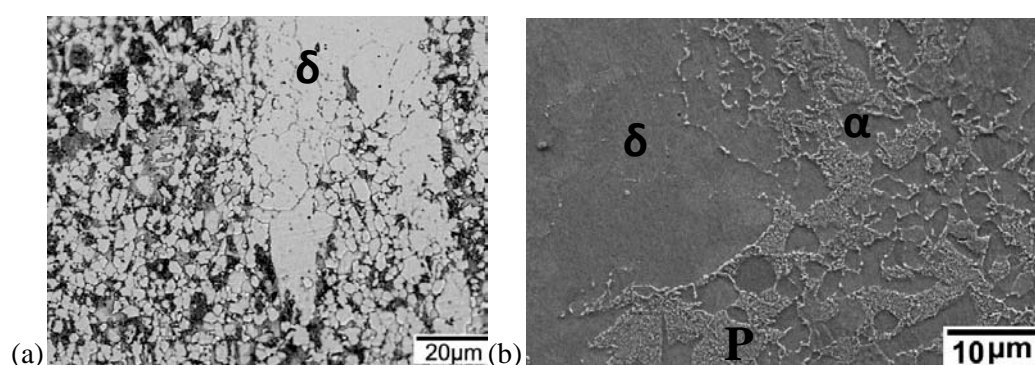


Figure 3.7: Alloy 7 after hot-rolling, (a) optical, (b) SEM

3.5 Conclusions

The δ -TRIP alloy system is based on the use of a relatively large concentration of aluminium, which should lead to the formation of a substantial quantity of ferrite dendrites at equilibrium. Much of this ferrite, which forms during solidification, should, in principle, resist transformation into austenite, when the steel is heated to the high temperatures typical of hot rolling deformation. That it does not do so in practice has been shown in previous work to be due to the fact that austenite is able to form by solid state transformation from δ -ferrite without the required level of partitioning of solutes, particularly aluminium. In the present work, it has been demonstrated that suitable

alloys, in which the δ -ferrite remains in the microstructure over the range 900-1200 °C, have been designed by increasing the aluminium and silicon concentrations, accompanied by a reduction in the manganese and copper contents. It has been possible, therefore, to produce a rolled variant of the alloy, which will be used in further investigations towards the commercialisation of the steel on a continuous production line.

Chapter 4 Extraordinary Ductility in Al-bearing δ -TRIP Steel

4.1 Introduction

There is a huge variety of steels available and many of these result in similar properties but are produced to satisfy particular requirements of cost, weldability, and design criteria [Joo *et al.*, 2009]. This overlap of properties is evident also in the formable alloys designed for the automotive industries, although an examination of Figure 4.1 shows that the distribution is not uniform; there are significant gaps at intermediate strength and ductility combinations, and when the strength exceeds about 1200 MPa. There already is research in progress on the stronger steels in order to enhance ductility and assess other engineering properties [Bhadeshia 2010; Edmonds *et al.*, 2006; Fan *et al.*, 2009a, b; Naderi 2007]. The same attention has not been paid to alloys which have a strength of 600-700MPa and at the same time exhibit elongations in excess of 30% since these materials are typically formed into components. Although the so-called TWIP steels fulfill these requirements, they are relatively expensive to manufacture and apply.

It is interesting in this context to explore the recent proposal of δ -TRIP steel in which the alloy is designed to retain a large quantity of δ -ferrite at all temperatures, with the residual microstructure consisting of a mixture of bainitic ferrite and retained austenite [Chatterjee *et al.*, 2007; Yi *et al.*, 2010a, b]. The δ -ferrite substitutes for the allotriomorphic ferrite that is normally introduced into TRIP-assisted steels by intercritical annealing or continuous cooling transformation [DeCooman 2004; Jacques 2004; Matsumura *et al.*, 1987a, b; Sakuma *et al.*, 1991a, b]. There are advantages to this, for example, that a fully martensitic structure cannot be produced in the heat-affected zone of a resistance spot weld. The steel also relies more on aluminium

rather than silicon to suppress the formation of cementite, which helps avoid the problem of the adherent fayalite scale [Fukagawa *et al.*, 1994; Okada *et al.*, 1995; Raman 2006] that forms on the surface during hot-rolling.

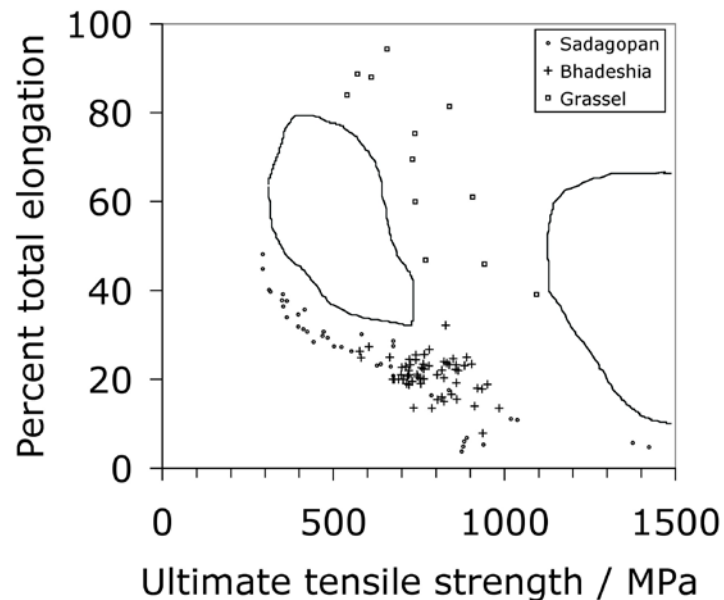


Figure 4.1: An illustration of the range of strength and elongation combinations available for automotive steels; data compiled from Sadagopan *et al.* [2003] on TRIP-assisted, dual phase, interstitial-free steels, from Grässel *et al.*, TWIP steels [2000] and from Bhadeshia [2001] on TRIP-assisted steels. Two domains are marked indicating combinations of properties which are not readily accessible.

The δ -TRIP steel has been demonstrated in the cast state to have an ultimate tensile strength of about 1000MPa and an elongation of 27% [Chatterjee *et al.*, 2007]. Subsequent experiments highlighted the fact that the alloy system is sensitive to non-equilibrium solidification which meant that δ -ferrite could not be reliably retained in the microstructure. Further intense research was necessary in order to characterise the transformation behaviour during and after hot-rolling in the two-phase field; the rolling

deformation is necessary to apply the steel in sheet form for use in the manufacture of automobiles. In the present work we report for the first time, some exciting mechanical property data for what we believe is a complete alloy design of a type consistent with large-scale manufacture.

4.2 Experimental

The alloy design procedures involving phase diagram calculations basically help ensure the presence of δ -ferrite under equilibrium conditions, at all temperatures in the solid state. Aluminium plays a key role in this and experience based on experiments has indicated that such calculations overestimate the amount of δ -ferrite expected when the real alloys solidify during casting under conditions which deviate from equilibrium. Therefore, the two alloys studied here (Table 4.1) have larger aluminium concentrations than in the Chapter 2.

Table 4.1: Chemical compositions (wt%) of the new alloys manufactured.

	C	Si	Mn	Al
Alloy 8	0.40	0.22	1.03	2.95
Alloy 9	0.39	0.21	0.51	3.84

The 1.2 mm thick cold-rolled sheets were used for heat treatments and tensile tests, the cold rolling process was fulfilled after the hot rolling seen Chapter 3.2. The heat treatments outlined in Table 4.2 were conducted using 1.2×40×110 mm samples in a CCT-AY (ULVAC-RIKO) simulator where the samples are heated at 20 °C s⁻¹ in a nitrogen atmosphere to allow some austenite to form, followed by cooling at -20 °C s⁻¹ to the temperature where bainitic ferrite is allowed to form, and finally at -10 °C s⁻¹ to ambient temperature. Samples for tensile tests were machined from these blanks to ASTM standard E8M-00 with elongation measured on a 10 mm gauge length following

tension at $3.3 \times 10^{-3} \text{ s}^{-1}$. All the mechanical data presented in this chapter represent the average of three tests; the reproducibility was excellent with the elongation varying by no more than $\pm 2\%$ and the strength by $\pm 5\text{MPa}$.

Table 4.2: Intercritical annealing and isothermal transformation heat treatments implemented on simulator. T and t stand for temperature and time respectively, V_{HR} and V_{IA} the fractions of $(\delta + \alpha)$ ferrite present in the microstructure in the hot-rolled and intercritically annealed conditions respectively. The values of V_{HR} for Alloy 8 and Alloy 9 are 0.71 ± 0.09 and 0.86 ± 0.02 respectively. The volume fractions were measured using point counting on scanning electron micrographs. ε_U and ε_T stand for uniform and total elongations in percent, respectively, and UTS for the ultimate tensile strength / MPa.

Intercritical		Isothermal		Alloy 8		Alloy 9		Alloy 8			Alloy 9			
$T / ^\circ\text{C}$	t / s	$T / ^\circ\text{C}$	t / s	V_{IA}	V_{IA}	ε_U	ε_T	UTS	ε_U	ε_T	UTS			
		350	1200			28	37	710	28	37	647			
850	180	400	600	0.66 ± 0.07	0.77 ± 0.08	34	43	709	31	41	648			
		450	120			33	40	740	32	41	661			
		350	1200			25	34	711	26	38	639			
		400	300			29	37	712	30	40	639			
950	180	400	600	0.69 ± 0.05	0.75 ± 0.07	30	39	688	30	41	622			
		400	900			29	38	693	29	40	629			
		450	120			30	38	725	31	40	649			

Microstructural evolution was studied using samples $2 \times 3 \times 10$ mm on a dilatometer described elsewhere [Pak *et al.*, 2008]. X-ray diffraction was done on metallographically prepared samples etched using 2% nital in order to remove any deformed surface, with Cu K α with Cu K α radiation with the data subjected to Rietveld analysis [Hill and Howard, 1987] and refinement [Rietveld 1967, 1969]. The austenite lattice parameter thus obtained was used to estimate the concentration of carbon using a published

equation [Dyson and Holmes, 1970].

Most phases could easily be identified using scanning electron microscopy. The austenite regions stand proud of the surface, and the bainite is in the form of sheaves which appear at these magnifications as plates. The δ -ferrite is given away by its coarse scale whereas the allotriomorphic ferrite appears as finer equiaxed grains. Pearlite present in the hot-rolled samples (without subsequent heat treatment) appears with dark contrast because the cementite and ferrite phases are intimately mixed. Martensite that forms during deformation could not be resolved but its presence is deduced from the decrease in the retained austenite content as measured using X-ray diffraction.

4.3 Microstructure

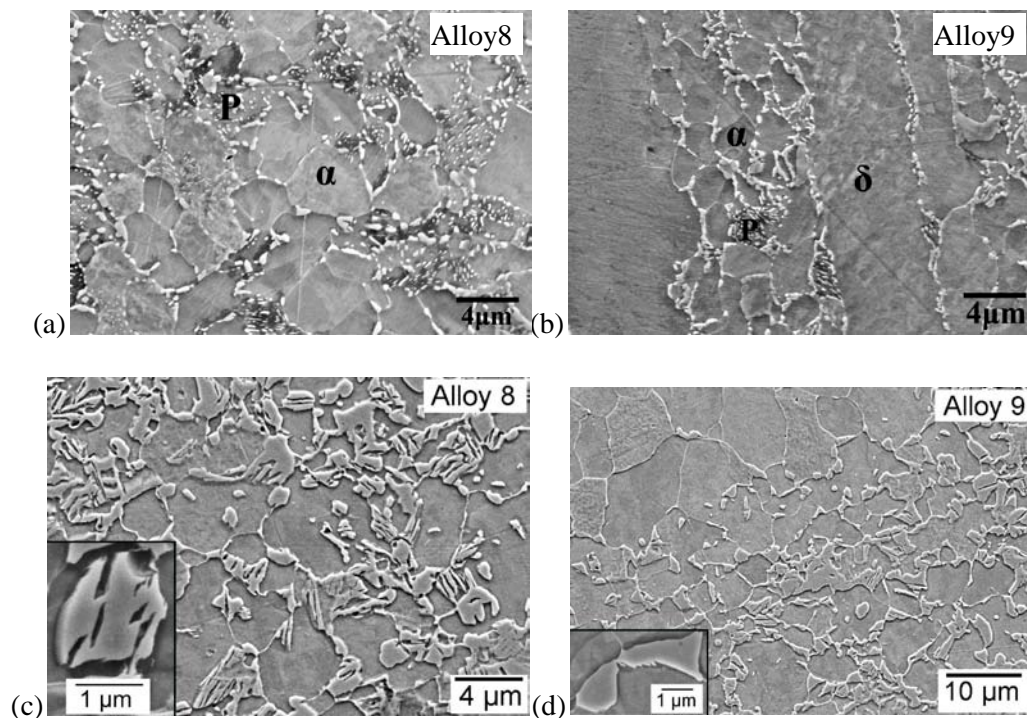


Figure 4.2: Microstructures in the hot-rolled (a, b) and heat-treated conditions (c, d). The heat treatment for the samples illustrated in (c, d) consisted of an intercritical anneal at

850 °C followed by isothermal holding at 400 °C for 600 s. Note that (d) is presented at a lower magnification to show that the relatively featureless region on the top-left corresponds to retained δ -ferrite.

The microstructure of the alloys in the hot-rolled condition is illustrated in Figure 4.2a,b, where δ -ferrite and α -ferrite is distinguished simply by identifying the former as having been retained from solidification and has persisted through the hot-deformation, whereas the α is a result of transformation from austenite. None of the δ -ferrite is retained in the microstructure of Alloy 8 which becomes fully austenitic during hot-rolling, resulting in a final microstructure of equiaxed grains of α ferrite and somewhat discontinuous pearlite. In contrast, Alloy 9, which contains more aluminium and less manganese, has the coarse elongated regions of ferrite which represents the δ -phase. The influence of composition is also reflected in the quantitative data given in Table 4.2 where the total fraction of ($\delta + \alpha$) is seen to be greater in Alloy 9.

Metallography was conducted on all of the heat-treated samples listed in Table 4.2 but only a few representative results are illustrated in Figure 4.2c,d for the particular case where the intercritical anneal was at 850 °C followed by isothermal transformation at 400 °C for 600 s. For the discussion below, the terms V_{HR} and V_{IA} represent the fractions of ($\delta + \alpha$) ferrite present in the microstructure in the hot-rolled and intercritically annealed conditions respectively.

Alloy 8 following heat treatment consists of fine and equiaxed allotriomorphic ferrite grains together with islands of retained austenite containing regions of bainitic ferrite. The intercritical annealing temperature is not high enough to fully austenitise the material so the total fraction of allotriomorphic ferrite has decreased only a little from $V_{HR} = 0.71 \pm 0.09$ in the hot-rolled state to $V_{IA} = 0.66 \pm 0.07$ - this general observation

is essentially correct for both alloys and intercritical annealing temperatures studied, as can be seen in Table 4.2. Retained austenite measurements are discussed in the next section.

Alloy 9 differs in that there is a mixture of the δ -ferrite together with allotriomorphic ferrite; the overall fraction of ferrite is larger by about 0.1 volume fraction, as expected from the composition difference relative to Alloy 8 (Table 4.2). The quantity of bainite within the retained austenite is also much smaller, because of the greater stabilisation of the residual austenite by carbon partitioned from the ($\delta + \alpha$). Most of the islands of austenite were featureless at high magnification, Figure 4. 2d.

4.4 Deformation

A summary of the mechanical properties obtained is presented in Figure 4.3 with the details listed in Table 4.2. The strength-elongation combination is impressive for all the heat-treatments applied, and approaches that of the high-Mn TWIP steels [Frommeyer *et al.*, 2003; Grässel *et al.*, 2000] which are more challenging to produce and apply. The data also fall in a domain which is not occupied by other automotive steels and furthermore, the ductility is comparable to that of the much weaker interstitial-free steels [Bayraktar *et al.*, 2007; Hayat *et al.*, 2009; Mukhopadhyay *et al.*, 2009]. The alloy also outperforms TRIP and dual-phase steels at the same strength level.

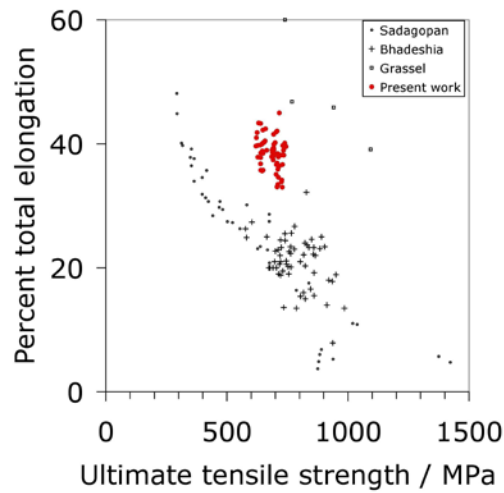


Figure 4.3: Summary of the mechanical properties obtained (red circles) in the context of published data (which are also illustrated in Figure 4.1 [Sadagopan *et al.*, 2003; Grassel *et al.*, 2000; Bhadeshia 2001]).

One reason for the large ductility observed is the presence of retained austenite in a form which transforms during deformation but has a stability which means that the transformation is gradual so that local stress concentrations which lead to damage can be accommodated to large strains. Figure 4.4 shows clearly that both the harder austenite [Furnemont *et al.*, 2002] which also contains the bainite, and the allotriomorphic and δ -ferrite deform in a compatible manner until final fracture occurs; the micrographs are taken in the close proximity ($\approx 1\text{mm}$) of the fracture surface and illustrate the elongation experienced by all the phases present.

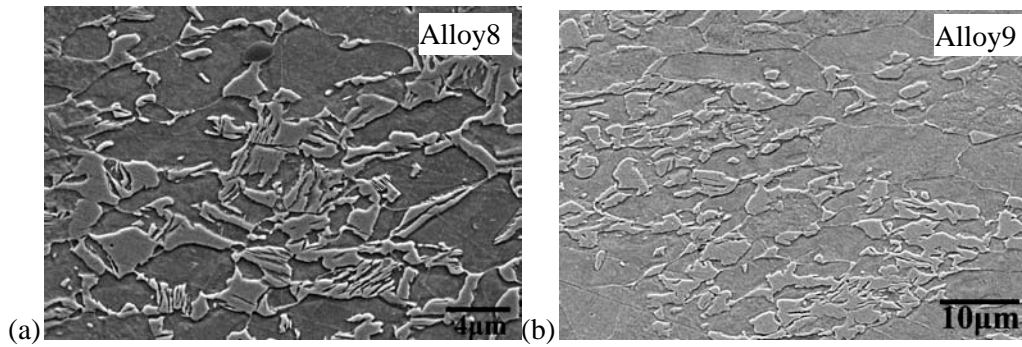


Figure 4.4: Micrographs taken from broken tensile specimens at locations about 1 mm away from the fracture surface. The samples were intercritically annealed at 850 °C followed by isothermal transformation at 400 °C for 600 s. (a) Alloy 8. (b) Alloy 9.

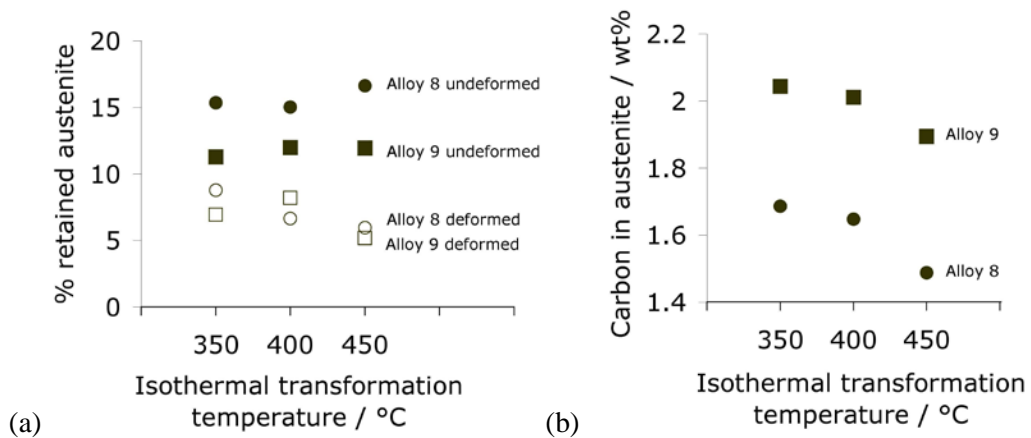


Figure 4.5: Data for samples intercritically annealed at 850 °C followed by isothermal transformation at the temperature indicated. (a) Retained austenite (with a maximum error of $\pm 0.30\%$ for 95% confidence). (b) Carbon concentration in the retained austenite.

Figure 4.5 shows the quantitative measurements of retained austenite both before and after deformation and it is evident that the austenite is reasonably stable given the large extent of plastic strain. The data also show that the austenite fraction is smaller in the case of Alloy 9, and its carbon concentration larger. This is because it contains a

greater aluminium and lower manganese concentration than Alloy 8, which means that a larger amount of ferrite is present at the intercritical annealing temperature (86% compared with the 71% in Alloy 7). The residual austenite is therefore enriched to a correspondingly greater degree due to the partitioning of carbon between the ferrite and austenite.

It should also be noted that the stability of the austenite increases if it survives the initial plastic strains and stresses, because the defect structure introduced during deformation can mechanically stabilise it to martensitic transformation [Chatterjee *et al.*, 2006; Fiedler *et al.*, 1955; Leslie and Miller, 1964; Machlin and Cohen, 1951].

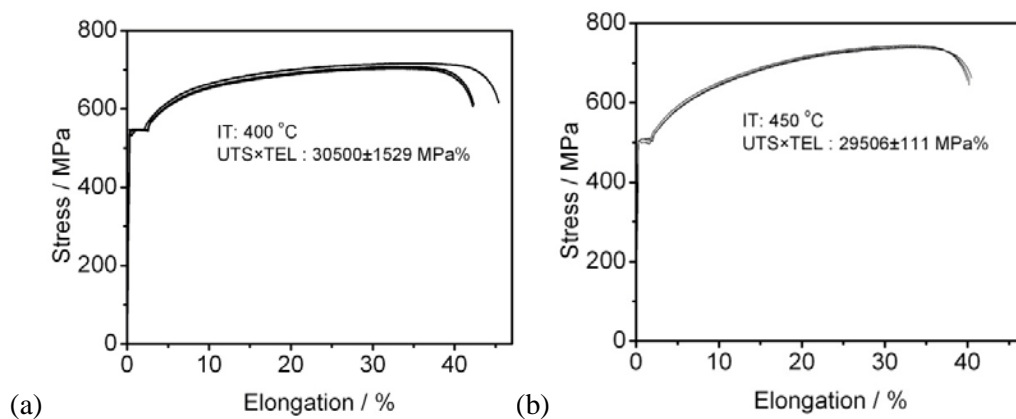


Figure 4.6: Typical tensile test data for Alloy 8 intercritically annealed at 850 °C for 180 s followed by isothermal transformation at (a) 400 °C for 600 s and (b) 450 °C for 120 s.

Alloy 8 in general shows better ductility than Alloy 9, presumably because of its finer structure. As pointed out earlier, the former becomes fully austenitic during Hot-rolling so that the coarse regions of δ -ferrite which exist in Alloy 9 are absent. Even though Alloy 8 in its final state does not fit the general concept of δ -TRIP steels, the work suggests that the properties of steels which do retain the δ -ferrite could be improved by refining this phase. This could be achieved by controlling the solidification

rate or by enhanced deformation during hot-rolling. This latter procedure would be practical when dealing with large castings than in the present work where small quantities of experimental alloys were fabricated.

Tensile curves for Alloy 8 are illustrated in Figure 4.6 showing a form consistent with the requirements of automotive steels; the small initial elongation at constant stress did not lead to any observable Lüders bands on the tensile specimen surfaces. It is not clear whether this would become an issue in the context of industrial production as opposed to the present laboratory experiments. Notice also the excellent reproducibility of the tests.

A detailed examination of the tensile data (Table 4.2) shows that the time at the isothermal transformation temperature does not significantly influence the mechanical properties, probably because the amount of bainite produced is rather small given the large carbon concentration of the austenite. It would be interesting in future work to eliminate the isothermal step altogether and assess the resulting properties.

4.5 Conclusions

A novel alloy system based on the concept of stabilising ferrite in the microstructure using aluminium as an alloying element has been found to exhibit promising combinations of tensile strength and elongation. These properties fall in a domain which is not represented by other commercially available or experimental steels designed for the automobile production.

The heat-treatments necessary to achieve the microstructure involve intercritical annealing followed by isothermal transformation at temperatures and time periods which are consistent with large scale production on the so-called continuous annealing

facilities [Yanagishima *et al.*, 1983]. The isothermal transformation can even be conducted at 450 °C which is compatible with a final galvanising treatment.

Chapter 6 will investigate the spot-welding characteristics; the key feature of the alloy design in this respect is that δ -ferrite can be retained permanently in the microstructure so that fully martensitic regions are not produced in the heat-affected zone of the spot weld.

Chapter 5 Mechanical Stabilisation of Retained Austenite

Excellent mechanical performance has been achieved in this research. Except the role of retained austenite playing as TRIP effect, its plastic deformation is found to contribute to the overall mechanical behavior by the composite effect as well. Mechanical stabilisation is a well known phenomenon for austenite. It has never before been discussed but as shown later, it plays a significant role in the alloys described here. A physical model has been proposed for the estimation of mechanical stabilisation and the result is consistent with experimental observations. It explains why retained austenite cannot transform fully into martensite even at very large plastic strains.

5.1 Introduction

δ -TRIP steel has a remarkable combination of strength and uniform ductility. This is attributed partly to the deformation-induced transformation of the retained austenite into martensite, resulting in an enhanced resistance to plastic instabilities [Chatterjee *et al.*, 2007]. Indeed, by tensile testing at 200 °C the alloys demonstrated that the consequent increase in the thermodynamic stability of the austenite led to a dramatic decrease in elongation without affecting strength. It is therefore well-known that considerable ductility can be obtained in spite of the high strength in TRIP-assisted steels. In addition to the elongation contributed from the dual phase effect, transformation plasticity plays a significant role for the extra elongation compared with dual phase steels. This relies on the formation of martensite from austenite during deformation, where the external mechanical free energy due to stress can compliment the inadequate chemical free energy change [Chatterjee *et al.*, 2007b]. On the other hand, mechanical stabilisation, a well known phenomenon for martensitic transformation [Chatterjee *et al.*, 2006a], may

play a role if the austenite does not transform until large plastic strains are achieved. Although the mechanical stabilisation is a well-established phenomenon [Fiedler *et al.*, 1955; Leslie and Miller, 1964; Machlin and Cohen, 1951], it has not previously been considered in TRIP-assisted steels.

The purpose of this research was to examine the mechanical stabilisation of retained austenite in δ -TRIP steel. The contribution of deformation of ductile austenite on the overall elongation is also been discussed.

5.2 Experimental

The hot-rolled alloy (Alloy 5) was manufactured as in Chapter 3.2 and its composition is listed in Table 3.1. Tensile specimens were soaked in a box furnace for intercritical annealing at 800 °C for 10 min, and then quenched and isothermally held in a salt bath at 330 °C for 30 min for bainitic transformation, followed by air cooling. The tensile tests and X-ray diffraction analysis were performed as in Chapter 4.2.

5.3 Mechanical behavior and microstructure

Table 5.1: Mechanical properties of alloy.

Strength / MPa		Elongation / %		UTS × TEL
YS	UTS	UEL	TEL	/ MPa %
573.3	881.7	31.4	37.7	33,247
540.9	880.3	30.7	37.4	32,940
535.9	893.5	30.6	36.6	32,691

This alloy exhibited excellent mechanical property (Table 5.1): UTS×TEL ~ 33,000 MPa %, which is much better than all the commercial automotive steel at comparable strength. It is even comparable with the best TRIP-assisted steels produced in laboratory experiments (Typical composition: Fe-0.4C-1.5Si-1.5Mn wt% [Matsumura

et al., 1987a, b)], alloys which have yet to be commercialized.

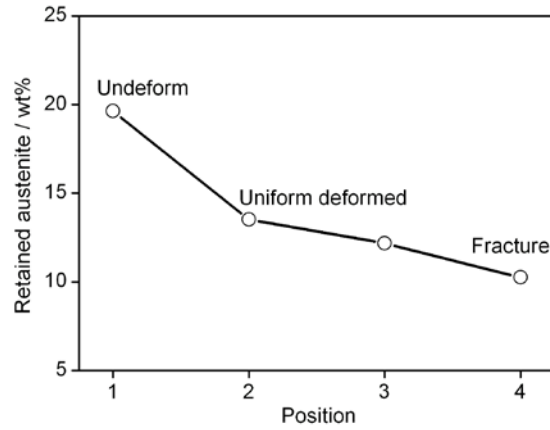


Figure 5.1: Retained austenite in different region

Table 5.2: Alloying element distribution in phases in heat-treated specimens, wt%

Phase	Al	Si	Mn	Cu
γ	2.56±0.14	0.32±0.08	1.87±0.17	0.55±0.13
α	3.13±0.05	0.40±0.06	1.15±0.05	0.44±0.06

As seen in Figure 5.1, the presence of 19.6±0.2 wt% retained austenite is revealed by X-ray diffraction analysis in the alloys before deformation, which contains about 1.33 wt% carbon estimated from the lattice parameter with the alloying elements in austenite in Table 5.2. 10.3±0.2 wt% of retained austenite persisted near the fracture surface of the tensile specimens. The gradual transformation of retained austenite to martensite during deformation is consistent with the contribution of TRIP to the overall mechanical behavior.

Although the TRIP effect is important, the transformation strains themselves can contribute at most 2% to the observed elongation given the small fraction of austenite present in these materials [Bhadeshia 2001]. The composite deformation behaviour of

the major phases as in phase steels contributes to the large uniform elongation of TRIP-assisted steels as well [Bhadeshia 2001; Jacques 2004]. The δ -TRIP alloy consists of ferrite (α), bainitic ferrite (α_b) and retained austenite (γ), including the blocky morphology formed by intercritical annealing and the films associated with bainitic transformation, as shown in Figure 5.2. As a consequence of deformation, the films of retained austenite clearly elongated to large strains probably consistent with the overall elongation (Figure 5.2a). This ductile deformation of austenite must contribute to the overall elongation a factor that has never been discussed in previous research on TRIP-assisted steels.

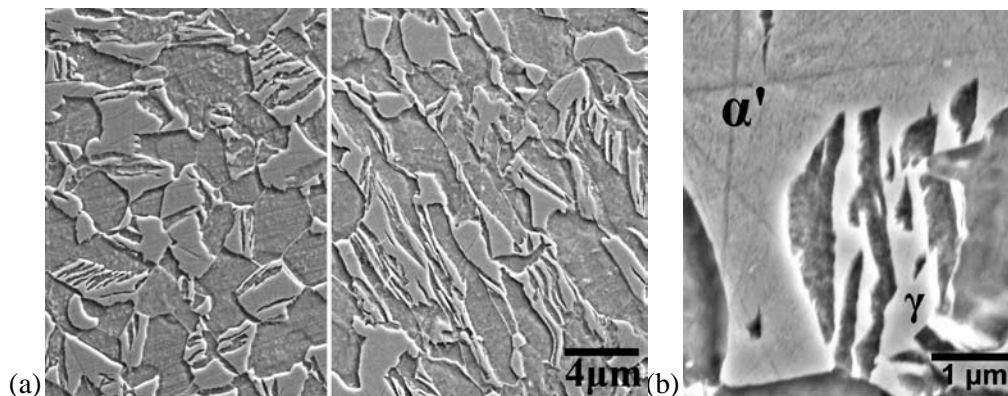


Figure 5.2: (a) Lath type retained austenite deformed plastically during tensile test, left-undeformed and right-necking region; (b) Martensite forming in blocky austenite (revealed as fold martensite plate) and austenite remaining untransformed in lath type one (revealed as clear surface).

5.4 Mechanical stabilisation of austenite in TRIP-assisted steels

Neutron diffraction has allowed the yield strength of individual phases in TRIP-assisted steel to be determined as 500 MPa, 650 MPa, 900 MPa and 2000MPa for ferrite, bainite, austenite and martensite, respectively [Furnémont *et al.*, 2002; Furnémont 2003]. Like

the behavior of dual phase steels, the application of stress at first causes yielding in the softer phase, ferrite, only. This explains the macroscopic yield strength is low, ~ 500 MPa. It is only after the ferrite has work hardened to be able to transfer sufficient load on to the stronger phases that the latter begins to deform plastically. When the stress on bainite becomes sufficiently high, it starts to deform. Then more load transfers onto the austenite, which might cause it to transform into martensite, or it might deform by slip. The resulting work hardening continues the process of slip or phase transformation. However, the stability of the austenite increases if it survives the initial plastic strains and stresses, because the defect structure introduced during deformation hinders the development of martensite. The films of austenite did not transform in contrast to the block morphology (Figure 5.2b). The stress concentrated on it should be very high due to the work hardening since it was elongated to large strains. It is postulated that the films are mechanically stabilised due to the defects introduced during deformation.

Martensitic transformation from austenite happens by the displacive transformation and involves the coordinated movement of atoms. In the case that sufficiently large strain exists in the austenite, the motion of glissile interfaces becomes impossible due to the high dislocation density, causing the transformation to halt. This is the essence of “mechanical stabilisation”. A theory for predicting the onset of mechanical stabilisation has been developed by balancing the force which drives the motion of the interface against the resistance of the dislocation debris created by the deformation of the austenite [Chatterjee *et al.*, 2006] as follows:

$$\tau_T = \phi \Delta G \quad (5.1)$$

where τ_T is the shear stress driving the motion of the interface, ϕ is a constant

assumed to be equal to unity, ΔG is the free energy change for the phase transformation. Mechanical stabilisation occurs when the stress driving the interface equals that opposing its motion as:

$$\tau_T = \tau + \tau_S \quad (5.2)$$

where τ is the opposing force from dislocation strengthening and τ_S is that from solid solution strengthening (solid solution hardening coefficients for a variety of solutes in austenite have been reported for tensile strength and were converted into shear stress equivalents τ_S using the Tresca criterion).

Combining Eqs. 5.1 and 5.2, we have

$$b\Delta G = \frac{1}{8\pi(1-\nu)} Gb^{3/2} \left(\frac{\varepsilon}{L}\right)^{1/2} + \tau_S b \quad (5.3)$$

where G is the shear modulus and ν the Poisson's ratio, b is the magnitude of Burgers vector, ε is the true strain and L is the average distance moved by the dislocations and $L = \delta D / (\delta + D\varepsilon)$ where D is the original grain size of austenite before straining, and δ is a coefficient equal to $\sim 1 \mu\text{m}$ [Barlat *et al.*, 2002].

In that model, the mechanical energy due to the composition of an external stress was not included in the driving force. The applied stress on austenite does supply the extra energy to drive the motion of interface and compensate for the shortage of chemical energy where the austenite is above its M_s temperature. The model has been modified here by including the mechanical energy as follows:

$$\Delta G = \Delta G_{Chem} + \Delta G_{Mech} - 600 \text{ J mol}^{-1} \quad (5.4)$$

where $\Delta G_{Chem} = G_\gamma - G_\alpha$ is the chemical free energy change, -600 J mol^{-1} is the stored energy in martensite and ΔG_{Mech} (positive) is the mechanical free energy. Both

ΔG_{Chem} and ΔG_{Mech} are considered as positive sign since they are driving force. For uniaxial loading, the ΔG_{Mech} per MPa is $\sim 0.86 \text{ J mol}^{-1}$ [Olson 1982]. The modified model can be rewritten as:

$$b(\Delta G_{Chem} + \Delta G_{Mech} - 600) = \frac{1}{8\pi(1-\nu)} G b^{3/2} \left(\frac{\epsilon}{L}\right)^{1/2} + \tau_S b \quad (5.5)$$

Table 5.3: Parameters used for the modeling in blocky and lath type of austenite.

Morphology	D / m	C / wt%	G / Pa	ν	b / m	$\tau_S b$ / N m ⁻¹	ΔG_{Chem} / J mol ⁻¹
Block	5×10^{-6}	1.2	8×10^{10}	0.27	2.52×10^{-10}	0.057640	1281
Film	0.5×10^{-6}	1.4				0.066444	1080

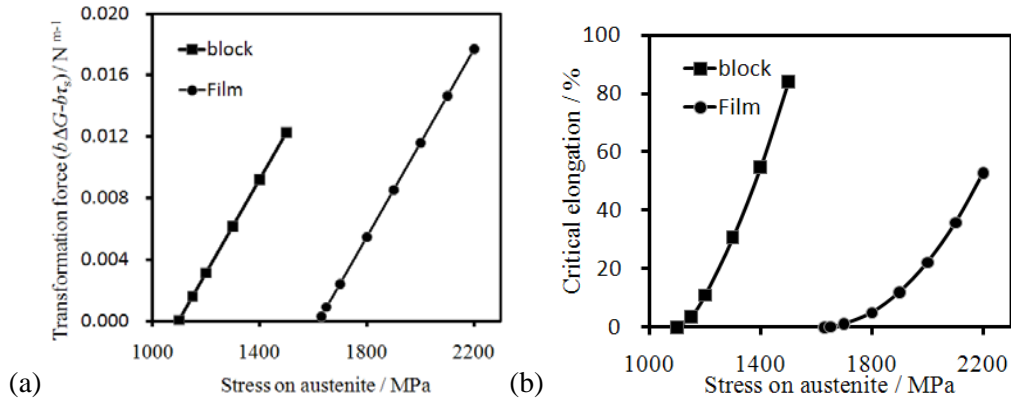


Figure 5.3: Effect of equivalent tensile stress on (a) the driving force ($b\Delta G - b\tau_s$) for induced martensitic transformation and (b) critical engineering strain for the triggering mechanical stabilisation in lath and blocky type of austenite.

ΔG_{Chem} was calculated using MTDATA combined with TCFE (1.21 version) database at 20 °C with the composition Fe-xC-0.32Si-1.87Mn-2.56Al-0.55Cu wt%, where the concentrations are measured by energy dispersive X-ray microanalysis as listed in Table 5.2. The average carbon concentration in austenite was estimated at ~ 1.33 wt% using a published equation [Dyson and Holmes, 1970] associated with the lattice parameter from X-ray diffraction results. However, the carbon enrichment in

blocky austenite forming during intercritical annealing is less than in the films one retained by bainitic transformation [Itami *et al.*, 1995], which was proven again in δ -TRIP steel related in Chapter A1. 1.2 wt% and 1.4 wt% of carbon are used in the modeling for blocky and film of austenite, respectively. The size of austenite is postulated as 5 and 0.5 μm for block and film of morphologies according to microscopic observations, respectively. The parameters for modeling are listed in Table 5.3.

When the total driving force $b\tau_T$ including both chemical and mechanical energy is less than the resistance from solid solution strengthening and dislocation strengthening, the stress-induced transformation becomes impossible. The total driving force increases with the mechanical energy by stress on austenite. The critical strain for initializing mechanical stabilisation increases therefore with the stress as well. The total transformation force for the stress induced transformation becomes positive at the stress ~ 1100 MPa in the blocky austenite (Figure 5.3a). A slight work hardening can achieve this strength level of them. If the stress on it is high to 1200MPa by strain hardening associated an engineering strain less than 11%, the martensitic transformation can be induced (Figure 5.3b). This blocky austenite therefore, transformed to martensite during deformation at the early stage of tensile process with slightly stress accumulation. This is supported by microstructure observations (Figure 5.2), where the blocky austenite was just deformed slightly and formed martensite.

The film austenite is stable against stress-induced martensitic transformation when equivalent uniaxial tensile stress on retained austenite is less than 1630 MPa (Figure 5.3a), since the total driving force $b\Delta G$ is less than the resistance from solid solution strengthening. To reach the critical driving force, 1630 MPa, for inducing martensitic transformation, the austenite must be strongly strain-hardened because the yield strength

of austenite was estimated at ~900 MPa by neutron diffraction [Furnémont *et al.*, 2002; Furnémont 2003]. The strain hardening however produces serious plastic deformation that, on the other hand, resists martensitic transformation. The lath type of retained austenite actually was elongated to large strains revealed in Figure 5.2. So TRIP effect does not happen in the lath type austenite since the extra mechanical energy supplied by stress is always accompanied with the plastic deformation, the resistance for martensitic transformation by mechanical stabilisation. Mechanical stabilisation can explain why the retained austenite can never fully decompose to martensite in deformed TRIP-assisted steels.

The addition of aluminium in δ -TRIP steel can shift the T_0 line to the right and therefore increase the carbon content in retained austenite [Bhadeshia 2001]. This makes it easier for mechanical stabilisation to occur in δ -TRIP alloys by enhancement of resistance from solid solution strengthening.

5.5 Conclusions

Promising mechanical properties have been achieved in the δ -TRIP alloy. The TRIP effect must contribute to the observed elongation. The composite phase effect, like dual phase steels, plays significant role as well, including not only the softer phase ferrite and bainite but also the deformation of ductile harder phase, austenite. Films of austenite did not however transform even at large plastic strains. This is because they are mechanically stabilised before they can be induced to transform into martensite.

Chapter 6 Spot Weldability

6.1 Introduction

Low-alloy steels containing a microstructure in which the predominant phase is allotriomorphic ferrite, with a residue consisting of a mixture of bainitic ferrite and retained austenite, are sometimes used in the manufacture of automobiles. This is because the austenite can transform during deformation and hence delay the onset of plastic instability, thus endowing a good combination of strength and formability to these so-called TRIP-assisted alloys. A typical composition would include Fe-0.15C-1.5Si-1.5Mn wt%. There are some 3000-5000 of spot welds in the manufacture of a single automobile [Rathburn *et al.*, 2003; Goldsberry 2007]. The carbon-equivalent of these alloys is large when compared with for example, interstitial-free or bake-hardening steels, making them somewhat more difficult to weld.

A new class of steels with a reasonable chance of being exploited in the automotive industries has been designated δ -TRIP [Chatterjee *et al.*, 2007; Yi *et al.*, 2010a, b] because δ -ferrite is retained in the as-cast microstructure due to their high aluminium contents. With suitable design, the ferritic phase remains stable even at temperatures in excess of 1000 °C so that rolling deformation is conducted in the two-phase $\alpha + \gamma$ region. The steel typically contains about 0.4 wt% carbon and hence should in principle be difficult to spot-weld. However, the persistence of ferrite in the microstructure should prevent the formation of fully martensitic microstructures in the regions affected by spot-welding so it is possible that different criteria determine the weldability of the steel rather than a description based on just the carbon-equivalent. These steels are stronger (≈ 1000 MPa) and more ductile than the conventional TRIP-assisted steels [DeCooman

2004; Jacques 2004; Bhadeshia 2001] so it would be particularly interesting to see whether they survive the welding operation.

The purpose of the work presented here was, therefore, to investigate the spot-welding behaviour of experimental δ -TRIP steels.

6.2 Method and Alloys

The alloys (alloy 5-9) used for spot welding is referred to as in Table 3.1 and 4.1. One problem with the alloy system is that the structure in the cast and rolled condition often does not follow the tenets of equilibrium, in the sense that the amount and stability of δ -ferrite is usually much less than expected from a phase diagram calculation. As a result, the concentrations of elements which stabilise the δ -ferrite has to be exaggerated, which is why there are a number of alloys listed in Table 6.1, Where the hot-rolled Alloy 8 and 9 were heat-treated to fulfill TRIP property (Intercritically annealed at 900 °C for 5 minutes in box furnace and followed by quenching into salt bath to 410 °C and isothermally soaking for 10 minutes there, finally cooled in the air to ambient temperature). This has had an unexpected benefit in permitting the study of spot welding as a function of the stability of the δ -ferrite.

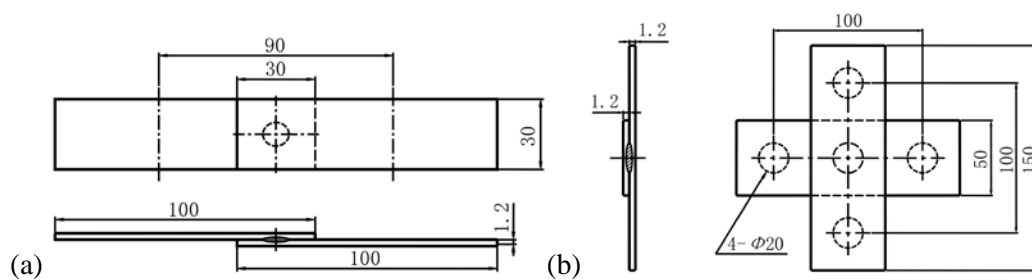


Figure 6.1: Spot-weld specimen geometries (dimensions in mm). (a) Shear tensile test samples. (b) Cross tensile test samples

Table 6.1: The compositions achieved during manufacture, wt% and other parameters related to spot-welding.

	Alloy 5	Alloy 6	Alloy 7	Alloy 8	Alloy 9	Ref.
	HR	CR	CR	CR/HR	CR/Hr	Heat-treated
Thickness /mm	1	1.2	1.2	1.2/2.5	1.2/2.25	1.8
Electrode force / kN	3.5	3.5	3.5	3.5/6	4.5/6	5.6
Squeeze time / cycles	40	40	40	40	40	-
Welding time / cycles	13	13	13	13/8	18/8	17
Hold time / cycles	13	13	13	13/30	10/30	25

where Ref. represents Sakuma and Oikawa [2003] with composition: Fe-0.08C-1.39Si-1.75Mn wt%.

The hardness was tested on a Vickers machine using a 10 kg or 5kg load with a dwell time of 10 s. The spot welding tests were carried on under the conditions shown in Table 6.1 according to the common standards [JIS Z 3136, 3137, 3139, 3140; ISO 18278-2]. The squeeze, weld and hold times are conventionally expressed in cycles, where 1 s equals 60 cycles, corresponding to a 60 Hz frequency of the alternating current used. The ‘up-slope’ which describes the ramping of the voltage was zero, and all the welds were made using a single pulse. There was no imposed cooling. A Draper type electrode was used with a tip diameter of 6 mm for sheets with thickness 1 and 1.2 mm, and 8 mm for sheets 2.25 and 2.5 mm in thickness.

The shear tensile tests and cross tensile tests specimens used, and weld locations are shown in Figure 6.1.

6.3 Results and discussion

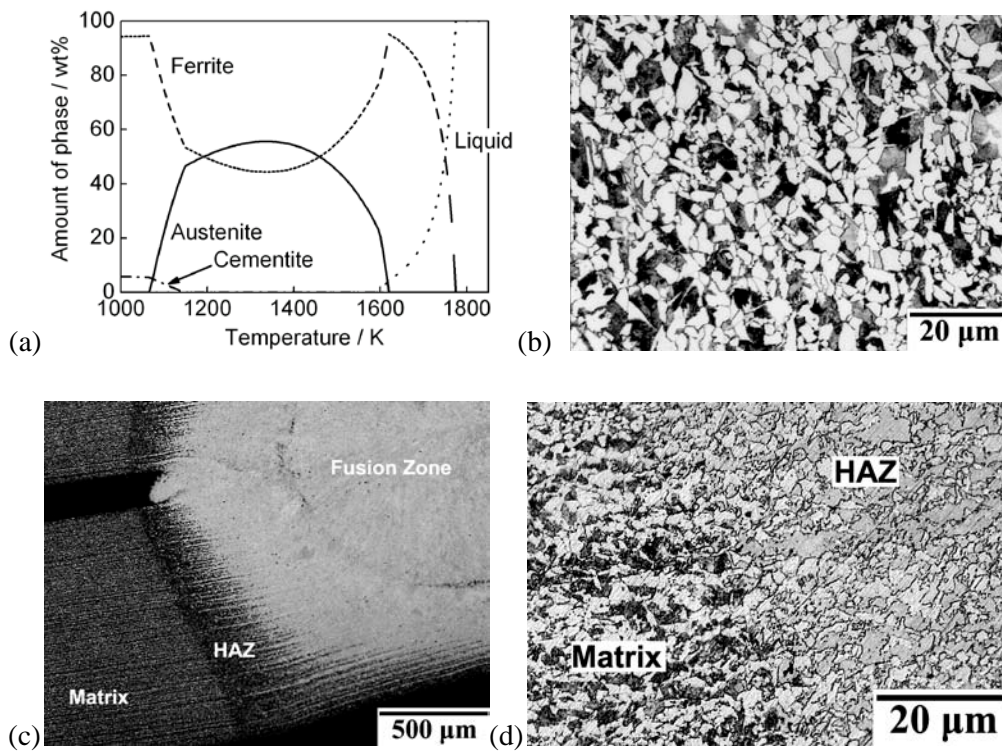


Figure 6.2: Alloy 5. Note that untempered martensite etches light-grey relative to allotriomorphic ferrite (white) and pearlite (dark). (a) Calculated equilibrium phase fractions. (b) Mixture of ferrite and pearlite following hot-rolling into sheet form. (c) Macrograph showing the spot weld and surroundings. (d) Higher magnification image showing the mixture of ferrite

Although equilibrium calculations indicate that Alloy 5 should at all temperatures contain at least 44 wt% of ferrite (Figure 6.2a), because the solid-state transformation to austenite following solidification to δ -ferrite occurs without the required level of solute partitioning, the cast material is not in an equilibrium state. In fact it becomes fully austenitic at 1100°C so that on cooling the hot-rolled sheet, the δ -dendrites present in the cast state are replaced by a mixture of allotriomorphic ferrite and pearlite as

illustrated in Figure 6.2b. The fusion zone of the spot weld therefore transforms completely into austenite during the heating stage and into a fully martensitic state with a hardness of 577 ± 16 HV following rapid cooling (Figure 6.3). It is interesting, however, that much of the heat-affected zone (HAZ) has a hardness less than that of martensite (Figure 6.3) because the microstructure there is a mixture of allotriomorphic ferrite and martensite because the high aluminium content of the alloy encourages the formation of ferrite.

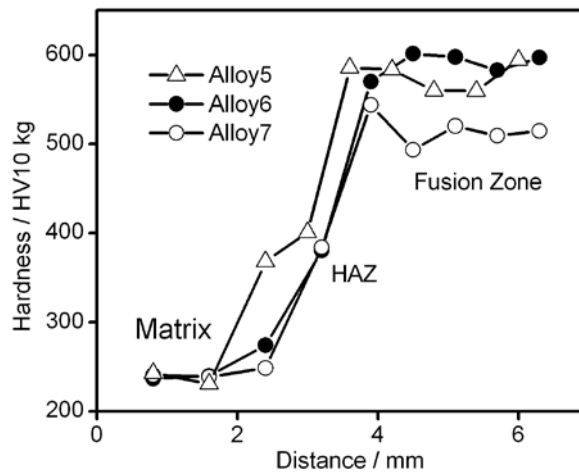


Figure 6.3: The distribution of hardness in typical welds of Alloys 5, 6 and 7.

Table 6.2: Summary of Vickers hardness data. HV_{fused} represents the hardness of the fusion zone of the spot weld, where HV10 kg for Alloy 5, 6 and 7, HV 5 kg for Alloy 8 and 9.

Alloy	HV_{Matrix}	HV_{HAZ}	HV_{fused}	$\frac{HV_{fused}}{HV_{HAZ}}$
5	237 ± 6	385 ± 23	577 ± 16	2.43
6	250 ± 14	381 ± 18	590 ± 13	2.36
7	243 ± 5	384 ± 16	516 ± 18	2.12
8	328 ± 9	353 ± 10	524 ± 33	1.60
9	311 ± 6	347 ± 30	406 ± 22	1.31

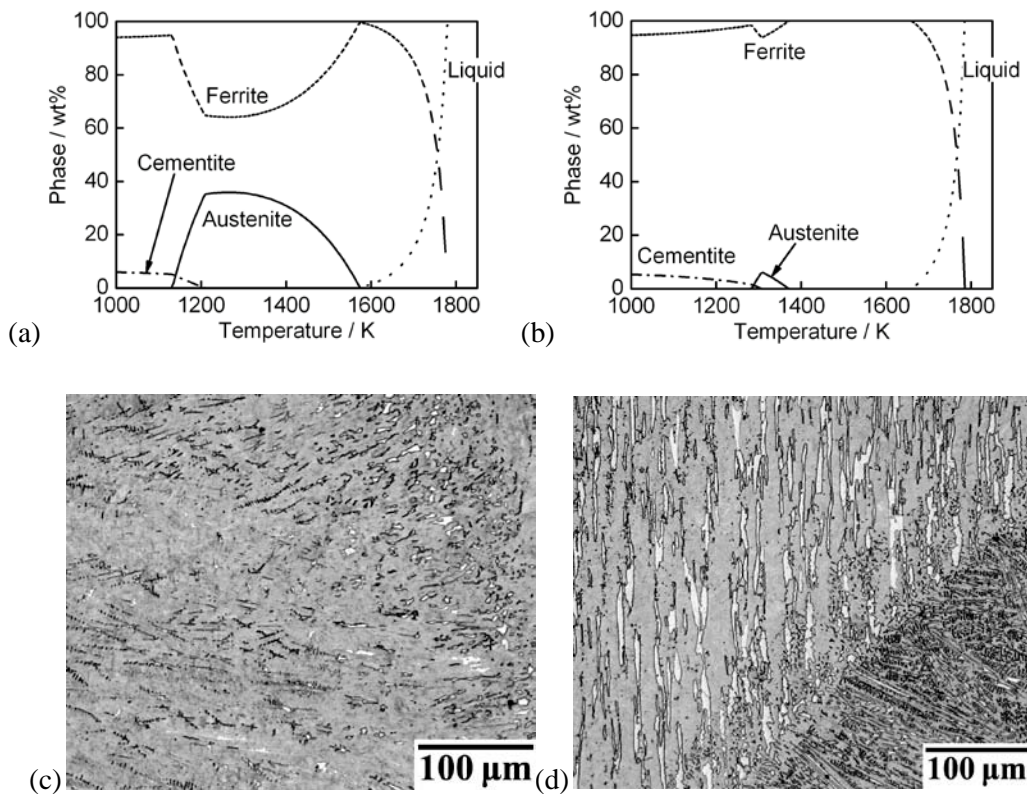


Figure 6.4: (a, b) Calculated equilibrium phase fractions for Alloys 6 and 7 respectively. (c, d) The structures of the fusion zones of spot welds in Alloys 6 and 7 respectively.

The original intention of retaining δ -ferrite throughout the entire weld zone was not achieved with Alloy 5, so Alloys 6 and 7 were made using larger concentrations of the ferrite-stabilising solutes Si and Al, as confirmed by the calculated phase diagrams and observations of the fusion zone in Figure 6.4. Small quantities of δ -ferrite were indeed retained in the fused region, leading to a small reduction in the hardness for Alloy 7 which has a larger concentration of aluminium. To further encourage the retention of δ -ferrite, the aluminium, silicon and manganese concentrations were further adjusted and resulted in dramatic reductions in the fusion zone hardness. Considerable quantities of δ -ferrite were retained in spite of that the cooling rate involved during spot welding is

of the order of $1000\text{-}2000\text{ K s}^{-1}$ [Chuko and Gould, 2002], as shown in Figure 6.5.

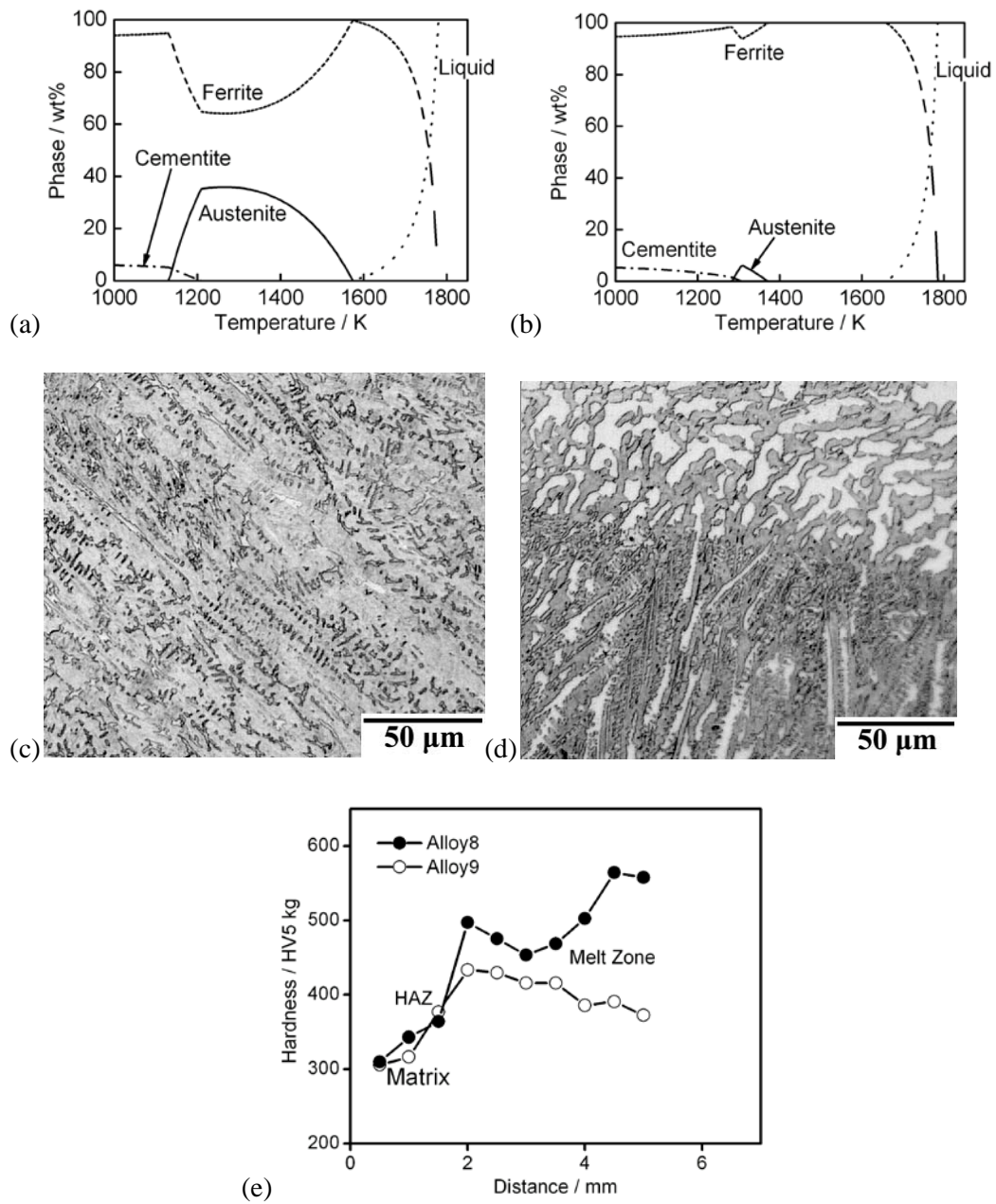


Figure 6.5: (a, b) Calculated equilibrium phase fractions for Alloys 8 and 9 respectively. (c, d) The structures of the fusion zones of spot welds in Alloys 8 and 9 respectively. (e) The distribution of hardness.

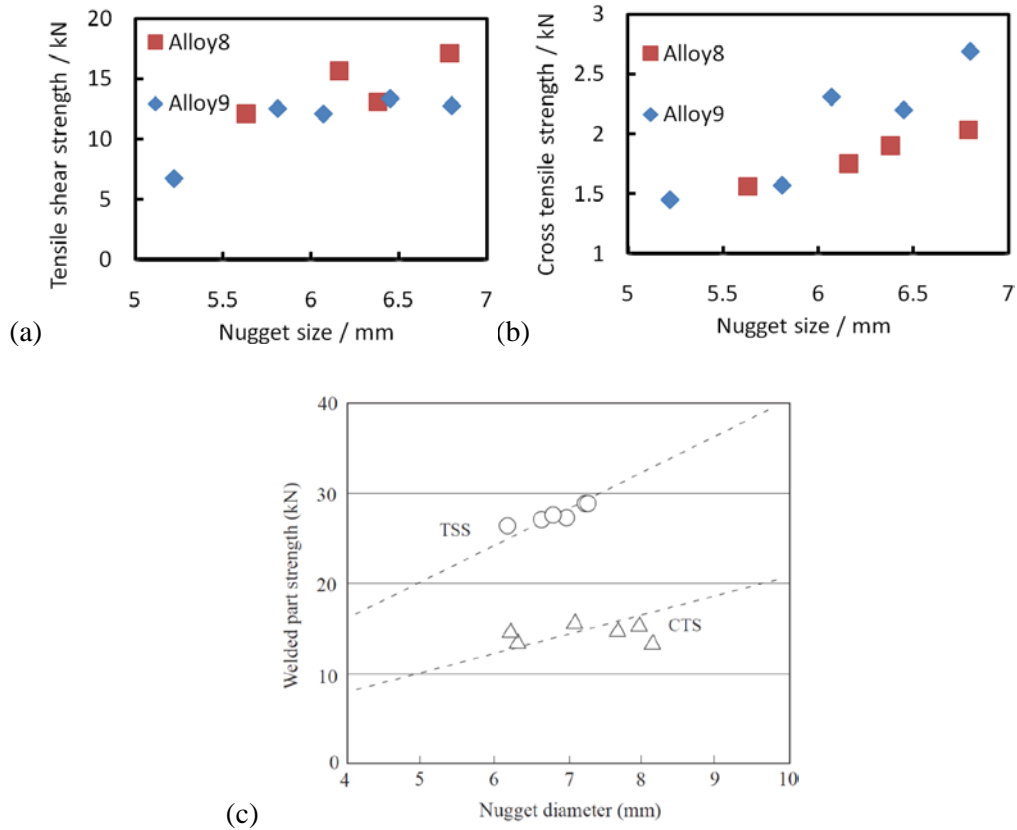


Figure 6.6: Change of loading on welds (TSS and CTS) with nugget size. (a) Tensile shear strength for 1.2 mm-thick cold-rolled alloys; (b) Cross tensile strength for 1.2 mm-thick cold-rolled alloys; (c) 1.8-mm-thick 780-MPa cold-rolled steel sheet (Ref. [Sakuma and Oikawa, 2003])

Hardness data are summarised in Table 6.2. The hardness distribution of welds in Alloys 8 and 9 are acceptable because they indicated the hardness ratio between fusion zone and matrix equals ~ 1.5 . The results from mechanical testing are presented in Figure 6.6. Compared with the reference data, 1.8-mm-thick 780 MPa steel sheet (Figure 6.6c), the cross tensile strength, however, are much lower than the acceptable value. The matrix or HAZ should be the tough zone in the δ -TRIP steels due to the dual phase microstructure. Fracture however happened in the matrix or heat affected zone in several

cross tensile tests in the welds of as-received cold-rolled sheet (Figure 6.7). This led to the poor weld property because of the brittle matrix resulted from the cold working.

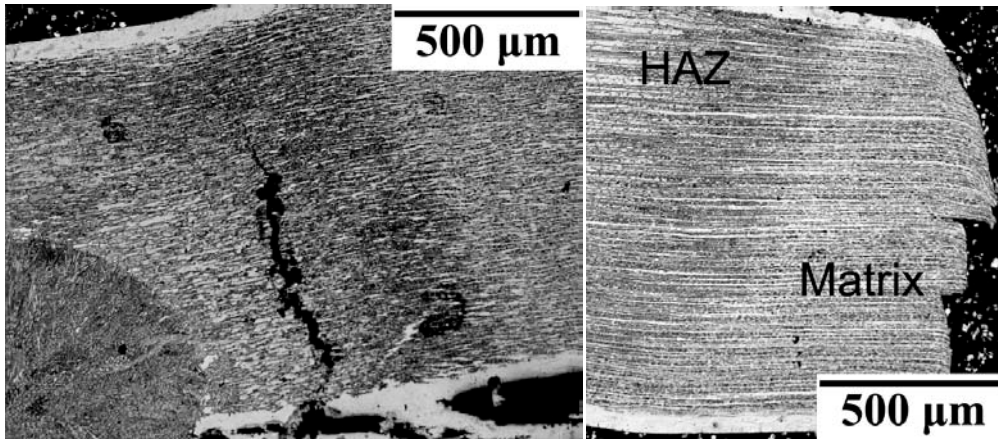


Figure 6.7: Microscopy of welds of alloy9 after cross tensile test, where cracks happened in the tough HAZ or matrix

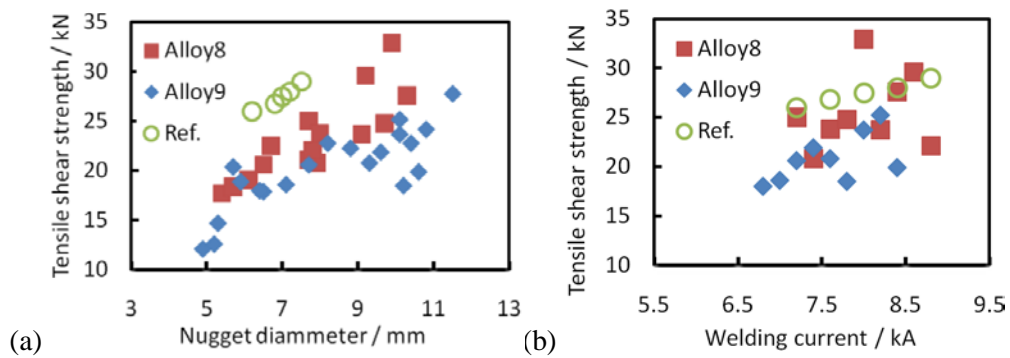


Figure 6.8: Spot welds property of hot-rolled sheets in heat-treated condition.

The heat-treated alloys have therefore been tested. The tensile shear strength of both alloys is just slightly lower, ~5 kN, than the reference alloy at the same nugget diameter (Figure 6.8), which contains only 0.08 wt% of carbon[Sakuma and Oikawa, 2003]. The weldable current range is however too narrow for the acceptable tensile shear strength (Figure 6.8b), and the fracture mode is interface or partial. The

weldability of δ -TRIP alloys has been not sufficient good for industry application yet. The spot welding property of δ -TRIP alloys containing 0.4 wt% carbon has been strongly improved by addition of high aluminium. This original idea has been proven to be possible in this research.

6.4 Conclusions

The hardness of welds of 0.4 wt% carbon containing δ -TRIP alloys was decreased drastically by introduction of δ -ferrite due to addition of strong ferrite stabilising element, aluminium, which performed promising mechanical properties that the current commercial steels have never achieved. The toughness in both fusion zone and heat affected zone was therefore improved strongly led by the dual-phase effect.

In two alloys with high aluminium addition performed excellent tensile shear strength that is comparable with the 0.08 wt% carbon containing dual phase steels at the same nugget size. The weldable current range is however too narrow for the actual industrial application. Modification of alloy design has to be investigated more to meet the industrial application requirement in the further research.

Chapter 7 Dual-Phase Hot-Press Forming Alloy

Hot-press forming steels are formed in a fully austenitic state followed by die-quenching in order to generate martensite and achieve a strong steel. The ductility however, tends to be limited. A novel steel design was explored here in which the forming operation is in the two-phase austenite and ferrite field, so that the quenching results in a dual-phase ferrite and martensite microstructure at ambient temperature. It is demonstrated that slightly better properties are achieved. The interpretation of the mechanisms of deformation during tensile testing indicate that the ductility can be further enhanced without compromising strength. The new steel also has the advantage that it can be formed in a softened state, at a lower temperature than conventional hot-press forming alloys.

7.1 Introduction

One application of strong steels in the context of automobiles is to enhance passenger safety by resisting damage to the passenger compartment during collisions. There are many varieties of such steels, for example those which are TRIP-assisted [Matsumura *et al.*, 1987a, b; Sakuma *et al.*, 1991a; Jacques 2004; DeCooman 2004; Bhadeshia 2006] or the dual-phase steels which are nicely reviewed in [Owen 1980]. These steels have to be formable and that requirement is difficult to achieve when the strength exceeds about 1000 MPa. Strong steels also suffer from an exaggerated change in shape due to the relaxation of elastic stresses when the steel is removed from the forming press [Kuhn 1967].

One solution to these difficulties was the invention in Sweden of the process known

as hot-press forming [Norrbottnens Jaernverk 1977; Berglund 2008], in which a hot sheet of steel in its austenitic state, is fed into a forming press with water-cooled dies which quench the material into a martensitic state. Following austenitisation at about 900 °C [Berglund *et al.*, 2008; Kusumi *et al.*, 2009], the steel is transferred to the press and the deformation occurs at high temperatures approximately in the range 800-600 °C [Hein and Wilsius, 2008] where the steel is soft and formability limitations insignificant. The quenching produces already-formed components with strength in the range 1200-1600MPa. There is little or no change in shape when the component is removed from the press. The steels typically have a composition Fe-0.22C, 1-2wt% Mn (depending on whether the steel also is alloyed with boron) and other trace elements to give a martensite-start temperature of about 400 °C [Fan *et al.*, 2009a]. The steel in its final condition after hot-press forming is fully martensitic and has a ductility of approximately 6-8%.

The purpose of the present work was to explore another option with the hope of improving ductility in the press-formed condition whilst maintaining the strength. An alloy was designed so that it consists of a mixture of allotriomorphic ferrite and austenite at the forming temperature, so that subsequent quenching leads to a dual-phase steel. A potential advantage of this mixture of allotriomorphic ferrite and martensite could be that the latter phase occurs in a finer state than in fully martensitic steels; this in itself should improve the resistance of the martensite to cracking [Bhadeshia *et al.*, 1983a, b; Chatterjee *et al.*, 2006].

7.2 Experimental Method

The steel studied is alloy 3 (Table 3.1) its calculated phase diagram is in Figure 7.1a. The combination of alloying elements, especially the aluminium, ensures that the alloy

has a large ferrite content at elevated temperatures. The alloy in fact was originally designed for a different purpose, the so-called δ -TRIP concept described in previous chapters. Nevertheless, by serendipity, the alloy proved useful to explore the dual-phase hot-press forming studied here.

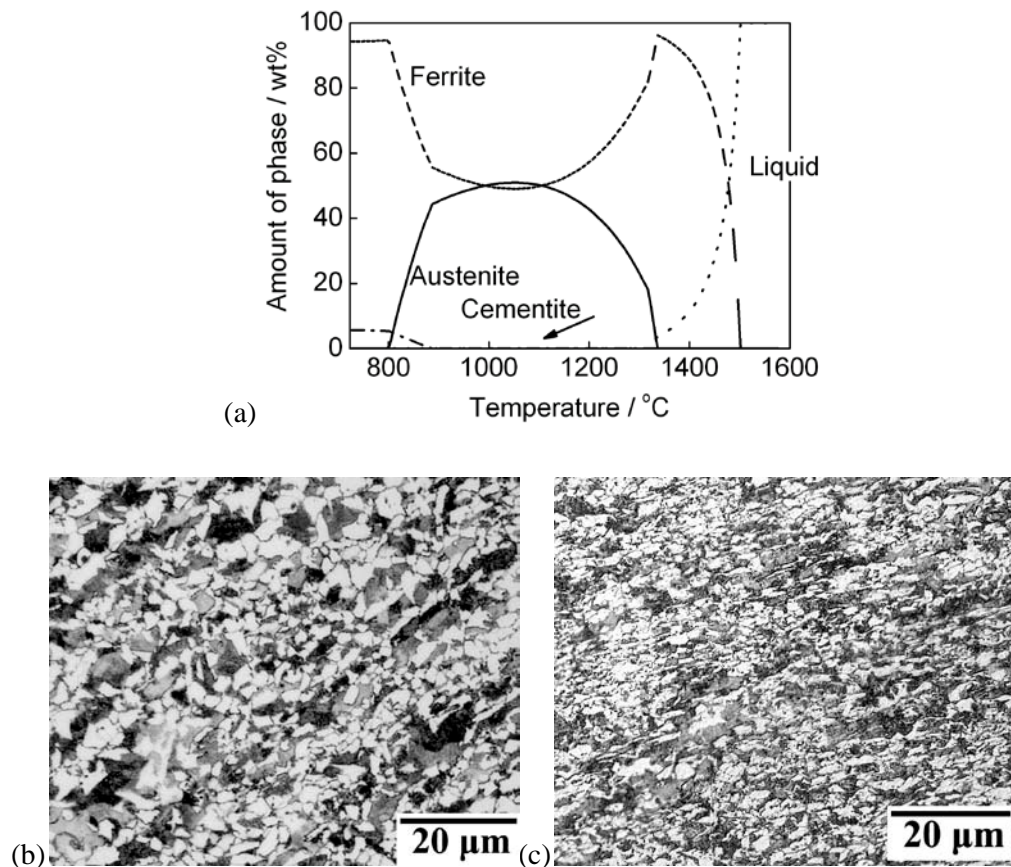


Figure 7.1: (a) Phase diagram calculated using MTDATA [2005] and the TCFE (version 1.2) database. (b) Optical microstructure in the hot-rolled state. (c) Optical microstructure in the cold-rolled state.

Heat treatments were conducted on a simulator, CCT- AY, made by ULVAC-RIKO. The cold rolled sheets for tensile testing were heated in a nitrogen atmosphere at 840, 860, 880 and 900 °C respectively for 3min at the heating rate

20 °C s⁻¹, followed by quenching at -40 °C s⁻¹ using nitrogen.

Conventional hot-rolling was conducted between 1200-900 °C; the fact that ferrite coexists with austenite at all temperatures in this range leads to a significant refinement, a grain size of just 3.1 ± 0.2 μm without using any thermomechanical processing (Figure 7.1b). The phenomenon is well-established in the field of superplasticity where two phase mixtures can resist coarsening during deformation [Maehara and Langdon, 1990]. The cold-rolled structure is illustrated in (Figure 7.1c).

7.3 Results and Discussion

Table 7.1: Quantitative metallographic data, and the carbon content of the martensite as estimated by mass balance from the average concentration.

Heat-treatment $T / ^\circ\text{C}$	$100V_\alpha$	$C_{\alpha'} / \text{wt}\%$	$\bar{L}_\alpha / \mu\text{m}$	$\bar{L}_{\alpha'} / \mu\text{m}$
840	38±5	0.64±0.05	1.2±0.1	1.7±0.3
860	34±9	0.60±0.07	1.1±0.1	1.9±0.1
880	32±6	0.58±0.05	1.1±0.2	2.4±0.2
900	26±6	0.54±0.05	1.0±0.1	2.5±0.4

Metallographic observations confirmed the dual-phase ferrite (α) and martensite (α') microstructure obtained following heat-treatment at 840, 860, 880 and 900 °C for 3min followed by quenching, Figure 7.2. Quantitative data are presented in Table 7.1, which show as expected from the phase diagram, that the fraction of ferrite decreases as the maximum heat-treatment temperature is increased. The size scales were characterised using standard metallographic theory [DeHoff 1968], with the mean lineal intercepts (\bar{L}) in the two phases given by

$$\bar{L}_\alpha = \frac{LV_V^\alpha}{N^\alpha} \quad \bar{L}_{\alpha'} = \frac{LV_V^{\alpha'}}{N^{\alpha'}} \quad (7.1)$$

where V_V and N represent the volume fraction and number of grains respectively of the

phase identified by the superscript. The observed grain sizes of the ferrite and of the martensite islands are remarkably small given the simple heat-treatment and the absence of any thermomechanical processing, Table 7.1.

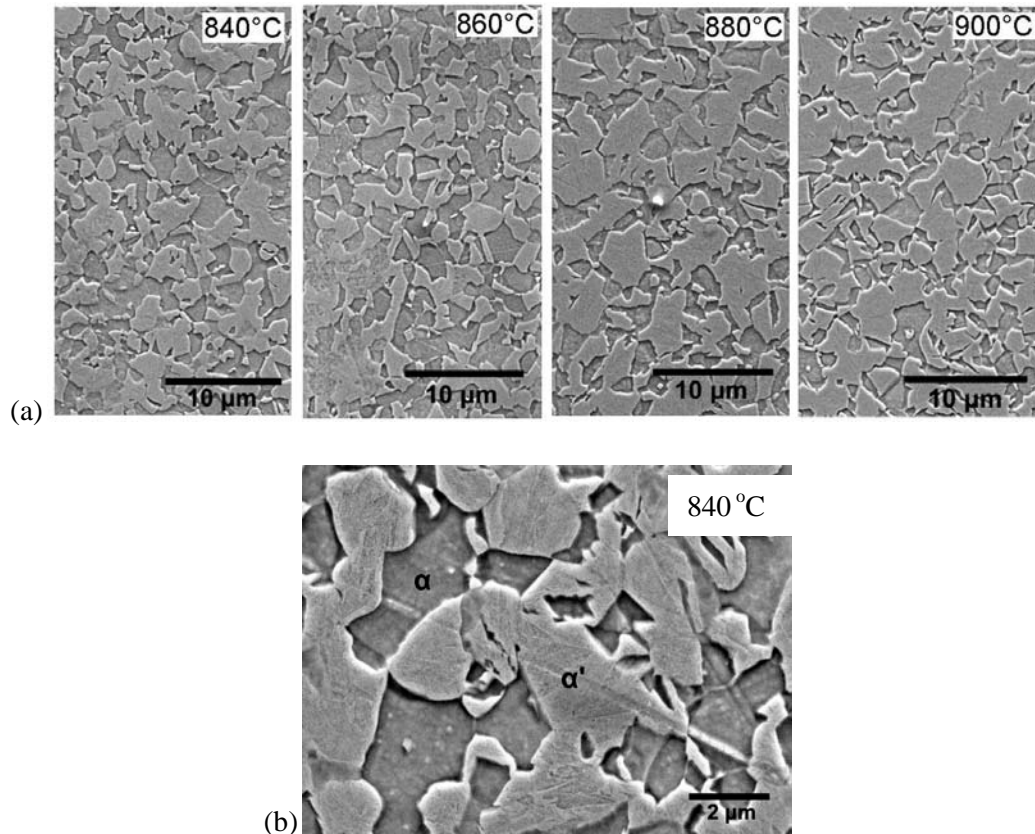


Figure 7.2: (a) Microstructures after heat treatment at the temperatures indicated followed by quenching. The light-etching regions which seem to protrude are martensitic. (b) Scanning electron micrograph showing martensite at higher resolution.

Tensile test results are illustrated in Figure 7.3 together with a comparison against some published data. There are a number of features which are striking, first that the yield strength is quite low, around 400 MPa, followed by work-hardening. This kind of behaviour is expected in dual-phase steels [Tomota *et al.*, 1976; Mileiko 1981;

Bhadeshia and Edmonds, 1980] consisting of two phases which have quite different yield strengths. The application of stress at first causes yielding in the softer phase only, but because the ferrite does not occupy the entire specimen, it yields at a stress less than that of the ferrite isolation. This explains the very low macroscopic yield strength observed.

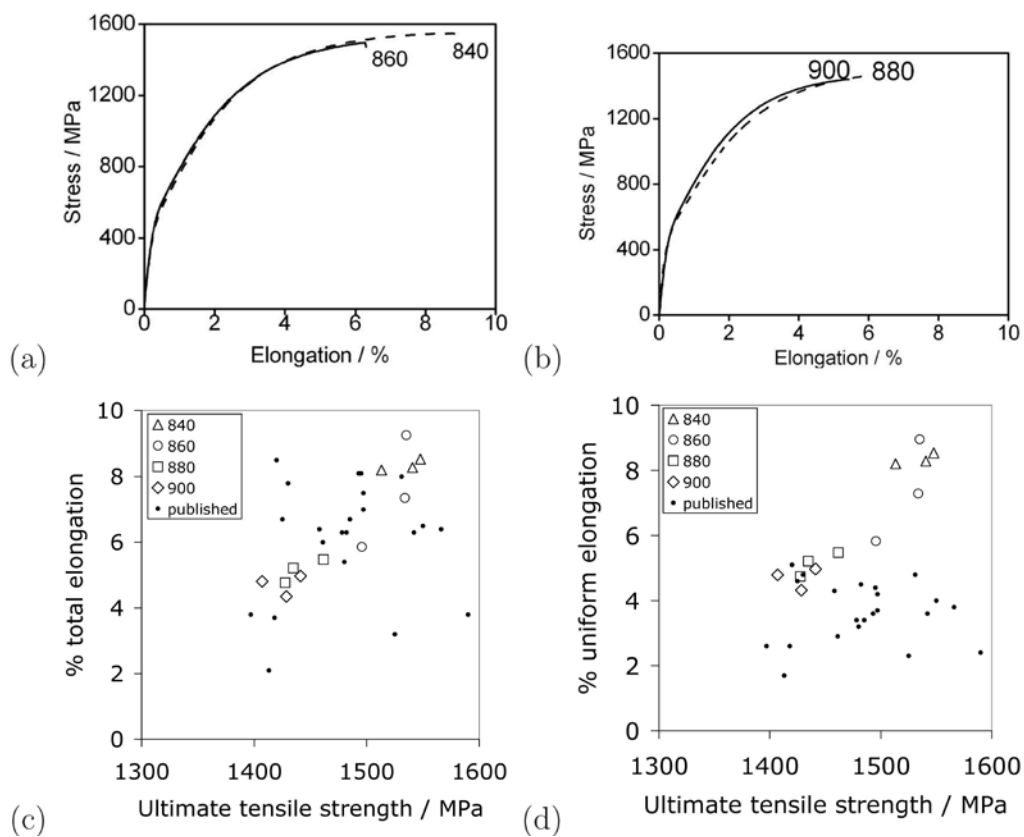


Figure 7.3: (a, b) Tensile test data. (c, d) Comparison of elongation against strength. The published data are from [Fan *et al.*, 2009a, b; Nader 2007; Suehiro *et al.*, 2003].

It is only after the ferrite has work hardened to be able to transfer sufficient load on to the stronger martensite that the latter begins to deform plastically. It is in this way that high-strength is achieved. However, fracture will occur when the martensite is no longer able to support plastic strain.

The surprising trend in the data illustrated in Figure 7.3c is that the total elongation increases as the heat-treatment temperature is reduced, in spite of the fact that the material at the same time becomes stronger. A recent idea explaining the ductility of another microstructure consisting of a hard and soft phase is that failure occurs in a tensile test when percolation is lost through the ductile phase [Bhadeshia 2008a, 2010]. Percolation theory is well-established [Garboczi *et al.*, 1995] and was used in the present case to estimate the volume fraction of equiaxed ferrite required to ensure continuity in the microstructures generated. It was found that a minimum of $V_V^\alpha = 0.29$ is needed so that the ferrite can be traversed in the microstructure without interruption. This is likely to be an underestimate given that a uniform grain size and distribution is assumed. It is interesting that the volume fractions of ferrite listed in Table 7.1 are quite close to the percolation fraction for the lowest ductility samples, *i.e.*, those heat-treated at 880 and 900 °C. Figure 7.4 shows cracks in the vicinity of the fracture surfaces of broken tensile samples. In the case of the sample heat-treated at 840 °C, which had the highest ferrite content and was ultimately the strongest, it is evident that the ferrite is able to accommodate a lot of damage before fracture propagates, whereas this is not so for the 880 °C sample where large cracks are able to develop without much hindrance within the martensite.

Referring back to Figure 7.3, the best total elongation achieved here are slightly better than for data corresponding to conventional hot-press forming martensitic steels [Fan *et al.*, 2009; Suehiro *et al.*, 2003]. However, with the interpretations presented above, it should be possible to further improve the dual-phase steel by reducing the carbon concentration to 0.3 wt% in order to make the martensite somewhat softer and to allow a greater quantity of ferrite relative to the percolation threshold. It remains to be seen as to how much tolerance there is for an increase in ferrite content since there must

come a point where strength is reduced.

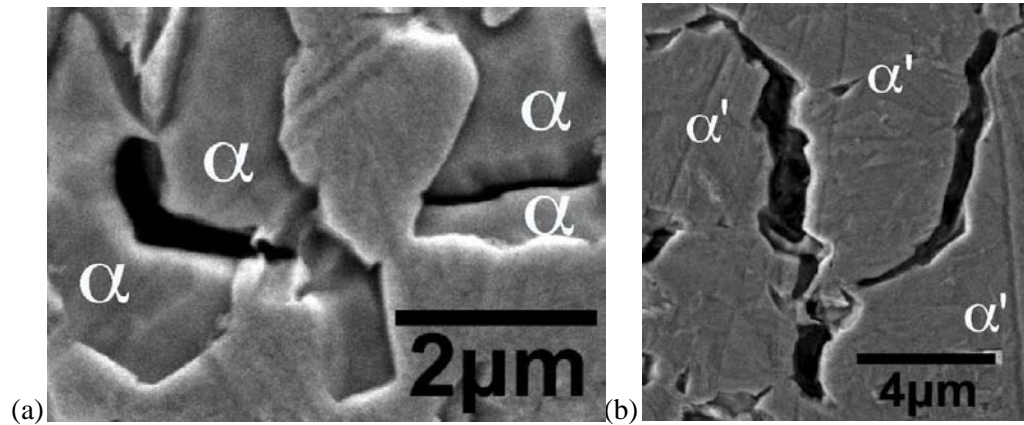


Figure 7.4: Typical cracks near under the fracture surface of broken tensile test specimens. (a) Non-propagating cracks in the ferrite, sample heat-treated at 840°C. (b) Cracks in large martensite regions in sample heat-treated at 880°C.

Finally, it is worth emphasising that the total elongation achieved for an ultimate tensile strength approaching 1550MPa is much greater than the 6% for an established dual-phase steel with a tensile strength of 1400MPa [Naderi 2007], and is comparable to that for another dual-phase steel which has an elongation of 9% but at a much lower tensile strength of 1000MPa [Naderi 2007]. This is undoubtedly because of the fine scale of the microstructure obtained in the present work, by hot-rolling in the two-phase field. In terms of the uniform elongation (Figure 7.3d), the steel investigated here significantly outperforms the fully martensitic variants reported in the published literature [Fan *et al.*, 2009a, b; Nader 2007; Suehiro *et al.*, 2003].

7.4 Conclusions

It has been demonstrated that it is possible to achieve a steel consistent with the requirement of hot-press forming, where the structure at the forming temperature

consists of a mixture of allotriomorphic ferrite and austenite, with the latter changing into martensite on quenching. This is in contrast to the fully martensitic variants in use today. It may be a commercial advantage that the maximum heat treatment temperature can be conducted at a temperature of 840 °C, which is at least 20-60 °C lower than convention. Furthermore, the total elongations recorded for the dual-phase steel are slightly better than those of the fully martensitic alloys, and our interpretation of the mechanisms of ductility and strength suggest that there is room for improvement. In terms of uniform elongation, the dual-phase steel significantly outperforms the fully martensitic counterparts.

Chapter 8 Conclusions

Based on the equilibrium phase diagram, the most significant alloying element to stabilize δ -ferrite is aluminium, which for kinetic reasons has to be as high as 2.49 wt% to retain substantial amounts of δ -ferrite. Even then, the amount retained is less than expected from equilibrium. The austenite that forms during cooling by solid-state transformation does so without the required partitioning of substitutional solutes. This conclusion is supported by microanalytical data and through calculations of limiting phase diagrams based on para equilibrium rather than equilibrium. Kinetic simulations support the conclusion that there are two stages involved in the formation of austenite, first when the latter forms as a part of the solidification process, and then through solid-state transformation of ferrite under circumstances where the substitutional solutes do not partition as expected from a local equilibrium condition at the transformation front.

In some cases, the δ -ferrite obtained by non-equilibrium solidification disappeared during reheating process in the common hot rolling temperature range. Suitable alloys have however been designed by increasing the aluminium and silicon concentrations, accompanied by a reduction in the manganese and copper contents, in which the δ -ferrite remains in the microstructure over the range 900-1200 °C,.

Promising combinations of tensile strength and elongation has been achieved in these δ -TRIP alloys. The novel alloy system is designed based on the concept of stabilising ferrite in the microstructure using aluminium as an alloying element. These properties fall in a domain which is not represented by other commercially available or experimental steels designed for automobile production. The heat-treatments necessary

to achieve the microstructure involve intercritical annealing followed by isothermal transformation at temperatures and time periods which are consistent with large scale production on the so-called continuous annealing facilities [Yanagishima *et al.*, 1983]. The isothermal transformation can even be conducted at 450 °C which is compatible with a final galvanising treatment.

TRIP effect did not happen on films of austenite and it participated in severe plastic deformation during tensile testing due to its higher carbon concentration and morphology, since aluminium shifts the T_0 line to larger carbon concentration. This ductile deformation of austenite contributes to the overall mechanical behavior by a composite phase effect. The plastic deformation of austenite leads to its mechanical stabilisation. This is supported by the modeling proposed in this research. This mechanical stabilisation explains the incomplete martensite transformation of retained austenite in TRIP-assisted steels as well.

The hardness of welds of δ -TRIP alloys was actually decreased drastically by the introduction of δ -ferrite due to addition of aluminium, a strong ferrite stabiliser. The toughness in both fusion zone and heat affected zone was therefore improved strongly led by the dual-phase effect. In two alloys with high aluminium addition performed excellent tensile shear strength that is comparable with the 0.08 wt% carbon containing dual phase steels at the same nugget size. The weldable current range is however too narrow for the actual industrial application. Modification of alloy design has to be investigated more to meet the industrial application requirement in the further research.

It has been demonstrated that it is possible to achieve a steel consistent with the requirement of hot-press forming, where the structure at the forming temperature consists of a mixture of allotriomorphic ferrite and austenite, with the latter changing

into martensite on quenching. This is in contrast to the fully martensitic variants in use today.

Appendix 1 Design of High Aluminium Containing δ -TRIP Steel by Calculation

A1.1 Introduction

A novel microstructure was developed in a high aluminium containing TRIP-assisted steel, called as δ -TRIP steel [Chatterjee *et al.*, 2007], which was evolved from as-cast alloys and consisted of dendritic δ -ferrite replacing the allotriomorphic ferrite in conventional TRIP-assisted steels, and the remanent bainite (alternate ferrite and retained austenite laths). The steel exhibited promising properties: an ultimate tensile strength in the as-cast condition of about 1000 MPa and a total elongation, almost all of which is uniform, of 23%. It has been demonstrated that the combination of strength and ductility is due partly to the deformation-induced transformation of the retained austenite into martensite, resulting in an enhanced resistance to plastic instabilities [Chatterjee *et al.*, 2007].

Since the microstructure and phase transformation kinetics are strongly different from the traditional TRIP-assisted steels due to the addition of high aluminium. The evolution of microstructure for TRIP cannot be designed simply based on the previous experience. In this research, the microstructure evolution in the δ -TRIP steel was designed by theory, MTDATA, MUCG83 [MAP a] and TRIP_PC_V [MAP b]. The actual experimental observations were compared with the theoretical calculation.

A1.2 Experimental

The alloy (alloy 2 in Table 3.1) investigated here was designed based on previous work of Chatterjee *et al.* [2007] and previous chapters. The alloy manufacture, microscopy,

microanalysis, X-ray diffraction and tensile test are performed as referred as in Chapter 4.2.

Microstructure evolution simulations were conducted on dilatometric samples of dimensions $2 \times 3 \times 10$ mm machined from as hot-rolled sheets using a push-rod BAHR DIL805 high-speed dilatometer with radio frequency induction heating. Tensile specimens were soaked in a box furnace for intercritical annealing and isothermally held in a salt bath for bainitic transformation followed by air cooling.

A1.3 Microstructure evolution

The solubility of carbon in ferrite is supposed to be 0.02 wt% during intercritical annealing. The partitioning of copper is ignored. Provided the phase transformations occur under para equilibrium condition during intercritical annealing, the composition of ferrite does not change and that of austenite can be calculated using a mass balance and assuming that the specimen has 40 wt% of ferrite and 60 wt% of austenite, Table A1.1.

Table A1.1: Measured composition of ferrite in as-rolled condition, that of austenite is calculated by mass balance assuming 40 wt% of ferrite and 60 wt% of austenite.

	C	Si	Mn	Al	Cu
Measured in ferrite / wt%	-	0.23	1.82	2.54	-
Calculated in austenite / wt%	0.60	0.23	2.11	2.46	0.49

The bainite and martensite start temperatures, TTT diagram, and carbon content (C_{T_0}) in austenite at T_0 temperature were calculated based on the composition using MUCG83, where T_0 means the temperature at which the Gibbs free energies of austenite and ferrite of the same composition are identical. Based on the composition of austenite listed in Table A1.1, those for the 2.46 wt% aluminium-containing austenite is

linearly extrapolated from the results simulated by MUCG83 for 1.0, 1.5 and 2.0 wt% of aluminium, because the permitted aluminium concentration is the range 0-2 wt% in MUCG83. The B_S and M_S temperature is fitted to be 500 and 288°C respectively. Sufficient carbon enrichment is necessary to achieve stable retained austenite. The lower the transformation temperature, the higher the concentration of carbon that can be partitioned into austenite due to the “incomplete reaction phenomenon” [Bhadeshia 2001]. A temperature of 330 °C is designed as the isothermal bainitic transformation temperature to enrich enough carbon in austenite. At $T_0 = 330$ °C, the carbon in austenite cannot exceed $C_{T_0} = 5.97$ at% ≈ 1.38 wt% (Figure 1 c). Ignoring carbon in ferrite, a maximum of 27 wt% of austenite can be retained on the basis of carbon mass balance. In fact, the actual amount of retained austenite should be less than that value because martensite might form due to the non-uniform carbon distribution and austenite morphology.

The as-received hot-rolled alloy consisted of 47 ± 2 wt% of ferrite and residual pearlite as shown in Figure A1.2. The A_{c1} and A_{c3} points are not possible to determine using dilatometry due to the aluminium content of the steel, Figure A1.3. The intercritical annealing temperature therefore can only be determined by optical microscopy of samples quenched from the intercritical annealing temperature. The specimens quenched from 800 °C and 760 °C contained 30 ± 4 wt% and 38 ± 4 wt% of ferrite respectively. The alloy is designed therefore to be intercritically annealed at 800 °C and 760 °C for 5 minutes.

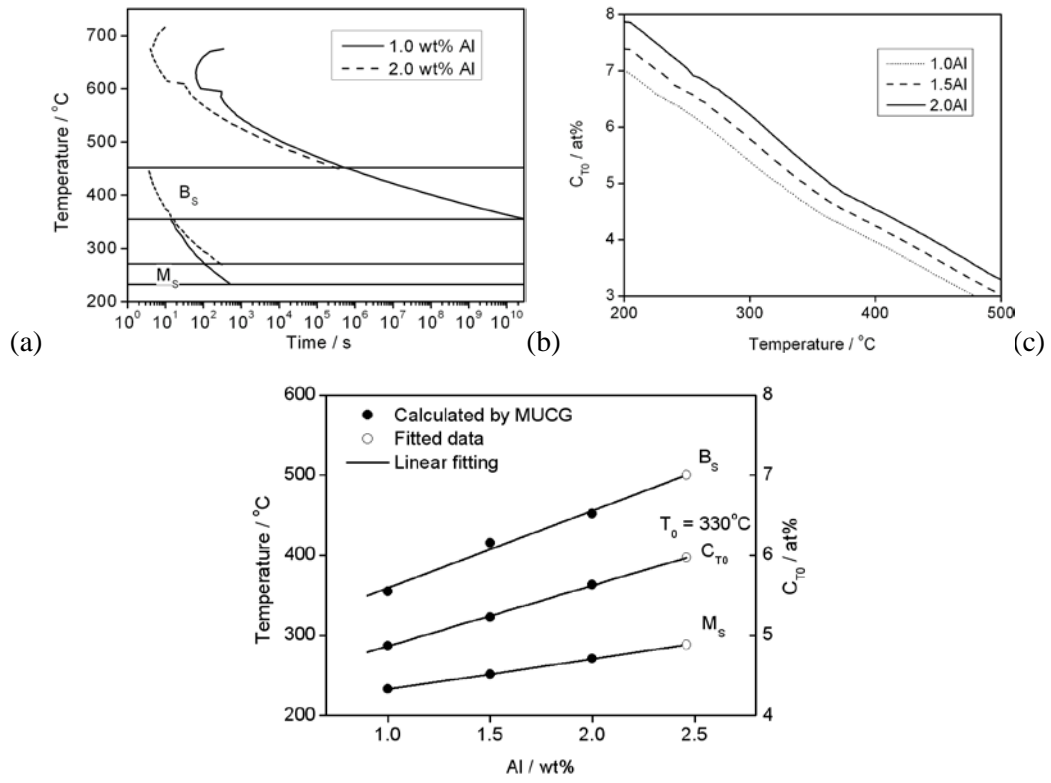


Figure A1.1: (a) TTT diagram, (b) carbon concentration in austenite at T_0 temperature, (c) Bainite and martensite starting temperature and carbon concentration in austenite at $T_0 = 330\text{ }^\circ\text{C}$, $C_{T_0} = 5.97\text{ at}\% \approx 1.38\text{ wt}\%$.

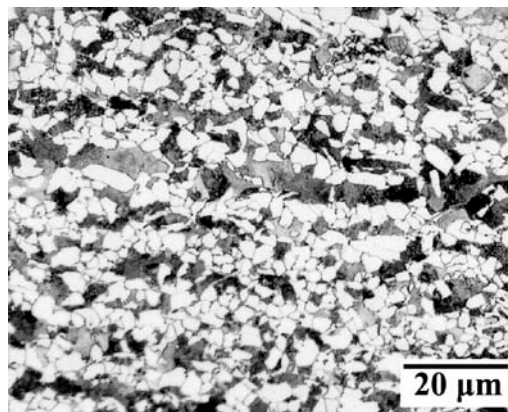


Figure A1.2: Optical image of as-received hot-rolled alloy.

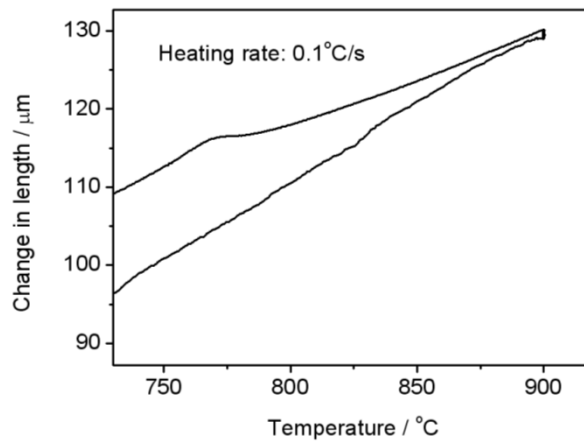


Figure A1.3: Change in length as the function of temperature in dilatometric study.

Table A1.2: Heat treatment cycle for tensile specimens and estimated retained austenite amount.

No.	Intercritical annealing		Isothermal holding		Estimated RA / wt% TRIP_PC_V
	Temperature / °C	Time / min	Temperature / °C	Time / min	
A	800	5	330	30	20 ± 23
B	760	5	330	30	23 ± 22
C	800	5	330	90	15 ± 44

In dilatometric study, the bainitic transformation is proportional to the change in length of specimens. The bainitic transformation is limited by carbon concentration C_{T_0} in austenite due to the “*incomplete reaction phenomenon*”. As shown in Figure A1.4a, for the specimens intercritically annealed at 800 °C, 73.4 and 97.2 wt% of bainitic transformation happened isothermally holding at 330 °C for 30 min and 90 min respectively. For the specimens intercritically annealed at 760 °C, 61.7 wt% of bainitic transformation finished after isothermally holding at 330 °C for 30 min due to the slower transformation kinetics resulted from the higher carbon content in the less austenite. Three heat-treatment cycles referred to as A, B, and C in Table A1.2 were designed. The

percentages of retained austenite in heat treatment A, B and C are estimated to be 20 ± 23 wt%, 23 ± 22 wt% and 15 ± 44 wt% respectively (Table A1.2), using a neural network model, TRIP_PC_V, where the error bars is large. These are consistent with the optimum retained austenite volume percentage in the 0.4 wt% carbon containing steels.

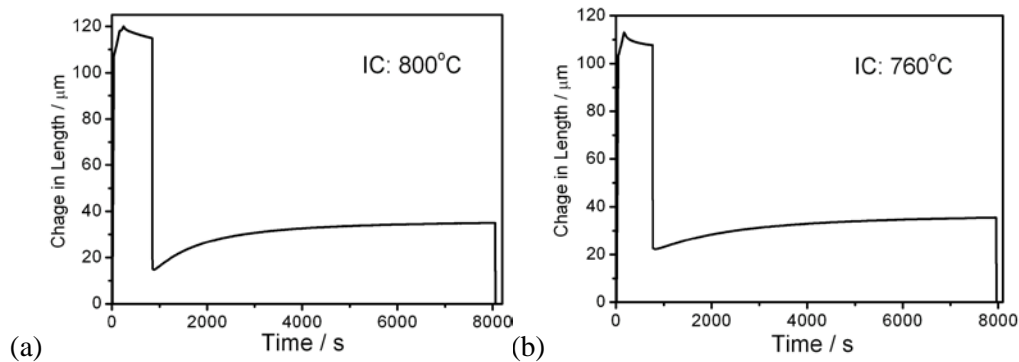


Figure A1.4: The change in length as a function of isothermal bainitic transformation at 330 °C in dilatometric study, intercritical annealed at (a) 800 °C and (b) 760 °C.

A1.4 Microstructure and mechanical properties

δ -TRIP steel consists of allotriomorphic ferrite (α), bainitic ferrite (α_b), retained austenite (γ) and martensite (α'). The majority of bainitic ferrite is in the form of laths shape and alternated with films of retained austenite, marked as α_{bL} . The retained austenite in δ -TRIP steel has three morphologies, γ_B : blocky austenite adjacent to allotriomorphic ferrite where no bainitic transformation has happened; γ_B' : blocky austenite adjacent to bainitic ferrite which is mildly enriched in carbon by bainitic transformation; γ_L : films of austenite alternating with bainitic ferrite and is strongly enriched in carbon. All three morphologies were enriched in carbon by intercritical annealing and isothermal bainitic transformation.

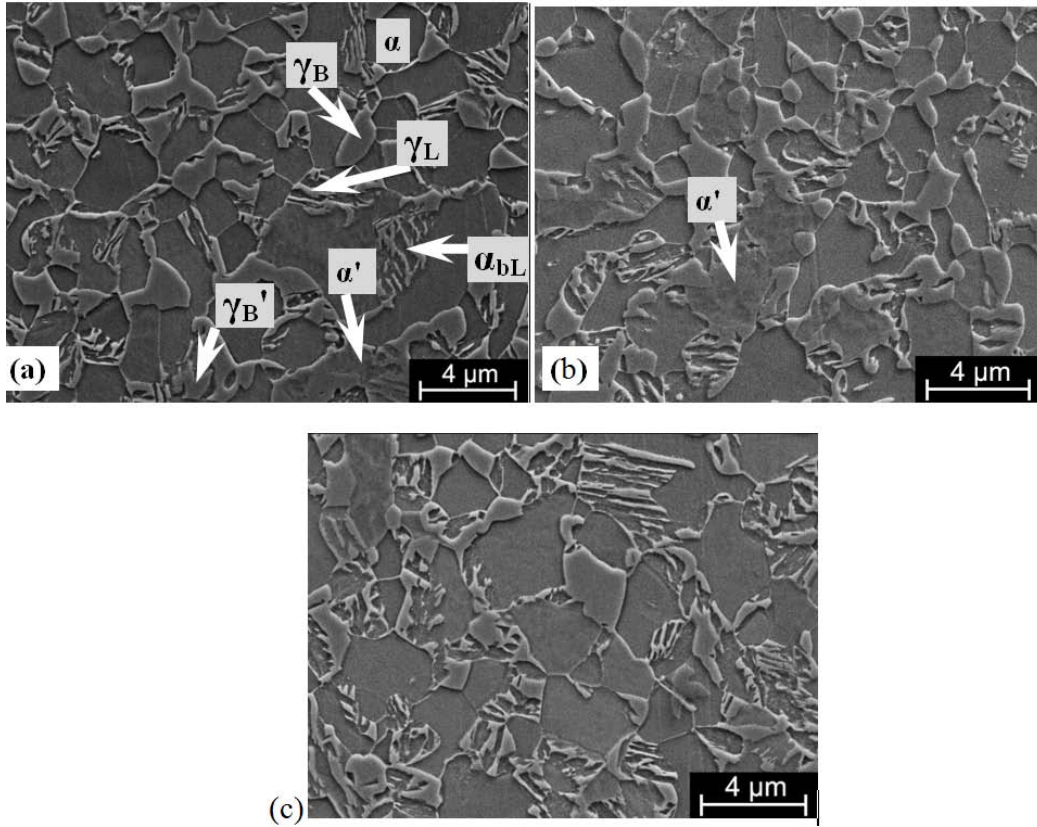


Figure A1.5: FE-SEM image of heat treated specimens. (a) heat treatment A, (b) heat treatment B, (c) heat treatment C.

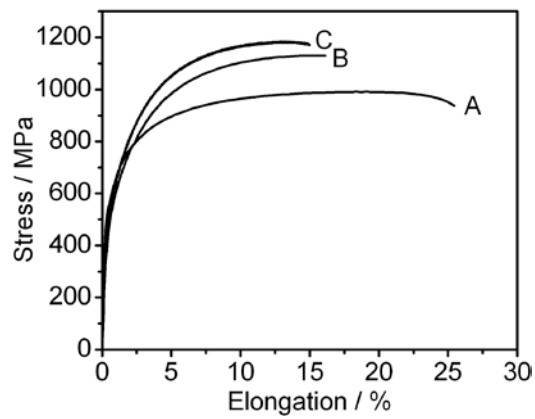


Figure A1.6: Flow stress of specimens A, B and C.

The carbon contents in them are different and in the following sequence: $C_{\gamma_L} > \gamma_{B'} >$

γ_B according to the previous work [Itami *et al.*, 1995]. The sequence of stability austenite is therefore $C\gamma_L > \gamma_B' > \gamma_B$ as well. It is seen in Figure A1.5, that some blocky austenite with big grain size transformed to martensite referred as α' because its M_s temperature increased due to the lower carbon and bigger grain size [Yang and Bhadeshia, 2009]. The grain size of blocky austenite in specimens B intercritically annealed at 760 °C is much smaller than that of A and C intercritically annealed at 800 °C. Less bainite formed in B compared with in A and C meanwhile more bainite formed in C than in A due to the long isothermal holding time. Consequently, the most martensite formed in specimen B and the least formed in C, in the big blocky austenite.

As shown in Figure A1.6, all the specimens exhibited continuous yielding like in dual phase steels. Continuous yielding is advantageous in forming operations as this helps to avoid stretcher strain or *Lüder bands*. The gradual yielding of dual phase steels is mainly due to the free dislocations present in the ferrite grains generated by the formation of martensite. Formation of bainite, instead of martensite, in TRIP-assisted steels is not as effective in inducing free dislocations in ferrite, resulting discontinuous yielding [Sugimoto *et al.*, 1993; DeCooman 2004]. The continuous yielding here was due to the formation of martensite in all specimens owing to the non-uniform grain size and carbon distribution in austenite.

Specimen A achieved the best mechanical properties, 991 MPa ultimate tensile strength, 19% uniform elongation and 25% total elongation. This is partly attributed to the amount and moderate stability of retained austenite. The X-ray diffraction results revealed that specimen A contained 19.0±0.1 wt%, 13.1±0.3 wt% and 9.5±0.2 wt% of retained austenite in the undeformed, uniformly deformed and fractured (necking) regions, respectively, as shown in Figure A1.7a. This is consistent with the results

calculated by modeling [Sherif *et al.*, 2004] (Figure A1.7b). Among specimens A, B and C, the more the retained austenite, the better mechanical properties that were achieved in specimen A. Specimen B and C had relatively poor mechanical properties because the retained austenite is too stable in specimen C, and that in B is not sufficiently stable.

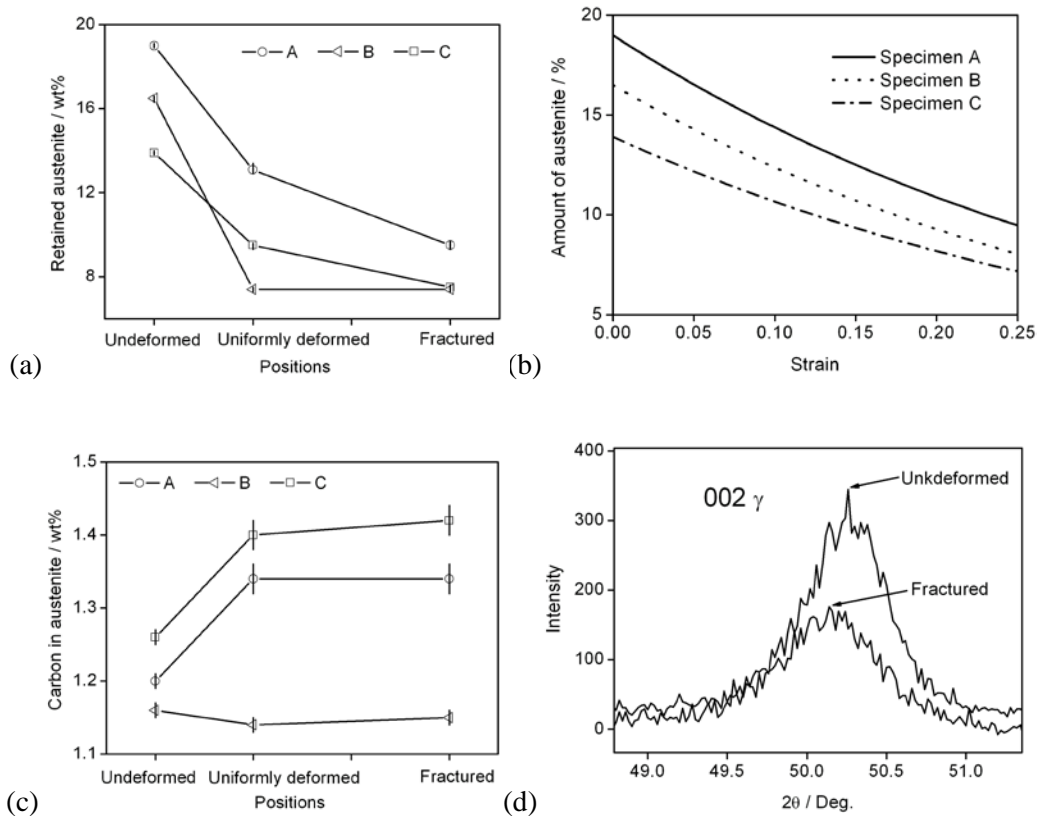


Figure A1.7: Retained austenite (a) revealed by X-ray analysis and (b) calculated by modeling [Sherif *et al.*, 2004], (c) carbon content in specimens, (d) (002) γ peak shifting with deformation in specimen A.

In specimen A, the blocky austenite contained less carbon and transformed first into martensite during deformation compared with the film (Figure A1.8). This is supported by X-ray diffraction data which revealed a higher carbon concentration in the deformed part than in undeformed part (Figure A1.7c). Figure A1.7d shows the peak of (0 0 2) γ

obviously shifted to the left after serious deformation in specimen A. This indicates the remanent retained austenite after serious deformation contains more carbon than that before deformation.

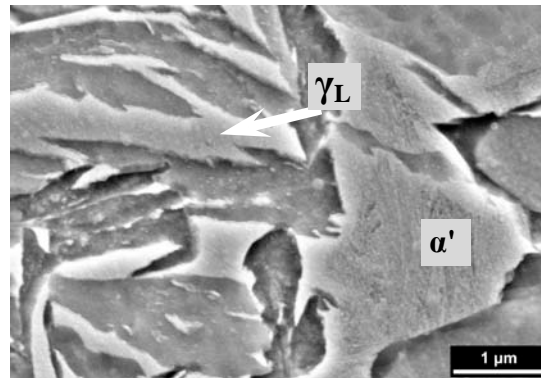


Figure A1.8: Martensite formed in blocky austenite and martensitic transformation didn't happen in austenite laths between bainitic ferrite in deformed specimen A.

A1.5 Conclusions

The microstructure evolution of δ -TRIP steel was successfully designed by sole calculations using MTDATA, MUCG and TRIP_PC_V. The fractions of retained austenite in heat treatments estimated by modeling are well consistent with those in actual alloys revealed by XRD. The best mechanical behavior was performed in the specimen containing high retained austenite fraction and its moderate stability compared with the weak stability and too strong stability in the other two specimens. Blocky austenite surrounded by allotriomorphic ferrite and lathy austenite between bainitic ferrite laths coexist in the microstructure. The blocky austenite transformed to martensite at early stage of deformation, meanwhile the lathy one can sustain until the fracture. More carbon can enrich in retained austenite during isothermal bainitic transformation in δ -TRIP steel compared the conventional TRIP-assisted steels because the addition of aluminium does shift the T_0 line to the right.

Appendix 2 Medium carbon fully pearlitic steel obtained by slow cooling

A2.1 Introduction

A pearlite colony is a bicrystal of cementite (θ) and ferrite (α), with these two phases growing at a common front with the austenite (γ). During equilibrium cooling of a binary steel, a fully pearlitic microstructure can only be obtained with a eutectoid composition. On the other hand, it is well established that supercooling the austenite in hypo- or hyper-eutectoid steels into a domain where the austenite is supersaturated with respect to both ferrite and cementite, permits it to evolve into a fully pearlitic state [Sorby 1986; Bhadeshia and Honeycombe, 2006]. This domain is known as the *Hultgren extrapolation region*, identified by extending the $(\alpha+\gamma)/\gamma$ and $(\gamma+\theta)/\gamma$ phase boundaries to temperatures below the eutectoid [Houin *et al.*, 1981]. To form a fully pearlitic microstructure in the hypo-eutectoid steel, the pearlitic transformation must happen at very low temperature corresponding to the carbon content along the extended $(\gamma+\theta)/\gamma$ phase boundaries. The fast cooling is necessary to retard austenite-ferrite transformation before pearlitic transformation. The lower the carbon contents, the lower the pearlitic transformation temperature with faster cooling rate before pearlitic transformation. A Fe-0.4C-0.62Mn-0.30Si-0.024Al wt% alloy can form fully pearlitic steels transforming between 670-560°C cooling from austenitizing temperature 900°C at very fast rate between 70 °C s⁻¹ and 140 °C s⁻¹ [Houin *et al.*, 1981]. However, such supercoolings may not be possible in practice when dealing with large dimensions of steels.

In this research, high aluminium contents were originally designed to replace

silicon to retard cementite formation during bainitic transformation and to stabilize δ -ferrite in the novel δ -TRIP steel. One of these designs allows a 0.4C wt% steel to be cast into a fully pearlitic state during slow-cooling, which consists of ultra fine discontinuous cementite lamellae dispersed in the ferrite matrix. The science behind this concept is discussed in the point view of the huge driving force for pearlitic transformation due to transition from the non-equilibrium state to equilibrium state.

A2.2 Experiment

The alloys used here are the alloy 1 and 2 in Table 2.1. Microhardness of pearlite in each alloy was measured on a Vickers hardness (FM -700) tester by using 300 gf loading and 15 s holding time. Room temperature tensile testing for the as-cast alloys was carried out using a computer controlled Zwick/Roell testing machine (Z-100) with an extensometer. The test specimens were prepared as per ASTM Standard (ASTM: Vol. 01.02: E8M-00). Uniaxial tensile tests of samples of 10 mm diameter and 50 mm gauge length was carried out at a strain rate of $3.3 \times 10^{-3} \text{ s}^{-1}$.

A2.3 Metallography and properties

The microscopic features of two alloys designed on the basis of equilibrium to contain substantial amounts of δ -ferrite, have been examined and found to display zero or much reduced fractions of this phase in the solidified condition. It is concluded that this is because the austenite that forms during cooling by solid-state transformation, does so without the required partitioning of substitutional solutes. This is responsible for the diminished quantities of δ -ferrite found in the cast microstructures (Chapter 2). The alloy 1 contains only 9 ± 1 wt% of allotriomorphic ferrite but not any dendritic δ -ferrite and the remain pearlite, where the dendritic solidification process is revealed through

coring effects that shows the original dendritic thickness is $89 \pm 9 \mu\text{m}$ (Figure A2.1a, b). That indicates the alloy was fully austenitized during the cooling process then followed by $\gamma \rightarrow \alpha + \theta$ transformation, where the $\alpha + \theta$ is consist of very small amount of allotriomorphic ferrite along the original austenite grain boundary and majority of pearlite. The allotriomorphic ferrite was transformed from austenite in the para equilibrium condition (Chapter 2) and was confirmed by the microanalysis and the thermodynamics data. The partition coefficient of alloying element is defined as concentration in ferrite / concentration in austenite before pearlite formation. The composition in austenite can be measured from the pearlite region because it in the final microstructure inherits the chemical composition of parent austenite. The partition coefficients of both manganese and aluminium are close to 1 which is far from the equilibrium value 0.32 and 3.00 listed in Table A2.1. It means the alloy elements don't partition during the allotriomorphic ferrite transformation from austenite.

The ferritic transformation before the cementite beginning was suppressed owing partially to the huge original austenite grain size. This can be confirmed by the fact that approximately $50 \pm 3\text{wt}\%$ allotriomorphic ferrite was found in the hot rolled steel due to the grain refinement for the same alloy (Figure A2.1c), where the original austenite is as small as only $3.1 \pm 0.2 \mu\text{m}$ using the mean lineal intercept method. The almost fully pearlitic microstructure is possible when transformation occurs at a low temperature, Figure A2.3. The phase diagrams of both alloys are calculated with the APPLICATION module of MTDATA. The low cementite fraction due to the low carbon concentration causes it to become discontinuous in the pearlite.

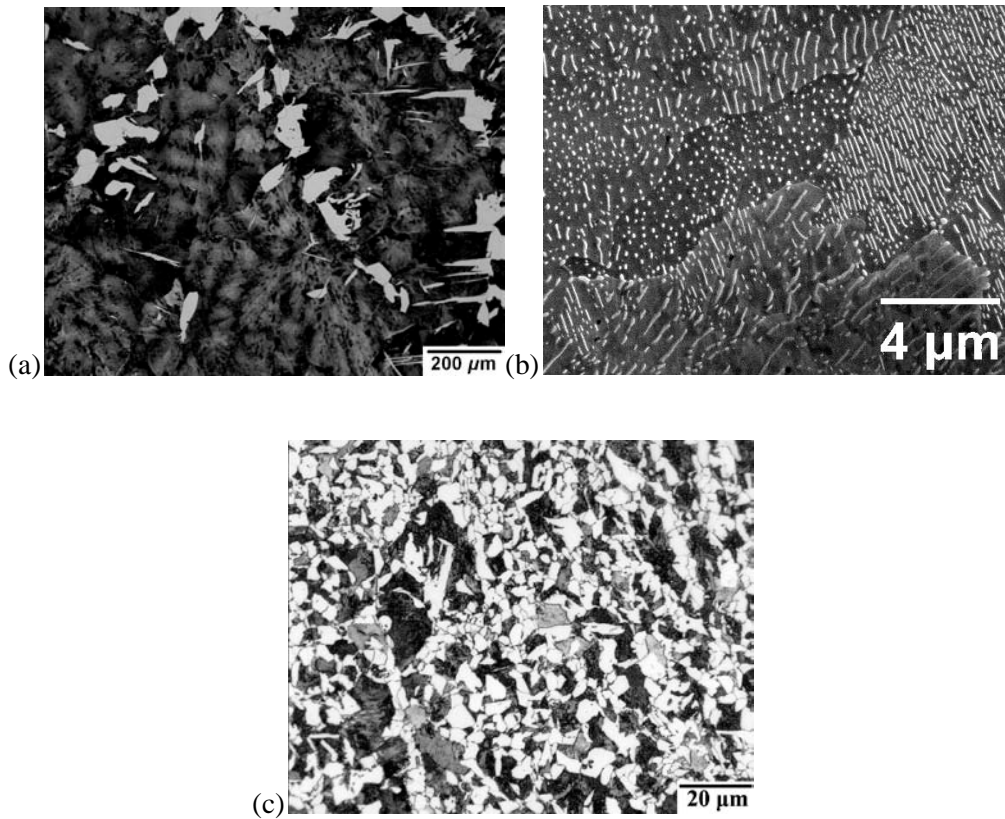


Figure A2.1. Microstructure of the cast Alloy1; the dark regions are fine pearlite and the white, ferrite. (a) General microstructure; (b) higher magnification image of the dark areas showing pearlite. (c) hot rolled indicating fine original austenite grain size.

Table A2.1: Partition of manganese and aluminium by equilibrium calculation at 1000 K and microanalysis results.

	Ferrite		'Austenite'		Partition coefficient	
	Mn	Al	Mn	Al	Mn	Al
Equilibrium at 1000 K	1.18	2.73	3.74	0.91	0.32	3.00
Measured	1.85±0.21	2.62±0.11	1.82±0.18	2.59±0.11	1.01	1.02

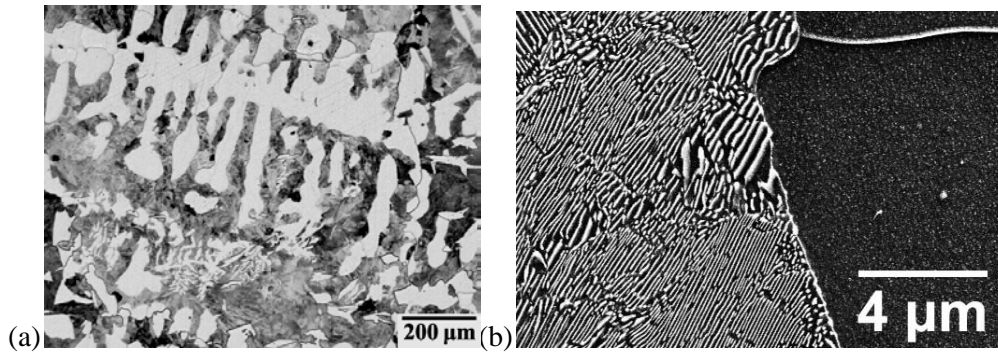


Figure A2.2. Microstructure of the cast Alloy2; the dark regions are fine pearlite and the white, ferrite. (a) General microstructure; (b) higher magnification image showing pearlite and ferrite.

It is emphasized again, that the para equilibrium calculation is a limiting estimate since the real process can be anywhere between local equilibrium and local para equilibrium. The interpretation presented here explains subsequent solid-state transformation under conditions where partitioning does not follow expectations from local equilibrium at the advancing interfaces. In conclusion, the allotriomorphic ferrite was suppressed in the cast alloy but not in the hot rolling process due to the large austenite grain size in cast condition and relevant kinetic reason proven by microanalysis.

Table A2.2: Microhardness and carbon content in pearlite and pearlite fraction in each alloy

	$V_{\text{Pearlite}} / \text{vol}\%$	$C_{\text{Alloy}}^c / \text{wt}\%$	$C_{\text{Pearlite}}^c / \text{wt}\%$	Hardness in pearlite / HV
Alloy1	90.7	0.36	0.39	266±20
Alloy2	67.1	0.37	0.54	253±16

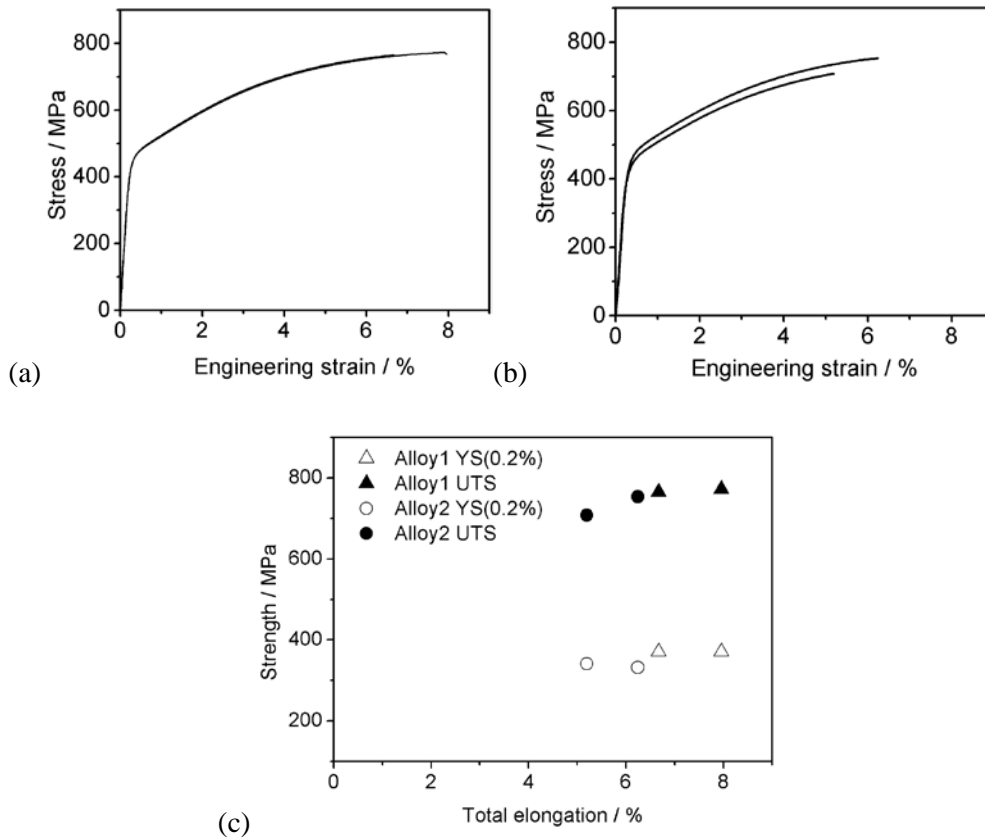


Figure A2.4: Tensile properties of as-cast alloys. (a) Flow stress of Alloy 1; (b) Flow stress of Alloy 2; (c) Comparison of mechanical properties between Alloy 1 and Alloy 2

In Alloy 2, 33 ± 2 vol% of dendritic δ -ferrite was retained to the ambient temperature and the remain phase is pearlite. The pearlite in Alloy 2 contains, therefore, both the perfect pearlite and discontinuous fine cementite dispersed in the pearlitic ferrite matrix.

Supposing 0.02 wt% carbon contains in allotriomorphic ferrite and δ -ferrite in as-cast alloys, the overall carbon concentration in pearlite can be calculated based on the carbon mass balance, illustrated in Table A2.2. The microhardness of Alloy 1 containing 0.39 wt% carbon in the pearlite region was measured to be 266 ± 20 HV compared with

253±16 HV in pearlite region of Alloy2 which contains 0.54 wt% carbon there. Alloy1 performed mechanically better in the cast condition than Alloy2 did, Figure A2.4. Alloy1 has similar yield strength and work hardening rate but slightly better ductility and resultant better ultimate tensile strength compared with alloy2. The ductility in alloy1 was probably enhanced by the fine and dispersed cementite in pearlite.

A2.4 Transformation driving force

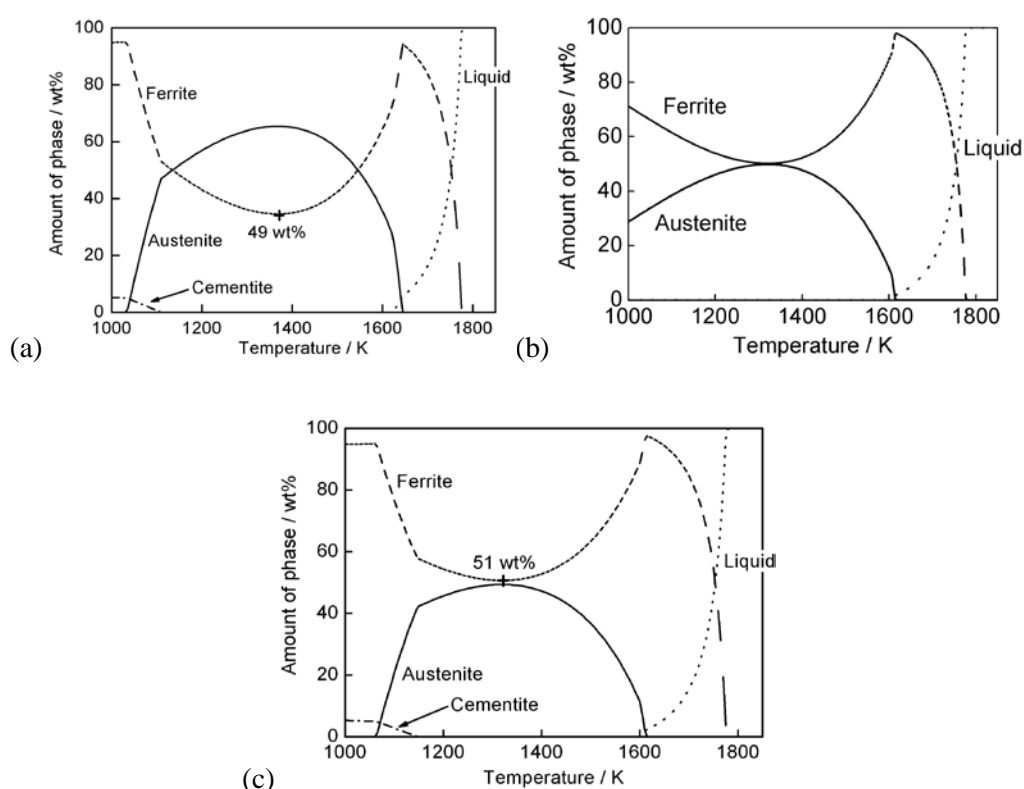


Figure A2. 4: Calculated phase amount as a function of temperatures and alloy based on equilibrium. (a) Alloy 1 including cementite, (b) Alloy 2 excluding cementite, (c) Alloy2 including cementite

The solid transformation is of para equilibrium approved in the previous work, it is however not possible to include cementite in para equilibrium calculation using

MTDATA with TCFE1.21 database due to a lack of thermodynamic data. Based on the metallography, the pearlitic transformation in alloy 1 in cast condition is considered to start from full austenite in the case ignoring the small amount of allotriomorphic ferrite, where the mother phases are in non-equilibrium state and the products are in equilibrium state, where the allotriomorphic ferrite was suppressed due to the large original austenite grain size and the kinetic reason. The equilibrium phase diagrams of both alloys including or excluding cementite phase are shown in Figure A2.4.

The driving force for pearlitic transformation at 1000 K can therefore be calculated by $\Delta G^{\gamma \rightarrow \alpha + \theta}$ in alloy1, where $\Delta G^{\gamma \rightarrow \alpha + \theta} = G^{\alpha + \theta} - G^{\gamma}$. In alloy 2, δ -ferrite persisted during the whole cast process, the pearlite at 1000K therefore transformed from a mixture of α and γ , where both mother phases and products are in equilibrium state. The Gibbs free energy is obtained from results of MTDATA. For 100 kg alloys, the total driving force for pearlitic transformation of Alloy 1 is almost 3 times as that of Alloy 2, illustrated in Table A2.3. The huge driving force for pearlitic transformation is coming from the strong trend of system state transition from non-equilibrium state to equilibrium state during pearlite transformation in Alloy1. As a conclusion, the ultra fine cementite lamellae or particle can form in Alloy 1 due to very high nucleation rate resulted from the huge chemical driving force due to state transmission from non-equilibrium to equilibrium resulting from the suppressed allotriomorphic ferrite formation, which may play a significant role for mechanical property.

Table A2.3: Driving force for pearlitic transformation for the 100 kg alloy at 1000 K.

	G^{Mother} / kJ	$G^{Product} / \text{kJ}$	$G^{Product} / \text{kJ}$
Alloy1	-89244.8 (γ)	-89709.8 ($\alpha + \theta$)	-4.65 ($\gamma \rightarrow \alpha + \theta$)
Alloy 2	-91019.3 ($\alpha + \gamma$)	-91192.8 ($\alpha + \theta$)	-1.74 ($\alpha + \gamma \rightarrow \alpha + \theta$)

A2.5 Conclusions

Almost fully pearlitic microstructure was obtained in a cast 0.4 wt% carbon containing steel with the approximate cooling rate 20 K s^{-1} , where only 9 ± 1 wt% of allotriomorphic ferrite formed compared with 50 ± 3 wt% of that was formed from during hot rolling process. The allotriomorphic ferrite transformation in para equilibrium condition during casting was suppressed by the kinetics reason because of the big austenite grain size proven by both microanalysis and DICTRA simulation. The suppressed ferritic transformation leads to a huge driving force for the pearlite formation confirmed by thermodynamics calculation, which encourages high nucleation rate and fulfils the fine divorced cementite lamellae.

References

- Andrews, K. W., Empirical formulae for the calculation of some transformation temperatures, *Journal of the Iron and Steel Institute*, 7 (1965) 721-727
- Ågren, J., Local equilibrium and prediction of diffusional transformations, *Scandinavian Journal of Metallurgy*, 20 (1991) 86-92
- Ågren, J., Computer simulations of diffusional reactions in complex steels. *ISIJ International*, 32 (1992) 291-296
- Allten, A. G., Discussion to “the effect of silicon on the kinetics of tempering”. *Trans. ASM*, 46 (1954) 812-829
- Auto/Steel Partnership (A/SP), High-Strength Steel Applications: Design and Stamping Process Guidelines, A Special Edition of In-Depth Advanced High-Strength Steel Case Studies, Auto/Steel Partnership Southfield, Michigan, June 2009, <http://www.a-sp.org/publications.htm>
- Barlat, F., Glazov, M. V., Brem, J. C. and Lege, D. J., A simple model for dislocation behavior, strain and strain rate hardening evolution in deforming aluminum alloys. *International Journal of Plasticity*, 18 (2002) 919-939
- Basuki, A. and Aernoudt, E. Influence of rolling of TRIP steel in the intercritical region on the stability of retained austenite, *Journal of Materials Processing Technology* 89-90 (1999) 37-43
- Basuki, A. and Aernoudt, E., Effect of deformation in the intercritical area on the grain refinement of retained austenite of 0.4C TRIP steel, *Scripta Materialia*, 40-9 (1999) 1003-1008
- Bayraktar, E., Kaplan, D., Devillers, L., Chevalier, J. P., Grain growth mechanism during the welding of interstitial free (IF) steels. *Journal of Materials Processing Technology*, 189 (2007) 114-125
- Bellhouse, E.M., Mertens, A.I.M. and McDermid, J.R., Development of the surface structure of TRIP steels prior to hot-dip galvanizing, *Materials Science and Engineering A* 463 (2007) 147-156
- Bentle, G. G. and Fishel, W. P., Gamma loop studies in the Fe-Si and Fe-Si-Ti systems, *Trans. Am. Inst. Min. Metall. Eng.*, 206 (1956) 1345-1348

- Berrahmoune, M.R., Berveiller, S., Inal, K., Moulin, A. and Pator, E., Analysis of the martensitic transformation at various scales in TRIP steel, *Materials Science and Engineering A* 378 (2004) 304-307
- Bhadeshia, H. K. D. H. and Edmonds, E. V., The Bainite Transformation in a Silicon Steel, *Metallurgical and Materials Transactions A*, 10 (1979) 895-907
- Bhadeshia, H. K. D. H. and Edmonds, E. V. Analysis of Mechanical Properties and Microstructure of High Dual-Phase Steel, *Metal Science*, (1980) 41-49
- Bhadeshia, H. K. D. H., A Rationalisation of Shear Transformations in Steels, *Acta Metallurgica* 29 (1981) 1117-1130
- Bhadeshia, H. K. D. H. and Edmonds, D. V., Bainite in Silicon Steels: A New Composition-Property approach. Part I, *Metal Science* 17 (1983) 411-419
- Bhadeshia, H. K. D. H. and Edmonds, D. V., Bainite in Silicon Steels: A New Composition-Property approach. Part II, *Metal Science* 17 (1983) 420-425
- Bhadeshia, H. K. D. H., Diffusional Formation of Ferrite in Iron and its Alloys, *Progress in Materials Science*, 29 (1985) 321-386
- Bhadeshia, H. K. D. H., The bainite transformation: unresolved issues, *Materials Science and Engineering A* 273-275 (1999) 58-66
- Bhadeshia, H. K. D. H. Bainite in Steels, IOM Communications Ltd, UK (2001)
- Bhadeshia, H. K. D. H., TRIP-assisted Steels? *ISIJ International* 42 (2002) 1059-1060
- Bhadeshia, H. K. D. H., Developments in martensitic and bainitic steels: role of the shape deformation, *Materials Science and Engineering A*, 378 (2004) 34-39
- Bhadeshia, H. K. D. H. and Honeycombe, R. W. K., *Steels: Microstructure and Properties*, Elsevier, UK, (2006)
- Bhadeshia, H. K. D. H., Properties of Fine-Grained Steels Generated by Displacive Transformation, *Materials Science and Engineering A*, 481-482 (2008)36-39
- Bhadeshia, H. K. D. H., Martensite in steels, lecture material in 2008 at GIFT of POSTECH, <http://cml.postech.ac.kr/a/lectures45.pdf>
- Bhadeshia, H. K. D. H., Nanostructured bainite. *Proceedings of the Royal Society of London A*, 466 (2010) 3-18
- Bhat, M. S., Microstructure and mechanical properties of AISI 4340 Steel modified with

Al and Si. PhD thesis, Lawrence Berkley Laboratories, California, USA, 1977

Berglund, D., Amundsson, K. and Hellgren, L. O., Hot stamped components with "soft zone" - Simulation and validation of material properties and product performance in: M. O. K. Steinhoff, B. Prakash (Eds.), Hot sheet metal forming of high-performance steel, 1st conference, CHS2, Luleå, Sweden, 2008, 4-10

Berglund, G., The history of hardening of boron steel in Northern Sweden, in: M. O. K. Steinhoff, B. Prakash (Eds.), Hot sheet metal forming of high-performance steel, 1st conference, CHS2, Luleå, Sweden, 2008, 1-3

Bolling, G.F. and Richman, R.H., Continual mechanical twinning: Part III: Nucleation and dislocation production Part IV: Cyclic twinning in Fe₃Be single crystals, *Acta Metallurgica*, 13 (1965) 745-757

Borgenstam, A., Engström, A., Höglund, L. and Ågren, L., DICTRA, a tool for simulation of diffusional transformations in alloys. *Journal of Phase Equilibria*, 21 (2000) 269-280

Bouet, M., Root, J., Es-Sadiqi, E. and Yue, S., The effect of Mo in Si-Mn Nb bearing TRIP steels, *Materials Science Forum*, 284-286 (1998) 319 -326

Chatterjee, S., Transformations in TRIP-assisted Steels: Microstructure and Properties, Ph.D these, 2006

Chatterjee, S., Wang, H. S., Yang, J. R. and Bhadeshia, H. K. D. H., Mechanical stabilisation of austenite, *Materials Science and Technology*, 22-6 (2006) 641-644

Chatterjee, S. and Bhadeshia, H. K. D. H., TRIP-assisted steels: cracking of high-carbon martensite, *Materials Science and Technology*, 22 (2006) 645-649

Chatterjee, S., Muruganath, M. and Bhadeshia, H. K. D. H., δ -TRIP Steel, *Materials Science and Technology* 23 (2007) 819-827.

Chatterjee, S. and Bhadeshia, H. K. D. H., Transformation-induced plasticity assisted steels: stress or strain affected martensitic transformation? *Materials Science and Technology*, 23 9 (2007) 1101-1104

Choi, B. Y., Krauss, G and Matlock, D. K. Bainite formation and deformation behavior in an intercritically annealed Fe-1.0Mn-0.09C steel, *Scripta Metallurgica* 22 (1988) 1575-1580

Choi, I. D., Bruce, D. M., Kim, S. J., Lee, C. G., Park, S. H., Matlock, D. K. and Speer,

- J. G., Deformation Behavior of Low Carbon TRIP Sheet Steels at High Strain Rates, *ISIJ International* 42 (2002) 1483-1489
- Chuko, W. and Gould, J., Development of Appropriate Resistance Spot Welding Practice for Transformation-Hardened Steels, Final Report of AISI/DOE Technology Roadmap Program, 2002 July
- Coldren, A.P. and Eldis, G.T., *J. Met.*, 32 (1980) 41-48
- De Cooman, B.C., Structure-properties Relationship in TRIP Steels Containing Carbide-free Bainite, *Current Opinion in Solid State and Materials Science*, 8 (2004) 285-303
- De Meyer, M., Vanderschueren, D., De Blauwe, K., De Cooman, B. C., ISS MWSP Conference proceeding, 37 (1999) 483-491
- De Meyer, M., Vanderschueren, D., De Cooman, B. C., 41st Mechanical Working and Steel Processing Conference Proceedings, Iron and Steel Society/AIME, USA, (1999) 265
- De Meyer, M., Vanderschueren, D., De Cooman, B. C., The influence of the substitution of Si by Al on the properties of cold rolled C-Mn-Si TRIP steels, *ISIJ International* 39 (1999) 813-822
- DeHoff, R. T. and Rhines, F. N., *Quantitative Microscopy*: McGraw Hill, New York, 1968
- Deliry, J., Nouveau carbure de fer transformation bainitique dans les aciers au carbone silicium. *Memoires Scientifiques Rev. Metallurg.*, 62 (1965) 527-550
- Denis, S., Gautier, E., Simon, A. and Beck, G., Stress phase-transformation interactions basic principles, modelling, and calculation of internal stresses, *Materials Science and Technology*, 1 (1985) 805-814
- Dyson, D. J. and Holmes, B., Effect of Alloying Additions on the Lattice Parameter of Austenite, *Journal of The Iron and Steel Institute* 208 (1970) 469-474
- Edmonds, D. V., He, K., Rizzo, F. C., Cooman, B. C. D., Matlock, D. K. and Speer, J. G., Quenching and partitioning martensite - a novel steel heat treatment, *Materials Science & Engineering A* 438-440 (2006) 25-34
- Engström, A., Höglund, L. and Ågren, J., Computer simulation of diffusion in multiphase systems. *Materials Science Forum*, 163-6 (1994) 725-730

- Epoxy 2003 Users' guide, Synaps Inc Fang, X., Fan, Z., Ralph, B., Evans, P. and Underhill, R. *Journal of Materials Processing Technology* 132 (2003) 215
- Fan, D. W., Kim, H. S. and De Cooman, B. C., A Review of the Physical Metallurgy Relate to the Hot Press Forming of Advanced High Strength Steel, *Steel Research International* 80 (2009) 241-248
- Fan, D. W., Kim, H. S. and De Cooman, B. C., in: K. S. M. Oldenburg, B. Prakash (Eds.), *Hot sheet metal forming of high-performance steel, 2nd conference*, Verlag Wissenschaftliche Scripten, Auerbach, Germany, 2009, pp. 7–16
- Fiedler, H. C., Averbach, B. L. and Cohen, M., The effect of deformation on the martensitic transformation, *Transactions of the American Society for Metals*, 47 (1955) 267-290
- Fischer, J. C., The free energy change accompanying the martensite transformation in steels, *Metals Transactions* 185 (1949) 688-690
- Frommeyer, G., Brüx, U. and Neumann, P., Supra-ductile and high-strength manganese-TRIP/TWIP steels for high energy absorption purposes. *ISIJ International*, 43 (2003) 438-446
- Fukagawa, T., Okada, H. and Maehara, Y., Mechanism of red scale defect formation in Si-added hot-rolled steel sheets. *ISIJ International*, 34 (1994) 906-911
- Furnémont, Q., Kempf, M., Jacques, P. J., Göken, M. and Delannay, F., On the measurement of the nanohardness of the constitutive phases of TRIP-assisted multiphase steels. *Materials Science and Engineering A*, 328A (2002) 26-32
- Furnémont, Q., Ph. D thesis, UCL, 2003
- Gallagher, M. F., Speer, J. G. and Matlock, D. K. Symposium on the Thermodynamics, Kinetics, Characterization and Modeling of: Austenite Formation and Decomposition, Minerals, Metals and Materials Society (TMS), USA, (2003) 563
- Garboczi, E. J., Snyder, K. A., Douglas, J. F. and Thorpe, M. F., Geometrical Percolation Threshold of Overlapping Ellipsoids, *Physical Review E* 52 (1995) 819-828.
- Gerberich, W. W., Thomas, G., Parker, E. R. and Zackay, V. F., Metastable austenite: decomposition and strength, *Proc. 2nd Int. Conf. on 'Strength of metals and alloys'*, Pacific Grove, CA, USA, August-September 1970, ASM International, 894-899
- Girault, E., Martens, A., Jacques, P., Houbaert, Y., Verlinden, B. and Van Humbeeck, J. ,

- Comparison of the Effects of Silicon and Aluminium on the Tensile Behaviour of Multiphase TRIP-Assisted Steels. *Scripta Materialia* 44 (2001) 885-892
- Goldberg, A. and Hoge, K.G., Effect of strain rate on tension and compression stress-strain behavior in a TRIP alloy, *Materials Science and Engineering*, 13 (1974) 211-222
- Goldsberry, C., Resistance welding technology advances. *Welding Magazine*, 80 (2007) 17-19
- Grässel, O., Kruger, L., Frommeyer, G. and Meyer, L. W., High strength Fe-Mn-(Al, Si) TRIP/TWIP steels development-properties-application. *International Journal of Plasticity*, 16 (2000) 1391-1409
- Guimaraes, J. R. C., THE DEFORMATION-INDUCED MARTENSITIC REACTION IN POLYCRYSTALLINE Fe 30.7 Ni - 0.06C, *Scripta Metallurgica* 6 (1972) 795-798
- Hall, J.A., Zackay, V.F. and Parker, E.R., *Transactions ASM*, 62 (1969) 965-976
- Hanzaki, A. Z., PhD Thesis, McGill University, (1994)
- Hanzaki, A. Z., Hodgson, P. D. and Yue, S., Hot Deformation Characteristics of Si-Mn TRIP Steels with and without Nb Microalloy Additions, *ISIJ International*, 35 (1995) 324-331
- Hashimoto, S., Ikeda, S., Sugimoto, K-I. and Miyake, S., Effects of Nb and Mo Addition to 0.2%C-1.5%Si-1.5%Mn Steel on Mechanical Properties of Hot Rolled TRIP-aided Steel Sheets, *ISIJ International*, 44 (2004) 1590-1598
- Hassani, F. and Yue, S. 41st Mechanical Working and Steel Processing Conference Proceedings, Iron and Steel Society/AIME, USA, 37 (1999) 493
- Hayat, F., Demir, B., Acarer, M. and Aslanar, S., Effect of weld time and weld current on the mechanical properties of resistance spot welded IF (DIN EN 10130-1999) steel. *Kovove Materialy*, 47 (2009) 11-17.
- Hein, P. and Wilsius, J., Status and Innovation Trends in Hot Stamping of USIBOR 1500 P, *Steel Research International*, 79 (2008) 85-91
- Hill, R. J. and Howard, C. J., Quantitative phase analysis from neutron powder diffraction data using the Rietveld method. *Journal of Applied Crystallography*, 20 (1987) 467-487.
- Hiwatashi, S., Takahashi, M., Katayama, T. and Usuda, M., *Journal of the Japan Society*

for Technology of Plasticity 35 (1994) 1109

Houin, J. P., Simon, A. and Beck, G., Relationship between Structure and Mechanical Properties of Pearlite between 0.2% and 0.8%C, Transactions ISIJ, 21 (1981) 726-731

Im, D. B., Lee, C. G., Kim, S. J. and Park, I. M. Journal of the Korean Institute of Metals and Materials 38 (2000) 447

Im, D. B., Lee, C. G., Song, B. H., Kim, S. J. and Park, I. M. Journal of the Korean Institute of Metals and Materials 38 (2000) 1328

Im, D. B., Lee, C. G., Kim, S. J. and Park, I. M. Journal of the Korean Institute of Metals and Materials 40 (2002) 8

Imai, N., Komatsubara, N. and Kunishige, K. Japan Technical Information Service (1992) 25

ISO 18278-2: 2004E. Resistance welding - weldability - part 2: Alternative procedures for the assessment of sheet steels for spot welding. International standard, International Standards Organisation, 2004

Itami, A., Takahashi, M. and Ushioda, K. Plastic stability of retained austenite in the cold -rolled 0.14%C-1.9%Si-1.7% Mn sheet steel, ISIJ International 35 (1995) 1121-1127

Jacques, P., Girault, E., Catlin, T., Geerlofs, N., Kop, T., van der Zwaag, S. and Delannay, F., Bainite transformation of low carbon Mn-Si TRIP-assisted multiphase steels: influence of silicon content on cementite precipitation and austenite retention, Materials Science and Engineering A, 273-275 (1999) 475-479

Jacques, P. J., Girault, E., Harlet, P. and Delannay, F., The Developments of Cold-rolled TRIP-assisted Multiphase Steels. Low Silicon TRIP-assisted Multiphase Steels, ISIJ International 41 (2001) 1061-1067

Jacques, P. J., Girault, E., Martens, A., Verlinden, B., Van Humbeeck, J. and Delannay, F., The Developments of Cold-rolled TRIP-assisted Multiphase Steels. Low Silicon TRIP-assisted Multiphase Steels, ISIJ International 41 (2001) 1068-1074

Jacques, P., Ladriere, J. and Delannay, F. On the Influence of Interactions between Phases on the Mechanical Stability of Retained Austenite in Transformation-Induced Plasticity Multiphase Steels, Metallurgical and Materials Transactions A 32 (2001) 2759-2768

Jacques, P., Furnemont, Q., Mertens, A. and Delannay, F., On the Course of Work Hardening in Multiphase Steels Assisted by Transformation-induced Plasticity, *Philosophical Magazine A* 81(7) (2001) 1789-19812

Jacques, P. J., Experimental investigation of the influence of the austenite grain size on the mechanism and kinetics of the bainite transformation in steels, *Journal de Physique IV* 112 (2003) 297-300

Jacques, P.J., Transformation-induced Plasticity for High Strength Formable Steels, *Current Opinion in Solid State and Materials Science*, 8 (2004) 259-265

Jeong, W.C., Matlock, D.K. and Krauss, G., Observation of Deformation and Transformation Behavior of Retained Austenite in a 0.14C-1.2Si-1.5Mn Steel with Ferrite-Bainite-Austenite Structure, *Materials Science and Engineering*, A165 (1993) 1-8

Jiao, S., Hassani, F., Donaberger, R. L., Essadiqi, E. and Yue, S., The Effect of Processing History on a Cold Rolled and Annealed Mo-Nb Microalloyed TRIP Steel, *ISIJ International*, 42 (2002) 299-303

JIS Z 3136. Specimen dimensions and procedure for shear testing resistance spot and embossed projection welded joints. Japanese industrial standard, Japanese Standards Association, 1999

JIS Z 3137. Specimen dimensions and procedure for cross testing resistance spot and embossed projection welded joints. Japanese industrial standard, Japanese Standards Association, 1999.

JIS Z 3139. Method of macro test for section of spot welded joint. Japanese industrial standard, Japanese Standards Association, 1978.

JIS Z 3140. Method of inspection for spot weld. Japanese industrial standard, Japanese Standards Association, 1989.

Joo, M. S., Ryu, J. H. and Bhadeshia, H. K. D. H., Domains of steels with identical properties, *Materials and Manufacturing Processes*, 24 (2009) 53-58

Kim, S. J. and Lee, C. G. *Journal of the Korean Institute of Metals and Materials* 37 (1999) 774

Kim, S. J, Lee, C. G., Choi, I. and Lee, S., Effects of Heat Treatment and Alloying Elements on the Microstructure and Mechanical Properties of 0.15 wt pct C Transformation-Induced Plasticity-aided Cold Rolled Steel Sheet. *Metallurgical*

Transactions A, 32A (2001) 505-14.

Kim, S. J., Lee, C. G., Lee, T. H. and Oh, C. S., Effects of Copper Addition on Mechanical Properties of 0.15C-1.5Mn-1.5Si TRIP-aided Multiphase Cold-rolled Steel Sheets, ISIJ International 42 (2002) 1452

Kim, S. J., Lee, C. G., Lee, T. H. and Oh, C. S., Effect of Cu, Cr and Ni on mechanical properties of 0.15 wt.% C TRIP-aided cold rolled steels, Scripta Materialia 48 (2003) 539-544

Kizu, T., Nagataki, Y., Inazumi, T. and Hosoya, Y., Effects of chemical composition and oxidation temperature on the adhesion of scale in plain carbon steels. ISIJ International, 41(2001) 1495-1501

Koh, H. J., Lee, S. K., Park, S. H., Choi, S. J., Kwon, S. J. and Kim, N. J., Effect of hot rolling condition on the microstructure and mechanical properties of Fe-C-Mn-Si multiphase steels, Scripta Materialia 38-5 (1998) 763-768

Koistinen, P. P. and Marburger, R. E., A general equation prescribing the extent of the austenite-martensite transformation in pure iron-carbon alloys and plain carbon steels, Acta Metallurgica 7 (1959) 59-60

Konieczny, A. A. Processing and Fabrication of Advanced Materials XI, ASM International, USA, (2003) 345

Kozeschnik, E. and Bhadeshia, H. K. D. H., Influence of silicon on cementite precipitation in steels. Materials Science and Technology, 24 (2008) 343-347

Kuhn, N.: Journal of the Australian Institute of Metals, 12 (1967) 71-76

Kung, C.Y. and Rayment, J.J., An Examination of the Validity of Existing Empirical Formulae for the Calculation of Ms Temperature, Metallurgical Transactions A, 13A (1982) 328-331

Kusumi, K., Yamamoto, S., Takeshita, T. and Abe, M., The effect of martensitic transformation on the spring-back behaviour of the hot stamping, in: K. S. M. Oldenburg, B. Prakash (Eds.), Hot sheet metal forming of high-performance steel, 2nd conference, Verlag Wissenschaftliche Scripten, Auerbach, Germany, 2009, 97-104

Langer, E. W., An investigation of carbide precipitation in iron. Metal Science Journal, 2 (1968) 59

Lee, C. G., Kim, S. J., OH, C. S. and Lee, S., Effects of Heat Treatment and Si Addition

on the Mechanical Properties of 0.1 wt% C TRIP-aided Cold-rolled Steels, ISIJ International 42 (2002) 1162-1168

Lee, C. G., Kim, S. J., Lee, T. H. and Lee, S., Effects of volume fraction and stability of retained austenite on formability in a 0.1C-1.5Si-1.5Mn-0.5Cu TRIP-aided cold-rolled steel sheet, Material Science and Engineering A 371 (2004) 16-23

Leslie, W. C. and Miller, R. L., The stabilization of austenite by closely spaced boundaries. ASM Transactions Quarterly, 57 (1964) 972-979

Li, S.H., Dan, W.J., Zhang, W.G. and Lin, Z.Q., A model for strain-induced martensite transformation of TRIP steel with pre-strain, Computational Materials Science,40 (2007) 292-299

Ludwigson, D. C. and Berger, J. A., Plastic behaviour of metastable austenitic stainless steels, Journal of The Iron and Steel Institute 207 (1969) 63-69

Maalekian, M., Lendinez, M. L., Kozeschnik, E., Brantner, H. P., Cerjak, H., Effect of hot plastic deformation of austenite on the transformation characteristics of eutectoid carbon steel under fast heating and cooling conditions, (2006, unpublished work)

Machlin, E. S. and Cohen, M., Burst phenomenon in the martensitic transformation. Trans. Metall. Soc. AIME 191 (1951) 746-754

Maehara, Y. and Langdon T. G., Superplasticity of Steels and Ferrous Alloys, Materials Science & Engineering A 128 (1990) 1-13.

Mahieu, J., De Cooman, B. C., Maki, J., and Claessens, S. Phase Transformation and Mechanical Properties of Si-Free CMnAl Transformation-Induced Plasticity-Aided Steel, Metallurgical and Materials Transactions A, 33 (2002) 2573-2580

MAP STEEL MUCG73 available freely in the world wide web, <http://www.msm.cam.ac.uk/map/steel/programs/mucg73-b.html>

Matas, S. J. and Hehemann, R. F. Trans. Met. Soc. AIME 221 (1961) 179

Matsumura, O., Sakuma, Y. and Takechi, H., Enhancement of elongation by retained austenite in intercritical annealed 0.4C-1.5Si-0.8Mn steel, Transactions ISIJ, 27 (1987) 570-579

Matsumura, O., Sakuma, Y. and Takechi, H., TRIP and its kinetic aspects in austempered 0.4C-1.5Si-0.8Mn steel, Scripta Metallurgica 27 (1987) 1301-1306

Matsumura, O., Sakuma, Y. and Takechi, H., Retained Austenite in 0.4C-Si-1.2Mn

- Steel Sheet Intercritically Heated and Austempered, *ISIJ International*, 32 (1992) 1014-1020
- Mileiko, S. T., The Tensile Strength and Ductility of Continuous Fibre Composite, *Journal of Materials Science* 4 (1981) 974-977.
- Mintz, B., Hot dip galvanising of TRIP and other intercritically annealed steels, *International Materials Reviews* 46 (2001) 169-197
- Mintz, B., The influence of aluminium on the strength and impact properties of steel, *International Conference on TRIP-aided High Strength Ferrous Alloys*, Ghent, 2002, 379-382
- Mintz, B., The Influence of Al on the Mechanical Properties of Hot Rolled Steel Plates, *Materials Science Forum* 426-432 (2003) 1219-1224
- Mohanty, O.N., On the Stabilization of Retained Austenite: Mechanism and Kinetics, *Materials Science and Engineering B32* (1995) 267-278
- Mori, K., Maki, S. and Tanaka, Y., Warm and Hot Stamping of Ultra High Tensile Strength Steel Sheets Using Resistance Heating, *CIRP Annals - Manufacturing Technology*, 54 (2005) 209-212
- MTDATA, National Physical Laboratory, Teddington, London, 2005
- Mukherjee, M., Mohanty, O.N., Hashimoto, S., Hojo, T. and Sugimoto, K., Strain-induced Transformation Behaviour of Retained Austenite and Tensile Properties of TRIP-aided Steels with Different Matrix Microstructure, *ISIJ International*, 46 (2006) 316-324
- Mukhopadhyay, G., Bhattacharya, S. and Ray, K. K., Strength assessment of spot-welded sheets of interstitial free steels. *Journal of Materials Processing Technology*, 209 (2009) 1995-2007.
- Naderi, M.: Hot stamping of ultra-high strength steels: Ph.D. thesis: RWTH Aachen: Germany (2007).
- Nagasaka, A., Sugimoto, K. and Kobayashi, M. *ASM International, USA*, (1996) 557
- Nagasaka, A., Sugimoto, K-I., Kobayashi, M., Shirasawa, H. *Tetsu-to-Hagane* 84 (1998) 218
- Nagasaka, A., Sugimoto, K-I., Kobayashi, M., Kobayashi, Y., Hashimoto, S. *Tetsu-to-Hagane* 85 (1999) 885

- Nagasaka, A., Sugimoto, K-I., Kobayashi, M. and Hashimoto, S. *Tetsu-to-Hagane* 85 (1999) 552
- Nagasaka, A., Sugimoto, K-I., Kobayashi, M., Kobayashi, Y. and Hashimoto, S-I., Effect of carbon content on deep drawability of TRIP-aided dual-phase sheet steels, *Tetsu-to-Hagane*, 87 (2001) 37-42
- Ojima, Y., Shiroy, Y., Taniguchi, Y. and Kato, K., Application to body parts of high strength steel sheet containing large volume fractions of retained γ , SAE paper 980954, Society of Automotive Engineers, Warrendale, PA, USA, (1998) 39-48
- Okada, H., Dukagawa, T., Okamoto, A., Azuma, M. and Matsuda, Y., Prevention of red scale formation during hot rolling of steels. *ISIJ International*, 35 (1995) 886-891
- Olson, G. B. and Cohen, M., Kinetics of strain-induced martensitic nucleation, *Metallurgical and Materials Transactions A*, 6 (1975) 791-795
- Olson, G. B., Transformation plasticity and the stability of plastic flow, *Processing and Structure*, American Society of Metals, USA, (1982) 391
- Owen, W. S., Can a Simple Heat Treatment Help to Save Detroit? *Metals Technology* 7 (1980) 1-13.
- Pak, J. H., Bhadeshia, H. K. D. H., Karlsson, L. and Keehan, E., Coalesced bainite by isothermal transformation of reheated weld metal. *Science and Technology of Welding and Joining*, 13(2008) 593-597
- Patel, J. R. and Cohen, M., Criterion for the action of applied stress in the martensitic transformation, *Acta Metallurgica* 1 (1953) 531-538
- Pereloma, E. V., Timokhina, I. B. and Hodgson, P. D., Transformation behaviour in thermomechanically processed C-Mn-Si TRIP steels with and without Nb, *Materials Science and Engineering A* 273-275 (1999) 448-452
- Pichler, A., Stiaszny, P., Potzinger, R., Tikal, R. and Werner, E. 40th Mechanical Working and Steel Processing Conference Proceedings, Iron and Steel Society/AIME, USA 36 (1998) 259
- Pichler, A., Traint, S., Arnoldner, G., Stiaszny, P., Blaimschein, M. and Werner, E. A. 44th Mechanical Working and Steel Processing Conference Proceedings, Iron and Steel Society/AIME, USA, 40 (2002) 121
- Pichler, A., Traint, S., Arnoldner, G., Stiaszny, P., Blaimschein, M., and Werner, E. A.

Iron and Steelmaker, USA, 30, (2003) 21

Pickering, F. B. Physical Metallurgy and the Design of Steels, Applied Science Publishers Ltd, England, (1978)

Pomey, J., Revenu de la martensite et reaction bainitique inferieure: Cas des aciers au carbonosilicium et des aciers au carbone. Memoires Scientifiques Rev. Metallurg., 63 (1966) 507-532

Pyshmintsev, I. Y., De Meyer, M., De Cooman, B. C., Savray, R. A., Shveykin, V. P. and Vermeulen, M., The influence of the stress state on the plasticity of transformation-induced plasticity-aided steel, Metallurgical and Materials Transactions A 33 (2002) 1659-1667

Radcliffe, S.V. and Schatz, M., The effect of high pressure on the martensitic reaction in iron-carbon alloys, Acta Metallurgica, 10 (1962) 201-207

Raman, R. K. S., Characterisation of 'rolled-in', 'fragmented' and 'red' scale formation during secondary processing of steels. Engineering Failure Analysis, 13 (2006) 1044-1050

Rathburn, R. W., Matlock, D. K. and Speer, J. G., Fatigue behaviour of spot welded high-strength sheet steels. Welding Journal, Research Supplement, 82 (2003) 207-218

Reisner, G., Warner, E. A. and Fischer, F. D., Micromechanical modeling of martensitic transformation in random microstructures, International Journal of Solid Structures, 35 (1998) 2457-2473

Rietveld, H.M., Line profiles of neutron powder-diffraction peaks for structure refinement. Acta Crystallographica, 22 (1967) 151-152

Rietveld, H. M., A profile refinement method for nuclear and magnetic structures. Journal of Applied Crystallography, 2 (1969) 65-71

Sadagopan, S., Wong, C., Huang, M., Yan, B. and Urban, D., Formability characterization of new generation of high strength steels. Tech. Rep. TRP 0012, American Iron and Steel Institute, 2003, Pittsburgh, USA.

Sadhukhan, S., Das, K. P., Bandyopadhyay, N. R. and Banerjee, M. K. Journal of the Institution of Engineers, India, 82 (2001) 65

Sakaki, T., Sugimoto, K. and Fukuzato, T., Role of internal stress for continuous yielding of dual-phase steels, Acta Metallurgica, 31-10 (1983) 1737-1746

Sakuma, Y., Matsumura, O. and Akisue, O., Influence of C Content and Annealing Temperature on Microstructure and Mechanical Properties of 400°C Transformed Steel Containing Retained Austenite, *ISIJ International*, 31 (1991) 1348-1353

Sakuma, Y., Matsumura, O. and Takechi, H., Mechanical-properties and retained austenite in intercritically heat-treated bainite-transformed steel and their variation with Si and Mn additions. *Metallurgical & Materials Transactions A*, 22 (1991) 489-498

Sakuma, Y., Matlock, D. K. and Krauss, G., Intercritically annealed and isothermally transformed 0.15Pct C steels containing 1.2 Pct Si-1.5Pct Mn and 4 Pct Ni: Part 1. Transformation, microstructure, and room-temperature mechanical properties, *Metallurgical and Materials Transactions A*, 23 (1992) 1221-1232

Sakuma, Y., Matlock, D. K. and Krauss, G., Intercritically annealed and isothermally transformed 0.15Pct C steels containing 1.2 Pct Si-1.5Pct Mn and 4 Pct Ni: Part 2. Effect of testing temperature on stress-strain behavior and deformation-induced austenite transformation, *Metallurgical and Materials Transactions A*, 23 (1992) 1233-1241

Sakuma, Y. and Oikawa, H., Factors to Determine Static Strengths of Spot-weld for High Strength Steel Sheets and Developments of High-strength Steel Sheets with Strong and Stable Welding Characteristics. *NIPPON Steel Technical Report*, 88 (2003) 34-38

Santella, M., Babu, S. S., Riemer, B. W. and Fang, Z., Influence of microstructure on the properties of resistance spot welds, *Materials Park, OH, ASM International*. in 'Trends in welding research', (ed. S. A. David et al.), 1999, 605-609

Scheil, E., *Zeitschrift für anorganische and allgemeine, Chemie* 207 (1932)

Schrader, A. and Wever, F. *Arch. Eisenhittenwesen* 23 (1952) 489

Sherif, M. Y., Garcia-Mateo, C., Sourmail, T. and Bhadeshia, H. K. D. H., Stability of retained austenite in TRIP-assisted steels, *Materials Science and Technology* 40 (2004) 319-322

Shipway, P.H. and Bhadeshia, H.K.D.H, Mechanical Stabilisation of Bainite, *Materials Science and Technology*, 11 (1995) 1116-1128

Song, S. M., Sugimoto, K-I., Kandaka, S., Futamura, A., Kobayashi, M. and Masuda, S., Effects of prestraining on high cycle fatigue strength of high strength low alloy TRIP steels, *Journal of the Society of Materials Science, Japan*, 50 (2001) 1091-1097

- Song, S. M., Sugimoto, K-I., Kandaka, S., Futamura, A., Kobayashi, M. and Masuda, S., Effects of prestraining on high cycle fatigue strength of high-strength low alloy TRIP-aided steels, *Materials Science Research International*, 9 (2003) 223-229
- Sorby, H. C., On the application of very high powers to the study of the microscopic structure of steel. *JISI* 1 (1886) 140-147
- Streicher, A. M., Speer, J. G. and Matlock, D. K. *Steel Research* 73 (2002) 287
- Suehiro, M., Maki, J., Kusumi, K., Ohgami, M. and Miyakoshi, T., Properties of aluminium-coated steels for hot-forming: Tech. Rep. 88: 16-21: Nippon Steel Corporation Technical Report (2003).
- Sugimoto, K-I., Kobayashi, M. and Hashimoto, S. I., Ductility and Strain-Induced Transformation in a High-Strength Transformation-Induced Plasticity-Aided Dual-Phase Steel, *Metallurgical and Materials Transactions A* 23 (1992) 3085-3091
- Sugimoto, K-I., Usui, N., Kobayashi, M. and Hashimoto, S. I., Effects of Volume Fraction and Stability of Retained Austenite on Ductility of TRIP-aided Dual-phase Steels, *ISIJ International*, 32 (1992) 1311-1318
- Sugimoto, K-I., Misu, M., Kobayashi, M. and Shirasawa, H., Effects of Second Phase Morphology on Retained Austenite Morphology and Tensile Properties in a TRIP-aided Dual-Phase Steel Sheet, *ISIJ International* 33 (1993) 775-782
- Sugimoto, K-I. and Kobayashi, M., *Iron and Steel Society/AIME, USA* (1994) 255-265
- Sugimoto, K-I., Nagasaka, A., Kobayashi, M. and Hashimoto, S. I., Effects of retained austenite parameters on warm stretch-flangeability in TRIP-aided dual-phase sheet steels, *ISIJ International* 39 (1999) 56-63
- Sugimoto, K. I., Muramatsu, T., Hashimoto, S. I. and Mukaid, Y., Formability of Nb bearing ultra high-strength TRIP-aided sheet steels, *Journal of Materials Processing Technology*, 177 (2006) 390-395
- Sugimoto, K.I, Microalloyed ultra high- and high-strength TRIP-aided sheet steels with different matrix structure, *Proceedings of the International Conference on Microalloyed Steels Emerging Technologies and Applications*, Kolkata, India, March 2007, 128-138
- Takahashi, M., Development of High Strength Steels for Automobiles, *Nippon Steel Technical Report*, 88 (2003) 2-7
- Takechi, H., Matsumura, O., Sakuma, Y. *Japan Kokai Tokyo Koho Japan Patent* 62, 188,

729 (1987)

Tobiyama, Y., Osawa, K. and Hirata, M, Kawasaki Seitetsu Gihou, 31 (1999) 181

Tomota, Y., Kuroki, K., Mori, T., Tamura, I., Tensile Deformation of Two-Ductile-Phase Alloys: Flow Curves of α - γ Fe-Cr-Ni Alloys, Materials Science and Engineering, 24 (1976) 85-94

Uenishi, A., Kuriyama, Y. and Takahashi, M., High-strength Steel Sheets Offering High Impact Energy-absorbing Capacity, Nippon Steel Technical Report (Japan), 81 (2000) 17-21

ULSAB -AVC Executive Summary, American Iron And Steel Institute, January 2002

Van Slycken, J., Verleysen, P., Degrieck, J., Bouquerel, J. and De Cooman, B.C., Dynamic response of aluminium containing TRIP steel and its constituent phases, Materials Science and Engineering A, 460-461 (2007) 516-524

Wei, X. C., Li, L., Fu, R. Y. and Shi, W. Acta Metallurgica Sinica (English Letters), China 15 (2002) 285

Wei, X., Fu, R., Li, L. and Shi, W., Shanghai Jinshu (Shanghai Metals), China, 24 (2002) 32

Wei, X. C., Li, L., Fu, R. Y. and Shi, W. Journal of Iron and Steel Research International, China, 10 (2003) 49

WorldAutoSteel, <http://www.ulsab.org/SteelBasics/Properties.aspx>

Yan, B. and Xu, K. 44th Mechanical Working and Steel Processing Conference Proceedings, Iron and Steel Society, AIME, USA 40 (2002) 493

Yanagishima, F., Nakazato, Y., Shimoyama, Y., Sunami, H., Ida, Y., Haga, T. and Irie, T., 1983. Development of a multipurpose continuous annealing line for cold rolled sheet steel. Iron and Steel Engineer, 60 (1983) 36-44

Yang, H. S. and Bhadeshia, H. K. D. H., Uncertainties in Dilatometric Determination of Martensite Start Temperature, Materials Science and Technology, 23 (2007) 556-560

Yang, H. S. and Bhadeshia, H. K. D. H., Austenite Grain Size and the Martensite-Start Temperature, Scripta Materialia, 60 (2009) 493-495.

Yoshitake, A., Saio, K. and Okita, T., Impact absorbed energy of hat square column in high strength steels, Paper 960020, Society of Automotive Engineers, Warrendale, PA,

USA (1996) 7-15

Zaefferer, S., Ohlert, J. and Bleck, W., A study of microstructure, transformation mechanisms and correlation between microstructure and mechanical properties of a low alloyed TRIP steel, *Acta Materialia* 52 (2004) 2765-2778

Zhu, Q., Sellars, C. M. and Bhadeshia, H. K. D. H., Quantitative Metallography of Deformed Grains, *Materials Science and Technology*, 23 (2007) 757-766

Acknowledgments

I am indebted to Professors H. K. D. H. Bhadeshia, Weijie Liu, Rongshan Qin and Ingee Kim for support, advice, inspiration and encouragement during the work and my stay here. I am grateful to Professor H. G. Lee, the Dean of Graduate Institute of Ferrous Technology, for the provision of laboratory facilities and the atmosphere at POSTECH. The work was financed by POSCO under the Blue Ocean Technology (BOT) project: δ -TRIP steel, and the Korea Science and Engineering Foundation under the context of the World Class University Programme (project no. R32-2008-000-10147-0).

I would like to thank Dr Kyoo-Young Lee, Principal Researcher in the Automotive Steel Products Research Group of Technical Research Laboratory, POSCO, who is the partner researcher of the BOT project in POSCO and gave me much needed support and advice for my research on δ -TRIP steel. I thank Dr Ji-Ho Lim, Senior Researcher in the Automotive Steel Applications Research Group, Technical Research Laboratory, POSCO, for his generous support and comments of experimental work on the spot welding of δ -TRIP steel. I thank Dr Young-Roc Im, Senior Researcher in the Sheet Products & Process Research Group of Technical Research Laboratory, POSCO, for the provision of laboratory facilities.

I wonder if this work would have been at all possible without Drs Swarup Ghosh, Shgh-Woei Ooi, Sangeeta Khare and Sadhan Ghosh, past or current members of the Computational Metallurgy Laboratory.

I shall cherish for a long time, the memory of being with the Computational Metallurgy Laboratory and I thank every member of the group for being so friendly with

me and helpful. This made my life really enjoyable here. I thank all of the members in GIFT for their kindness. I thank all my friends who supported me during this period.

Finally, I wish to record my deep sense of appreciation to my parents, wife and my two sons for their love and support during the entire period.

CURRICULUM VITAE

Name: Yi, Hongliang (易红亮)

Date of birth: Jan. 12, 1981

Place of birth: Chongqing, P. R. China

Email: knuyihl@yahoo.com.cn



Education

B. S.: Sept., 1998 – July, 2002, in materials engineering of the Department of Materials Science and Engineering, Harbin Institute of Technology (HIT), Harbin, P. R. China

M. S.: Sept., 2003 – July, 2005, in materials science of the Department of Materials Science and Engineering, Harbin Institute of Technology (HIT), Harbin, P. R. China

Ph. D: March, 2007 – July, 2010, in Computational Metallurgy of the Graduate Institute of Ferrous Technology (GIFT), Pohang University of Science and Technology (POSTECH), Pohang, Korea (South)

Experience

July, 2005 – Dec., 2006, assistant researcher, in Department of Materials Technology, China Automotive Engineering Research Institute, Chongqing, P. R. China

Special activity

Sept., 2007: China Award for Science and Technology Improvement in Automotive Industry (Second grade), based on the work between 2005 and 2006 in China Automotive Engineering Research Institute

May, 2010: 2009 Chinese Government Award for Outstanding Self-financed Students Abroad, based on the work during Ph. D program in GIFT, POSTCH